



POLITECNICO DI TORINO

Master of Science Degree in MECHANICAL ENGINEERING

MASTER THESIS

Numerical modelling of the energetic behaviour of hybrid lattice structures

Supervisor:

Prof. Giorgio DE PASQUALE

Candidate:

Luca SAVIGLIANO

s262537

ACADEMIC YEAR 2019 - 2020

Abstract

Every year more and more collisions between vehicles involve between twenty and fifty million injuries, as proven by Association for Safe International Road Travel that discloses the annual statistics. One of the solutions to this problem would be to invest in materials and innovations that allow better absorption of energy from impact. In recent years, the demand for lightweight structures with high energy absorption capacity has grown exponentially. Automotive and aerospace world are not distant from this evolution; in fact many solutions are under development.

In this thesis finite element models have been developed to analyse the compression response of lattice structures based on two different architectures in metallic material, 316L. The first structure has a Body Center Cubic lattice with vertical uprights on the Z axis lattice (BCC) while the second one has a similar lattice reinforced with vertical uprights on the Z axis (BCCZ). Three-dimensional (3D) models of polymeric material were also made and used to model structures under quasi-static compressive loads. The results of the Finite Element (FE) models of the lattice structures, as well as those of the polymeric models are compared with the experimental data and proved to be in good agreement. From the simulations carried out on the metal models it is demonstrated how the rigidity and the energy capacities could be improved by varying the geometry of the unit cell. Further tests were carried out on modified reticular structures to verify how the energetic behaviour varies as a function of combined elements. The modification consists in the infiltration of the lattice structure with a polymeric material. In this regard, this study focuses deeply on examining the experimental static behaviours of hybrid materials for both different cell topologies. In the last stages of this investigation, the hybrid structures were subjected to a dynamic stress test in order to estimate the energy absorbed by the compression structures.

Contents

1	Introduction	1
1.1	Objective of the thesis	1
1.2	Organization of the thesis	3
2	State of Art	4
2.1	Lattice structure	4
2.1.1	Introduction	4
2.1.2	Type of lattice structures	5
2.1.3	Previous studies	8
2.2	Lattice structure fabricated by AM	8
2.2.1	Story of lattice structures manufacturing	8
2.3	Additive Manufacturing methods	9
2.3.1	Electron Beam Melting	12
2.3.2	Electron Beam Additive Manufacturing	13
2.3.3	Selective Laser Melting	14
2.3.4	Direct Metal Laser Sintering	16
2.3.5	Laser Deposition	16
2.4	Infiltrated lattice	17
2.4.1	Definition	17
3	FE models definition and calibration	20
3.1	Definition	20
3.2	Calibration of 50x50x50mm ³ model	20
3.2.1	A30	26
3.2.2	A60	29

3.3	Mesh Sensitivity	32
4	Static Analysis	34
4.1	Polymer	34
4.1.1	A30	36
4.1.2	A60	38
4.1.3	F- δ curves comparison	40
4.2	Lattice structures	41
4.2.1	Design	43
4.2.2	BCC	46
4.2.2.1	BCC d=0.55mm	46
4.2.2.2	BCC d=0.65mm	48
4.2.2.3	BCC d=0.75mm	51
4.2.3	BCC comparison	54
4.2.4	BCCZ	55
4.3	Hybrid Material	56
4.3.1	BCC1/A30 & BCC1/A60	57
4.3.2	BCC2/A30 & BCC2/A60	59
4.3.3	BCC2/A30 & BCC2/A60	60
4.3.4	BCC/A30 comparison	62
4.3.5	BCC/A60 comparison	63
4.3.6	BCCZ/A30 & BCCZ/A60 comparison	64
5	Energy absorption analysis	67
5.1	BCC/A30	68
5.2	BCCZ/A30	70
5.3	BCC/A60	72
5.4	BCCZ/A60	74
5.5	Influence of the number of cells	75
6	Dynamic analysis	78
6.1	Modal analysis	78
6.2	Harmonic analysis	85

7 Conclusion and future development	98
References	100

Glossary

K_{eq}	Equivalent stiffness.
σ - ϵ	Stress-Strain.
3D	three-dimensional.
ADV	Advantage.
AM	Additive Manufacturing.
BCC	Body Center Cubic lattice.
BCCZ	Body Center Cubic lattice with vertical uprights on the Z axis.
CAD	Computer Aided Design.
CT	Compression Test.
DMLS	Direct Metal Laser Sintering.
DSV	Disadvantage.
EBAM	Electron Beam Additive Manufacturing.
EBM	Electron Beam Melting.
F-δ	Force-Displacement.
FCC	Face Centered Cubic lattice.
FE	Finite Element.
FEM	Finite Element Method.
FRF	Frequency Response Function.
IPCM	Integrated Process Chain Management.
LD	Laser Deposition.

MDOF Multi-Degree-Of-Freedom.

PCM Periodic Cellular Metals.

PU Polyurethane.

SDOF Single-Degree-Of-Freedom.

SLM Selective Laser Melting.

SOA State Of Art.

STL Standard Triangulation Language.

SW Solidworks.

W Tungsten.

WB Ansys Workbench.

ZTA Thermally Altered Zone.

List of Figures

2.1	CAD models of several unit cells for lattice structure design and manufacturing (left column); CAD models of lattice structures with corresponding unit cell designs (middle column); and photographs of corresponding SLM-processed lattice structures; (a–c) BCC; (d–f) BCCZ; (g–i) FCCZ. [2].	6
2.2	The designed lattice structures (a, b) tetrakaidecahedron-structure, (c) diamond-structure and (d) BCC. [3]	6
2.3	a) Tetrahedron, b) Pyramid, c) Octahedron, d) Kagome, e) Cube, f) Octet. [4]	7
2.4	F- δ curves of BCC and BCCZ lattice structures submitted to a compression test	7
2.5	Process of Additive Manufacturing	11
2.6	Slicing	11
2.7	EBM working principle	13
2.8	EBAM working principle	14
2.9	SLM working principle	15
2.10	LD working principle	17
2.11	Honeycomb structure & sandwich structure	18
3.1	Polymers characteristic curves	22
3.2	Tendency line of polymers	24
3.3	A30 Simulation condition and F- δ curve y=-8mm	26
3.4	Stress condition	27
3.5	A30 Simulation condition and F- δ curve y=-35mm	27

3.6	A30 Stress condition	28
3.7	A60 Simulation condition and $F-\delta$	29
3.8	A60 Simulation condition and $\sigma-\epsilon$	29
3.9	A60 $F-\delta$ curves	30
3.10	A60 $\sigma-\epsilon$ curves	30
3.11	A60 Comparison experimental vs simulation curves	31
3.12	$F-\delta$ curves as a function of mesh size	32
4.1	Polymer mesh generation	35
4.2	A30 simulation results	37
4.3	A60 simulation results	39
4.4	Polymers $F-\delta$ curves comparison	40
4.5	BCC (a) and BCCZ (b) lattice structures [4]	42
4.6	Sweep and circular repetition	43
4.7	Definition of parameters for static analysis	44
4.8	Lattice mesh generation	45
4.9	BBC1 compression simulation results	46
4.10	BBC1 stress simulation results	47
4.11	BBC2 compression simulation results	49
4.12	BBC2 stress simulation results	50
4.13	BBC3 compression simulation results	52
4.14	BBC3 stress simulation results	53
4.15	BCC $F-\delta$ curves comparison	54
4.16	BCCZ $F-\delta$ curves comparison	55
4.17	Hybrid material design	56
4.18	BCC1/A30 & BCC1/A60 simulation results	58
4.19	BCC2/A30 & BCC2/A60 simulation results	60
4.20	BCC3/A30 & BCC3/A60 simulation results	61
4.21	BCC/A30 $F-\delta$ curves comparison	62
4.22	BCC/A60 $F-\delta$ curves comparison	63
4.23	BCCZ/A30 $F-\delta$ curves comparison	64
4.24	BCCZ/A60 $F-\delta$ curves comparison	65

5.1	BCC/A30 energy comparison	69
5.2	BCCZ/A30 energy comparison	71
5.3	BCC/A60 energy comparison	73
5.4	BCCZ/A60 energy comparison	75
5.5	Energy absorption as a function of displacement [4]	76
6.1	Definition of parameters for modal analysis	79
6.2	Frequency Response Function of the hybrid materials	82
6.3	Influence of the lattice on the natural frequency of the hybrid material	84
6.4	Definition of parameters for harmonic analysis	85
6.5	Frequency Response Function of damped hybrid materials	89
6.6	Half power method of damped hybrid materials	93
6.7	Spring-mass-damper system	94
6.8	Influence of the lattice on the energy absorption of the hybrid material	97

List of Tables

2.1	ADV & DSV of EBM process	13
2.2	ADV & DSV of EBAM process	14
2.3	ADV & DSV of SLM process	16
2.4	ADV & DSV of LD process	17
3.1	Polymer specification	21
3.2	Loading condition and chord modulus	25
3.3	A30 results	28
3.4	A30 results	31
3.5	Mesh sensitivity results	33
4.1	Polymer specification	35
4.2	A30 results	37
4.3	A60 results	39
4.4	Comparison F- δ results	40
4.5	Lattice dimensions	42
4.6	Mechanical properties of 316L	44
4.7	BCC1 results	48
4.8	BCC2 results	51
4.9	BCC3 results	53
4.10	BCC comparison results	54
4.11	BCCZ comparison results	55
4.12	BCC1/A30 & BCC1/A60 results	59
4.13	BCC2/A30 & BCC2/A60 results	60
4.14	BCC3/A30 & BCC3/A60 results	61

4.15 BCC/A30 results	62
4.16 BCC/A60 results	63
4.17 BCCZ/A30 results	65
4.18 BCCZ/A60 results	66
6.1 Results of modal analysis	83
6.2 Damping coefficient	86
6.3 Results of harmonic analysis	90
6.4 Results	95

Chapter 1

Introduction

1.1 Objective of the thesis

Lightweight and energy-absorbing materials have received constant interest in recent years, thanks to the continuous development of Additive Manufacturing (AM). The lattice structures possess excellent mechanical properties in terms of stiffness and strength. They are characterized by a high percentage of voids and show a very high strength-to-weight ratio. This is a key factor for industrial sectors like automotive, aerospace, and medical. Thanks to the unique structural properties that characterize the lattice structures, the lightweight reticular materials show a high capacity for absorbing energy. The properties of reticular materials are defined by the internal architecture and can be tailored by acting on the topology of the structure or on the relative density.

The progress of AM techniques has been a determining factor for the development and production of reticular materials, which are difficult to achieve with traditional techniques. The use of this type of structures is becoming increasingly intensive in sectors such as automotive and aerospace due to their excellent properties of energy absorption during impacts. For these reasons the market has grown in the last decades, several additive manufacturing processes have been developed, and the additive sector is undergoing an exponential increase.

To reduce production costs, Finite Element Method (FEM) plays a key role in the

design of lattice structures. The FEM process allows to easily vary the materials that make up the part to compare the different response in the simulation of impacts, and calculate the energy absorbed by the component before its realization.

The purpose of this thesis work is to study the energy absorption of hybrid materials in relation to the components that constitute them. The parts are composed of a metal reticular structure that undergoes a post-treatment of polymer infiltration. Among the samples, the same metal alloy is used (316L steel by SLM process) and polymers with variable ShoreA hardness are used for filling. 316L stainless steel produced via additive manufacturing is studied. Concerning the polymeric part, two types of rubbers with different hardnesses are tested.

The available component was designed from a high packing of reticular cells of different nature and vacuum infiltrate. Then, produced by AM and tested in the laboratory under compression. The work starts initially with the study and design the components individually, namely the reticular structures and the polymeric component, using specific three-dimensional software. They are then assembled into the final component.

Using the simulation software, we started by calibrating the model previously built and then subsequently isolating individual cells. The purpose of the work is not only to modify the geometry of the structure but also to act on other parameters such as materials, mesh size, constrain and displacement. Once the calibration is performed it is possible to isolate a single lattice structure and study its behaviour applying the model. Another interesting application of the model is to study the effect of varying the material of the component. In this thesis work after calibration, simulation tests on single lattice structures are performed. The single lattice cell is made with a totally new approach, using FEM simulation software. The various components are tested for an uniaxial compressive load along the vertical. From the simulation the response of the material to the stress is extracted and considerations are made from the engineering point of view. The new designed component is analysed by examine in depth its behaviour from an energy point of view. The same procedure is then followed for infiltrated structures.

1.2 Organization of the thesis

The thesis is divided into seven chapters, here summarized for a for a quick understanding of the whole structure:

Chapter 1: Brief introduction, focusing the thesis goal and valence.

Chapter 2: State Of Art (SOA) presenting actual market and technologies, with a specific focus on lattice structures and hybrid materials, with a final outline additive manufacturing processes.

Chapter 3: detailed description of the re-designed model, from tridimensional design to an in-depth view of the simulation process to model characterization.

Chapter 4: testing phase is here explained in its various declination, from simulations as FEM and Compression Test (CT) to energy absorption test. Important aspect of the testing is the data analysis, method to prove the reliability of the simulation, and to find and fix different kind of errors in the mathematical model.

Chapter 5: is dedicated to the comparison between different hybrid materials. This is done to verify the increasing of energy absorption with respect the starting materials.

Chapter 6: dynamic analysis is done in order to study how the behaviour of hybrid material submitted to a CT is connected in term of energy. A half power method allows to establish the correlation between Frequency Response Function (FRF) and energy absorption.

Chapter 7: the thesis end with conclusions on the work done and ideas for future possible development.

This said, welcome into my thesis.

Chapter 2

State of Art

2.1 Lattice structure

2.1.1 Introduction

Lattice structures are a class of architectures with uprights and nodes interconnected in a three-dimensional space [1]. Compared to natural cellular materials, the lattice ones have a more homogeneous configuration. Their physical properties can be more easily controlled by acting on specific parameters such as relative density of filler and structural material or topology. The mechanical properties of the lattice can be optimized by acting on the distribution of material on its surface or on its geometry. In recent years, these aspects allowed the spreading of lattice structures in the industrial field as advanced lightweight materials. Until a few decades ago, the predominant obstacle to their fabrication was represented by the complex geometry of the structures. Therefore, their use was very limited. With the development of Additive Manufacturing, that is a layer-by-layer construction strategy of the part, lattice structures have gradually assumed an increasingly important role in the applications of lightweight components. Lattice structures have good design features and obvious advantages over typical foam or honeycomb structures. The shape of the cells and the mechanical properties of the lattice can be tailored on the specific applications where they will be used.

One of the main characteristics that favour lattice structures over other cellular structures is that they can be more easily designed and modelled, while this is generally not

possible for cellular structures. This makes the properties of lattice materials not only exactly controllable, but it also allows a wide range of optimizations.

Since lattices can be engineered, their properties can also be optimized by modifying the structural configuration. This would not be possible for other types of cellular structures.

Chunze Yan et al. [2] reported how lattice materials show a strength/mass ratio comparable with those of honeycomb constituent materials. In addition they guarantee excellent heat conduction, impact insulation and sound absorption properties. In case of low relative density, lattice materials highlight even more significant mechanical performances than other cellular materials.

Mechanical testing of lattice structures has recently attracted the interest of researchers. Xiaoliang Geng et al. [3] tested various lattice material with different volume fraction and unit cell sizes. They observed that there is a clear relationship between the compression modulus and strength of the material and their volume fraction and unit size.

2.1.2 Type of lattice structures

Different geometries of lattice metal structures are available on the market, such as octahedral, pyramidal, tetrahedral and Kagome structures. Each geometry is defined by a unit cell, i.e. the smallest repeating unit having the full symmetry of the lattice structure. Each of them is basically composed of struts stacked with a different arrangement and the air occupies most of the volume. In Fig.2.1 three different CAD (Computer Aided Design) models of several unit cells for lattice structure design and manufacturing technique are presented. Figure 2.1c display also the evolution from 3D design up to the fabrication via Additive Manufacturing. The lattice structures are in Fig.2.1a, Fig.2.1d and Fig.2.1g are BCC, BCC and Face Centered Cubic lattice (FCC) type respectively.

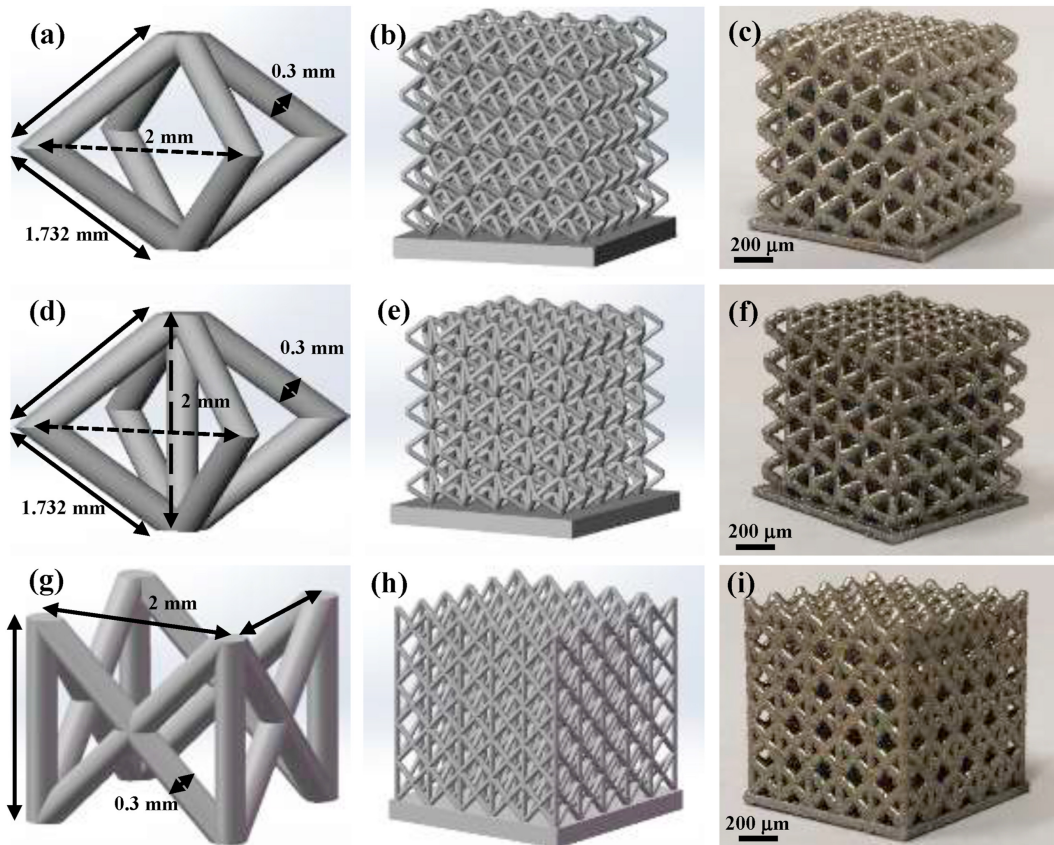


FIGURE 2.1: CAD models of several unit cells for lattice structure design and manufacturing (left column); CAD models of lattice structures with corresponding unit cell designs (middle column); and photographs of corresponding SLM-processed lattice structures; (a–c) BCC; (d–f) BCCZ; (g–i) FCCZ. [2].

Other types of lattice unit cells are reported below, in Fig.2.2, Fig.2.3.

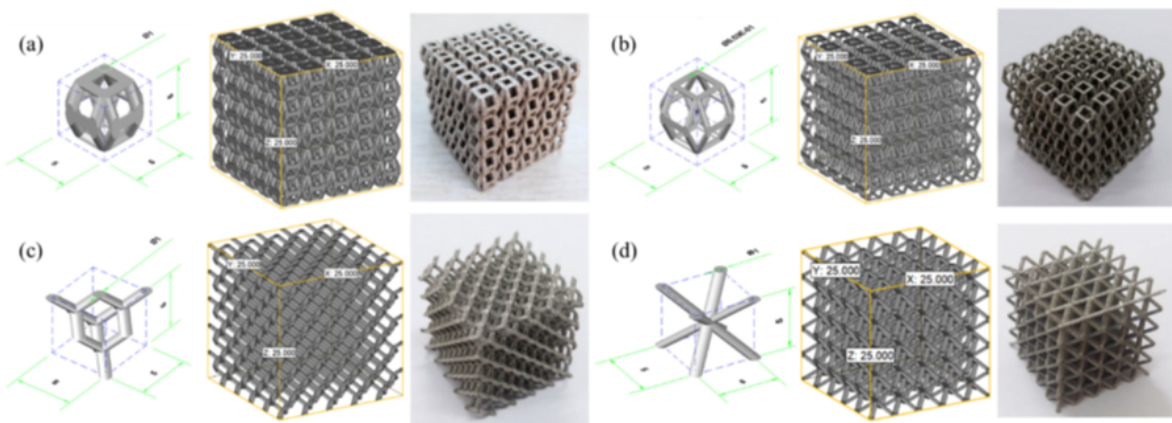


FIGURE 2.2: The designed lattice structures (a, b) tetrakaidecahedron-structure, (c) diamond-structure and (d) BCC. [3]

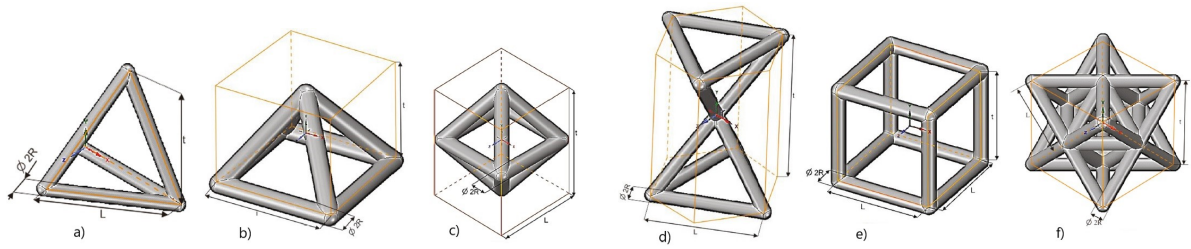


FIGURE 2.3: a) Tetrahedron, b) Pyramid, c) Octahedron, d) Kagome, e) Cube, f) Octet. [4]

Truss lattice materials can be considered as mechanical metamaterials where their mechanical properties are dependent on the design of their unit cell and the properties of the starting material from which they are fabricated.

Different unit cells can be more fitting for different applications, for example BCC and BCCZ structures are very suitable for use as energy absorbers [4]. In fact, they present in the Force-Displacement ($F-\delta$) diagram a plateau zone, Fig.2.4. Plateau zone is the name given to the section of the $F-\delta$ curve where the force remains almost constant despite increasing displacement. From this it can be deduced how the BCC structure in the plateau zone is able to absorb energy from the deformation of the lattice itself.

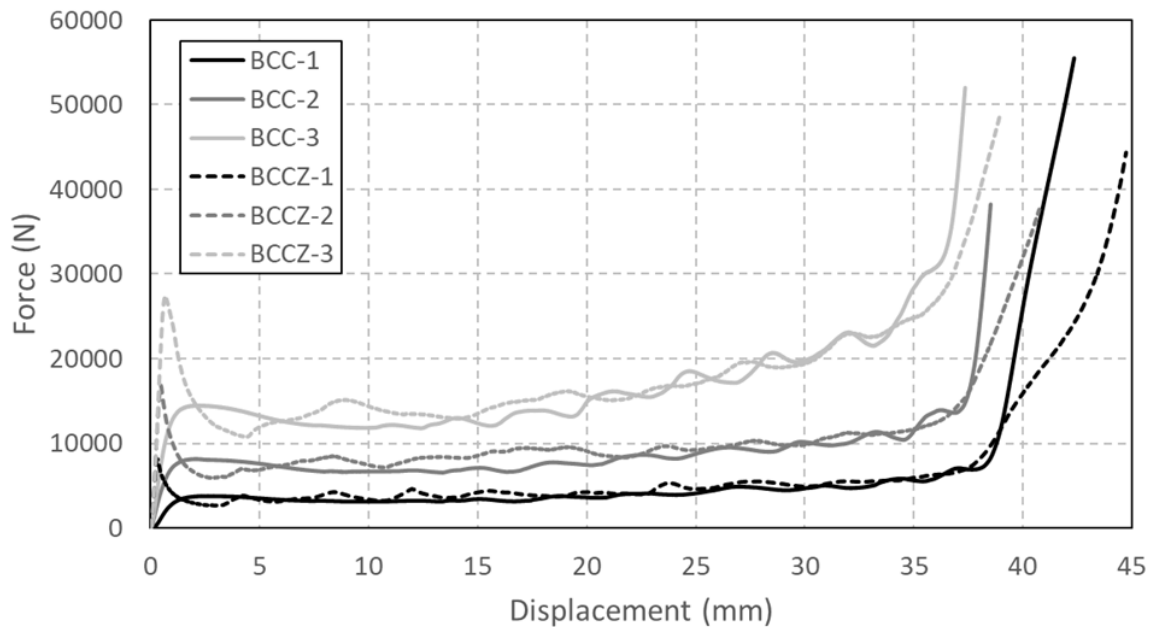


FIGURE 2.4: $F-\delta$ curves of BCC and BCCZ lattice structures submitted to a compression test

2.1.3 Previous studies

The energy absorber capabilities of cellular solids are always topic of interest for scientists and materials engineers. H. Niknam et al. [5] studied how the energy performance of different cellular structures can be improved. Initial studies were carried out on hexagonal honeycombs since they were considered the most common periodic solids. After applying an uniaxial and biaxial compression, the study suggests empirical relationships between stress and strain. In the following a classification of varies lattice structures was provided. Finally, it was investigated how the addition of reinforcements at the edges are effective in improving the energy absorption and impact resistance of a cellular structure.

Other study found in the literature highlight how reinforcing auxetic lattice structures with polymer fillers improves the elastic modulus as well as compressive strength and energy absorption of the structure [6].

2.2 Lattice structure fabricated by AM

2.2.1 Story of lattice structures manufacturing

Many technologies have been developed to manufacture lattice structures but the most used are the folding of perforated sheets or welding of thin rods. Although these technologies can produce many different architectures, their limitations are still evident, particularly in the fabrication of small structures and complex geometries. The choice of matrix materials is also a problem that has not yet been overcome. During their manufacture, welding or bonding processes are usually necessary. The stability of the structure could be compromised if the joints are not properly designed. This can lead to a reduction in the mechanical properties of the material used. To overcome these drawbacks, attempts have been made to produce reticular materials by liquid forming without the need for welding or adhesives, i.e. injection molding. This process is still rather complicated and requires times and costs that are still high now, as presented by Yingying Xue et al. [6].

Up to few decades ago, the manufacturing of lattice structures was the main obstacle

in their realization, limiting the possibilities to study their properties. The progress of Additive Manufacturing has marked an important step in the industrial field. It brought about changes in the modelling and construction of cellular structures and allowed for much more complex designs to be developed. The advantage of these new production systems is the ability to provide exceptional control over the lattice geometry. New structures can be obtained with minimum lattice dimensions that reach down to the order of magnitude of micrometres. These are classified as micro-structures.

The structures to be built are modelled using 3D design software. Lattice structures fabricated via Additive Manufacturing are set apart from the structures produced using traditional techniques by the absence of mechanical joints such as welds, that would be fundamental for this type of geometry. The mechanical properties are the best possible because there is not a Thermally Altered Zone (ZTA), as for example in the joints by welding. In fact this ZTA would drastically reduce the mechanical characteristics, as pointed out by Uzair Ahmed Dar et al. [7]. Unlike traditional and subtractive manufacturing methods, Additive Manufacturing is based on incremental manufacturing layer by layer. Therefore, the most relevant AM technologies commonly use powder or wires. The raw material is selectively melted from a heat source and consolidated by subsequent cooling to form a part.

The reticular or micro-lattice structures produced by Additive Manufacturing guarantee better mechanical characteristics of compressive strength, impact resistance and energy absorption compared to those produced with traditional techniques. This is allowed by the greater complexity that can be obtained with these new production systems [7].

2.3 Additive Manufacturing methods

Additive Manufacturing has attracted a lot of attention over the past decade due to its benefits such as unrivalled design freedom and short lead times [8]. Additive Manufacturing techniques have been known for more than twenty years but were initially limited to rapid prototyping of porous structures and prototypes. With the development of technology, the density and quality of manufactured parts have improved. It has become possible to reliably produce full dense finished parts with outstanding

properties.

From early applications tool inserts with integrated cooling channels have now evolved [9]. In the medical field complete dental prostheses are now made [10].

There is a wide range of usable materials on the market, including steel, aluminium and titanium. Compared to other manufacturing techniques, additive production techniques allow to create objects with a high degree of complexity from custom-made CAD models. Between the many technologies available on the market, only a few are able to guarantee dimensional tolerances that are in good agreement with the requirements of industrial applications.

AM techniques can essentially be classified according to the nature and aggregate state of the raw material. For the production of metal components, the starting material is used in the form of powder, or more rarely in threads. In the construction process, the powder is selectively melted by a localized heat source and transformed layer by layer into a solid part. The most common processes for the production of metal components are:

- Electron Beam Melting (EBM);
- Electron Beam Additive Manufacturing (EBAM);
- Selective Laser Melting (SLM);
- Direct Metal Laser Sintering (DMLS);
- Laser Deposition (LD);

Despite differences in the part construction process, they follow the same approach. Fig.2.5 shows the process flow of Additive Manufacturing, which is basically independent on method of choice. The starting point is the realization of the 3D model of the component. In AM, the universal conversion standard for mathematical models is the STL (Standard Triangulation Language) format. The CAD file is converted into a shell model in which the outer surface is approximated through triangles of different sizes. Once the 3D model has been inserted into the machine, the orientation is studied to ensure that the number of construction supports is as low as possible. The supports fasten the model in the work area by and avoid deformations due to its weight. They

also have the function of supporting protruding parts. After the generation of the supports, the model is virtually cut into planes parallel to the construction platform, i.e along the z-axis, and spaced apart by a quantity $\Delta(z)$, Fig.2.6. The data obtained from this operation are used directly by the machine. The orientation of the part and the slicing are of fundamental importance for the quality and tolerances of the finished component. On the basis of these data, the physical part is then constructed by repetitive deposition of individual layers and local melting of the material by a heat source. Once the construction process is finished, the supports are removed, the piece is cleaned, and any finishing operations are carried out.

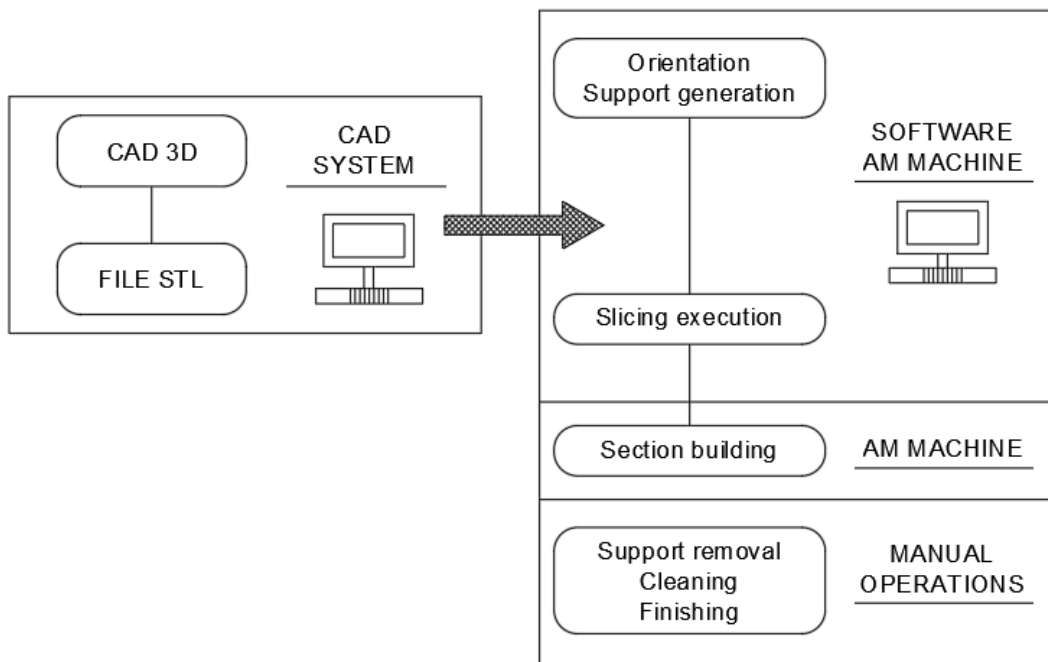


FIGURE 2.5: Process of Additive Manufacturing

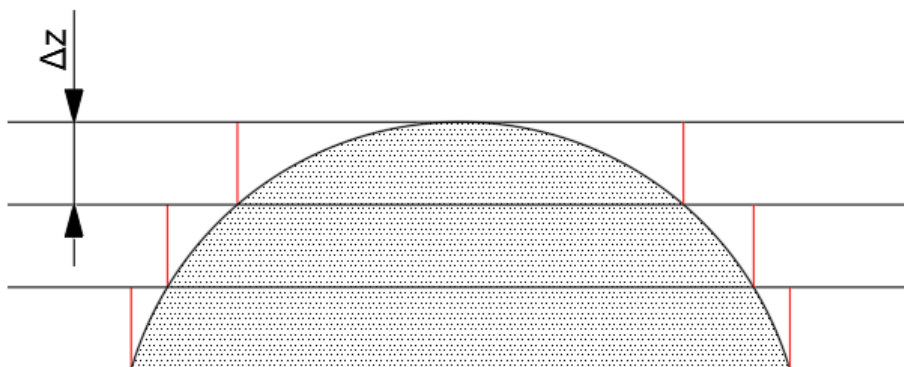


FIGURE 2.6: Slicing

Below, some information are reported on the most common processes used into the production of metal components.

2.3.1 Electron Beam Melting

The EBM process, Fig.2.7, uses metal powders as raw material. It is a process born after the 2000s and has been consolidated for the construction of turbine blades [11]. The process consists of an emission of electrons from a Tungsten (W) filament heated to a temperature greater than 2500°C. The electrons are accelerated via anode potential and conveyed in a ray. The ray is controlled by two electromagnetic lenses. The first one focuses the glimmer to the desired diameter while the second one deflects it. The beam can be concentrated up to a diameter of 10^{-1} mm. The deflection of the electron ray is controlled only with the use of electromagnetic lenses, therefore there are no moving mechanical parts. To prevent air molecules from deflecting the beam, inside the working chamber is necessary to work in high vacuum condition, where the pressure is within a range of 10^{-4} - 10^{-2} Pa. The construction process begins when the ray impinges on the powder. The kinetic energy of the electron beam is transformed into heat which melts the powder into metal. Since the temperature gradient that is generated is very high, there is a preheating phase to avoid internal tensions and deformations before casting. In this phase the working chamber is brought to a temperature around 800-900°C. In the EBM technique, thanks to the preheating of the part, the supports are reduced by 90% compared to the other AM techniques.

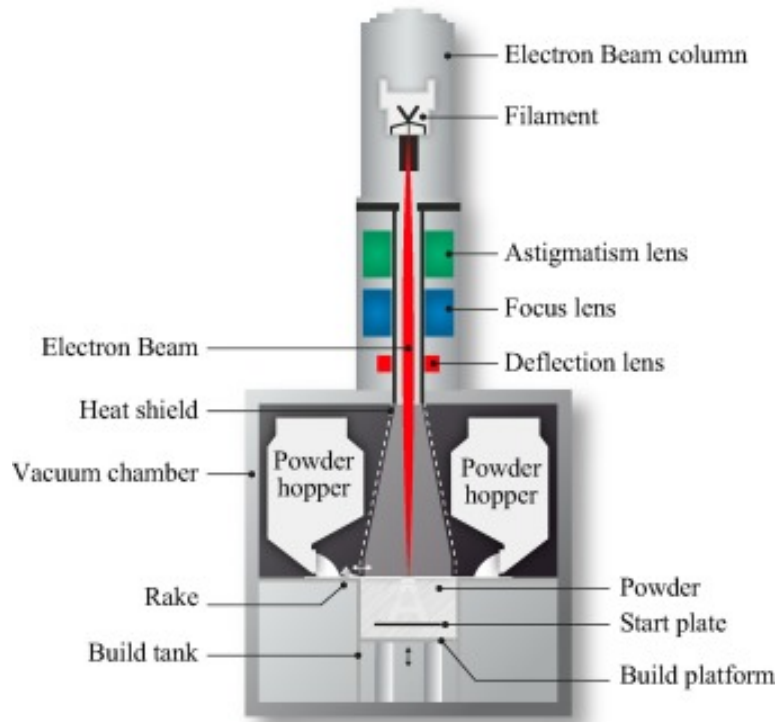


FIGURE 2.7: EBM working principle

The materials used are titanium alloys, in particular Ti6Al4V, Cobalt Chromium, super alloys such as TiAl. The Advantage (ADV) and Disadvantage (DSV) of this technique are reported in Tab.2.1.

ADV	DSV
Excellent material properties	Mechanical removal of supports
Density close to 100%	Slow cooling
Possibility to recycle unused powder	Requires specialized operator
Low operating costs	Lower tolerances with respect SLM process
Excellent accuracy in trajectory control	

TABLE 2.1: ADV & DSV of EBM process

2.3.2 Electron Beam Additive Manufacturing

The EBAM process, Fig.2.8, is a niche process and represents the evolution of the welding system, again based on the electron beam and used mainly for repair operations.

The process consists in the fusion of a metal filament by means of an electron beam source. Source and wire are a phase. The process allows a high ratio of depth of penetration with limited distortions. Volumes of work have potentially no limitations in space since they are defined by the radius of action of the head on which the filament is mounted. So it is possible to work with large volume components. The materials that can be used by this technique include all those that can be welded.

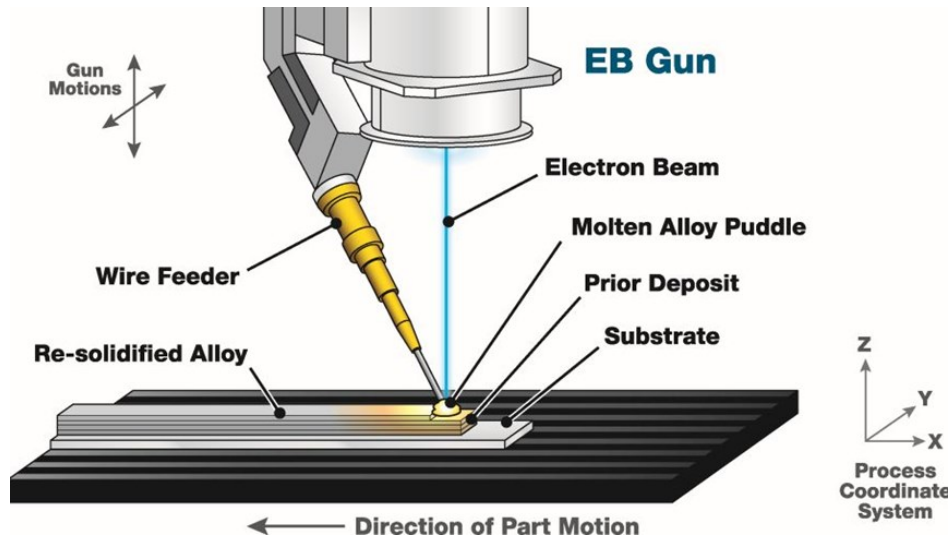


FIGURE 2.8: EBAM working principle

The Advantage and Disadvantage of this technique are reported in Tab.2.2

ADV	DSV
High productivity	Need to generate vacuum
Large volumes of work	Difficult management system
Wide range of available materials	
Possibility of making the desired alloy in the machine	

TABLE 2.2: ADV & DSV of EBAM process

2.3.3 Selective Laser Melting

The Selective Laser Melting process, Fig.2.9, is a full-melt powder bed AM technique for the production of metal components. It uses metal powders excluding organic

bonds between the particles. The thermal energy is generated through an yttrium crystal aluminium doped (Nd-Yag) laser source. Alternatively, a CO₂ laser is used to generate the ray. The laser glimmer melts not only a layer of powder but also a portion of previously solidified material. This guarantees the correct adhesion of the layers and avoids the phenomenon of delamination if the process is correctly controlled. The construction process takes place layer-by-layer in a controlled atmosphere. The powder is stored in containers adjacent to the construction zone and transported via a roller to the melting zone. The roller also performs the function of ensuring that each layer is laid out flat.

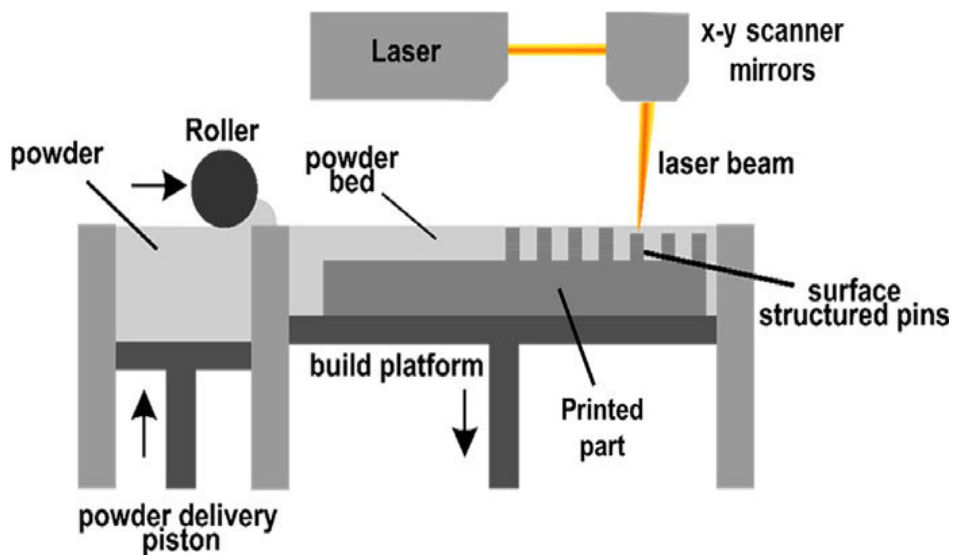


FIGURE 2.9: SLM working principle

The materials used in the SLM process are aluminium alloys, Ti and its alloys, stainless steel and noble metals alloys. The Advantage and Disadvantage of this technique are reported in Tab.2.3.

ADV	DSV
Good mechanical properties of materials	Post-processing operation needed
Better dimensional tolerances with respect to EBM process	Presence of supports
Possibility of creating complex geometries	Supports of the same material as the part
Density close to 100%	

TABLE 2.3: ADV & DSV of SLM process

2.3.4 Direct Metal Laser Sintering

The DMLS process is analogous in many aspects to the previously described SLM process. The technique was patented by EOS [12]. It consists of a different construction strategy of the part to avoid porosity within the components produced. Unlike the standard SLM, DMLS requires the scanning direction to be opposite to that of the blanket gas flow in the work chamber. Furthermore, the management of materials through Integrated Process Chain Management (IPCM) has been improved compared to the standard process. It is composed of three different stations. The first is the powder conveying module, where particles are stored after the completion of the process, the second one is the powder sieving module in which the particles are sieved to take back to the original sizes. Finally, the powders are put back inside the machine via the lifting trolley. The materials used as well as the ADV and DSV are the same of SLM process formerly discussed.

2.3.5 Laser Deposition

Laser Deposition is an AM process in which the powder is selectively deposited by two or more nozzles and then melted by a laser source, Fig.2.10. The laser source and the nozzles are both positioned on a single processing head that can move freely in a very large working space. The process takes place in a controlled atmosphere with a protective gas to prevent any oxidation of the material in contact with oxygen.

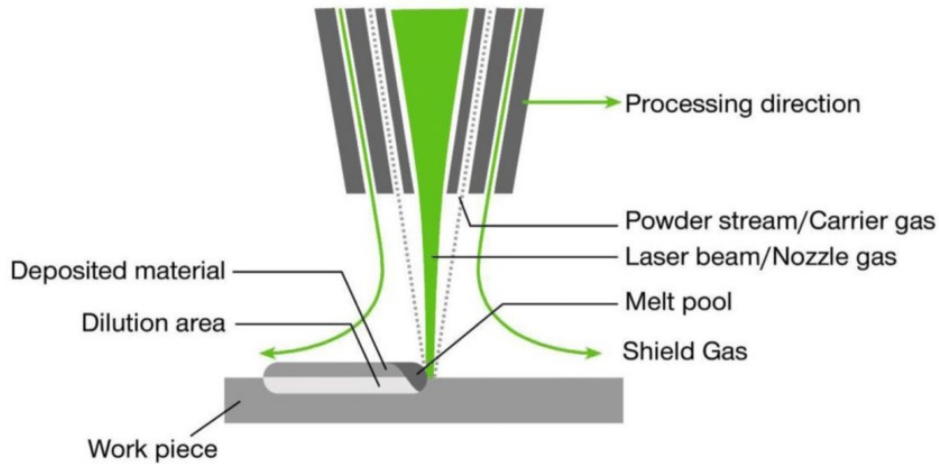


FIGURE 2.10: LD working principle

The materials used in the LD process are super alloys, i.e. Inconel IN625, aluminium alloys, titanium alloys, stainless steel and cobalt chromium. The Advantage and Disadvantage of this technique are reported in Tab.2.4.

ADV	DSV
Possibility of making multi-material components	Post-processing operation needed
Possibility of making final alloy in the machine	Sophisticated process control
No size limit	Limits on geometries
Good dimensional tolerances	High material cost
	Difficult recovery of dust

TABLE 2.4: ADV & DSV of LD process

2.4 Infiltrated lattice

2.4.1 Definition

A wide range of materials is available on the market for energy absorbing applications, each having different limitations on the mechanical properties. These limitations are evident especially when combinations of properties belonging to different materials are

required. Although some of these limitations can be overcome with the production of new alloys or polymers, the study of the union of materials can be the right tool for solving various engineering problems.

An hybrid material is defined as the fusion of two or more monolithic materials combined in a predetermined shape and scale that exhibit properties that are combination of those of the starting materials [13]. It therefore consists of a heterogeneous material whose final properties are usually better than the linear combination of the materials that constitute it.

Campbell et al. [14] investigated how the properties of Periodic Cellular Metals (PCM) vary when these are reinforced with rigid Polyurethane (PU) foams. The paper demonstrates how the strength of the hybrids was greater than that of the PCM or PU alone, and in most configurations the strength was greater than the linear sum of the strength of the periodic cellular metals and the PU foam.

The classification of hybrid materials includes not only the best known composite materials, namely a material formed by a matrix and a reinforcement in the form of fibres such as Kevlar, but also different types of structures such as sandwich structures or honeycomb structures, in which the composition of materials is based on shape and not on chemical composition. The infiltration of lattice structure with polymer also falls into this category of materials.

Fig.2.11 shows an example of the hybrid materials just described.

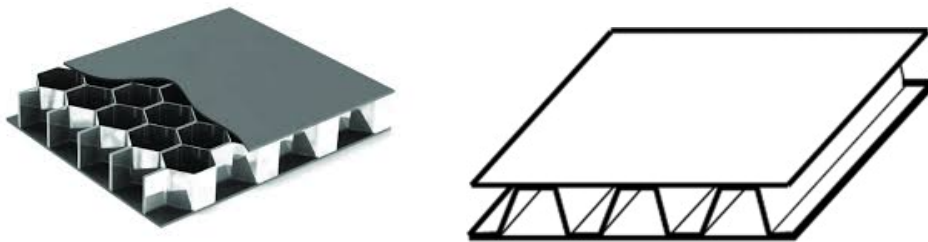


FIGURE 2.11: Honeycomb structure & sandwich structure

The main disadvantages of currently available infiltrated lattice materials are the irregularity of the cross-linked structure or the non-homogeneous distribution of the cells within the polymeric matrix. Consequently, the control of the design parameters is of particular importance to obtain the desired properties of the lattice structures.

Recently, several studies have been carried out [15][6] which have demonstrated how the desired reticular structures can be produced by Additive Manufacturing techniques and which guarantee better strength and stiffness to weight ratios than traditional foam materials.

In the literature, few studies have dealt with the use of microlattice structures as the basis for a hybrid composite structure [6][16][17]. A hybrid composite material, based on BCC microlattice additively manufactured from 316L stainless steel and rubber-like material, was developed by Gümruk et al. [13].

Chapter 3

FE models definition and calibration

3.1 Definition

In this subsection the study is done from a feasibility study engineering point of view. The starting point to carry out predictive considerations at the energy level, is the calibration of the model designed using 3D software. The calibration of the part consists in a comparison of the simulation results with reference measurements on a real sample. Once the results of the model are in agreement with those of the real sample, the model is considered to be ready. At this point it is possible to modify the architecture of the truss structure.

Thanks to a previous work, the results of the polymeric component in cubic form with dimensions $50 \times 50 \times 50 \text{mm}^3$ were provided. Therefore, the model calibration is performed on the rubber component.

3.2 Calibration of $50 \times 50 \times 50 \text{mm}^3$ model

The first step of the work was to calibrate the model on the polymeric material obtained in the laboratory. The real geometry is numerically modelled by means of the Ansys Workbench (WB) simulation platform, simulating a compression behaviour for small displacements. This operation allows to have a traced comparison with the experimental data considering in the first instance only the purely elastic behaviour of the polymer.

In the previous work [4], compression tests were carried out on the part in the laboratory. The experimental data collected on that occasion are exploited to calibrate the model. With the experimental data in possession, we want to create a mathematical model that allows to implement the mechanical characteristics within WB. The goal of this work is to obtain a reliable mathematical model that allows to extract correct results regardless of the geometry one wants to analyse.

The polymeric materials considered for the study are two types of rubbers that differ from each other by their chemical compositions. They have different amount of “Extender” present within the polymer, Tab.3.1.

Sample name	Polymer hardness	Sample size [mm ³]	Mixture ratio [%]			Sample weight [g]
			Polyol	Isocyanate	Extender	
A30	Shore A30	50x50x50	1	1	4.5	132
A60	Shore A60				2.0	135

TABLE 3.1: Polymer specification

The first phase of the calibration process consists in the design of the three-dimensional model using a 3D-CAD software (Solidworks). The calibration is carried out in two steps, the first one aims to reproduce the elastic properties of the polymer evaluated in the laboratory. The next step allows the implementation of the non-linear effects that occur in rubbers subjected to large displacements in the compression test, also resulting from the experimental tests, Fig.3.1.

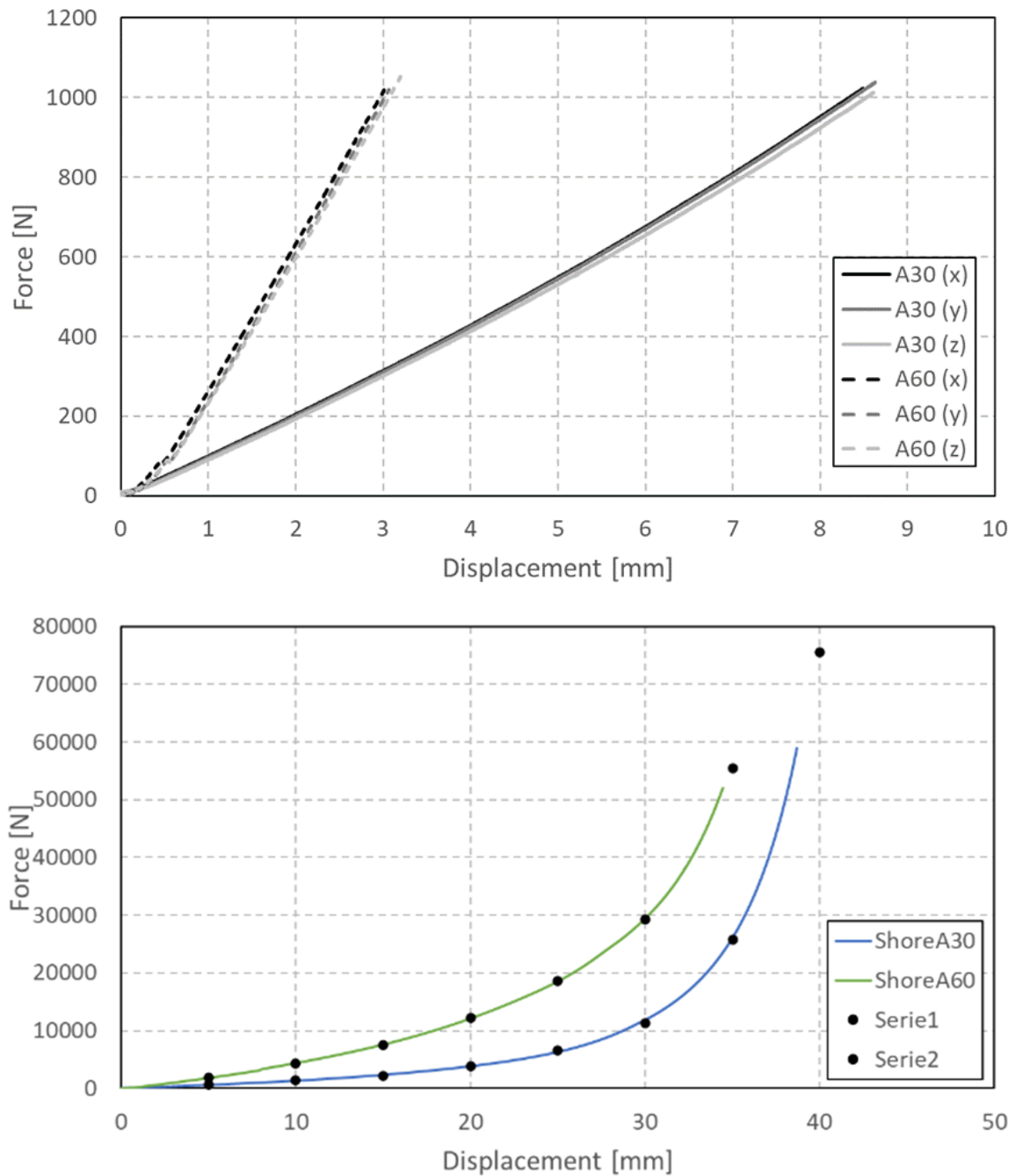


FIGURE 3.1: Polymers characteristic curves

Aiming to reproduce the elastic properties of the polymers, the experimental Force-vs-Displacement characteristic curves are analysed. The region of the curve at small displacement is considered, where it can be assumed that the behaviour of the polymer follows a purely elastic trend. This assumption is verified when the slopes of the lines are almost constant, as in Fig.3.1. This assumption has been made for both the

hardness of the polymers used in the study, namely on Shore 30 and Shore 60.

From the analysis of the experimental data, all the information necessary to be included in the simulation software is obtained. The chord modulus is obtained from the trend line, whereas the maximum displacement and maximum load are read on the F- δ curve.

To evaluate the elastic modulus analytically from the experimental data, the trend line of the initial linear portion of the load extension curve was plotted, Fig.3.2. By dividing the difference in stress corresponding to any segment on this straight line by the corresponding difference in deformation, it is possible to calculate its stiffness, Eq.3.1 The correlation factor R^2 is also calculated.

$$E_f = \frac{\sigma_{f2} - \sigma_{f1}}{\epsilon_{f2} - \epsilon_{f1}} \quad (3.1)$$

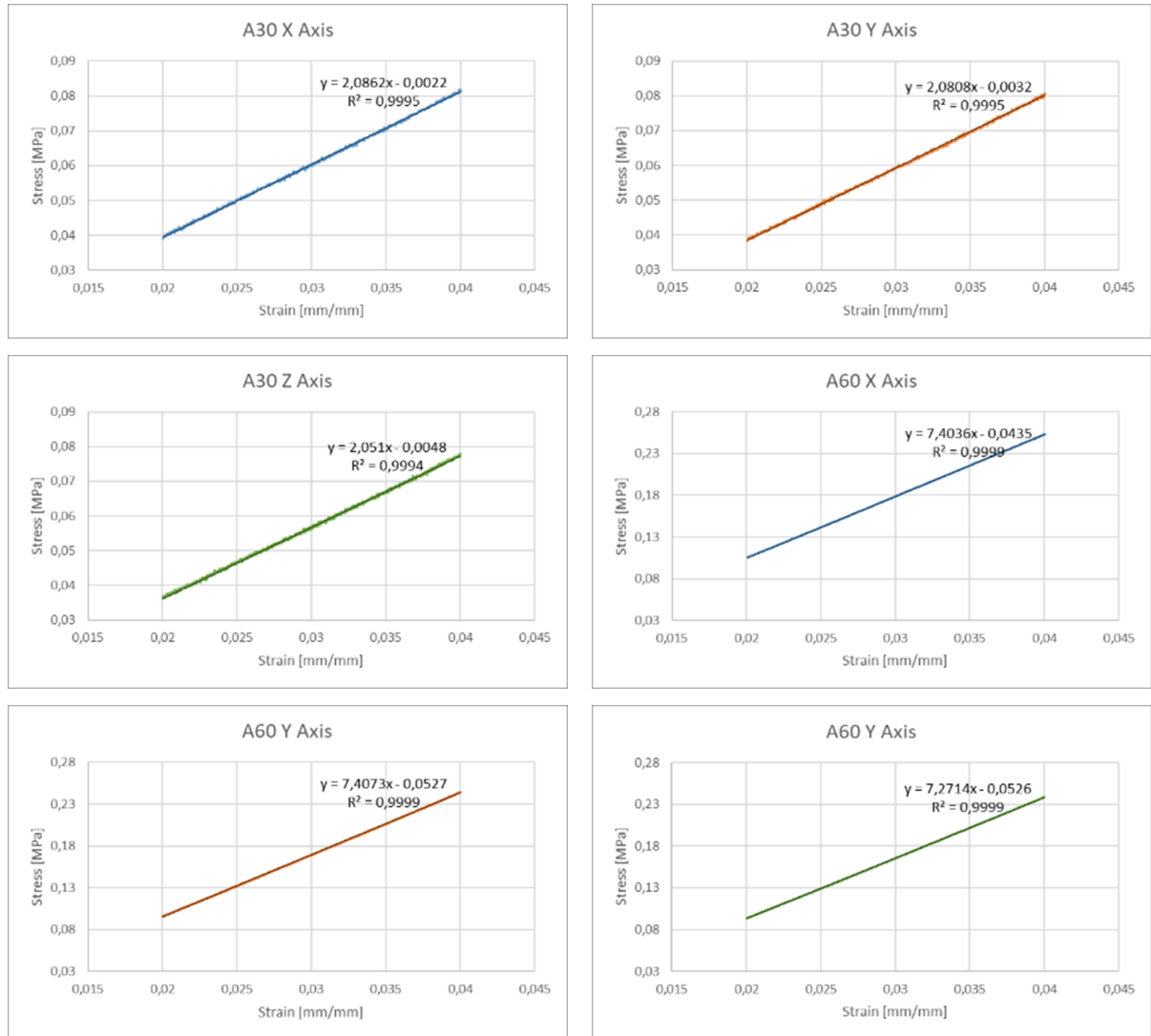


FIGURE 3.2: Tendency line of polymers

Data were computed on the three Cartesian loading directions, and subsequently averaged, Tab.3.2. This operation is correct as the material taken into consideration is isotropic, as can be deduced from the previous graph.

		Max Load	Max Stress	Max Strain	Chord Modulus
		[N]	[MPa]	[-]	[MPa]
A30	X-axis	1022.6	0.41	0.1698	2.115
	Y-axis	1038.2	0.42	0.1725	2.126
	Z-axis	1012.6	0.41	0.1722	2.070
Average		1024.5	0.41	0.1715	2.104
Std Deviation		10.6	0.004	0.0012	0.024
A60	X-axis	1019.2	0.41	0.0602	7.377
	Y-axis	1020.7	0.41	0.0614	7.424
	Z-axis	1052.1	0.42	0.0640	7.249
Average		1030.6	0.41	0.0618	7.350
Std Deviation		15.2	0.006	0.0016	0.074

TABLE 3.2: Loading condition and chord modulus

After the design of the geometry, it is saved with the .IGS extension and subsequently imported into Ansys. Now it is possible to set the properties of the materials to be analysed in the appropriate section of the software.

At this point the simulations are carried out for the two polymers hardness taken into consideration, namely Shore A30 and Shore A60. The polymer's cube has a dimension of 50x50x50mm³. A compression test is simulated in Ansys WB by setting the boundary conditions. It is necessary to apply some boundary conditions to the model in order to faithfully reproduce the real test. Boundary conditions are generally represented by external supports, loads or displacements. Defining limitations is a necessary condition for performing a correct static analysis. A fixed constraint is

applied to the model to the lower face of the polymer's cube, which defines a fully constrained state to simulate the locking on the machine for the compression test to avoid the sliding phenomenon that can occur with the machine platform. At the upper face is applied a downward shift in the direction of the Y-axis. The displacement along the Y axis is varied during the simulations.

3.2.1 A30

The first analysis is carried out for a displacement along the vertical (Y-axis) of 8mm in order to be sure to fall within the linear part of the deformation. The simulation results are shown below, Fig.3.3.

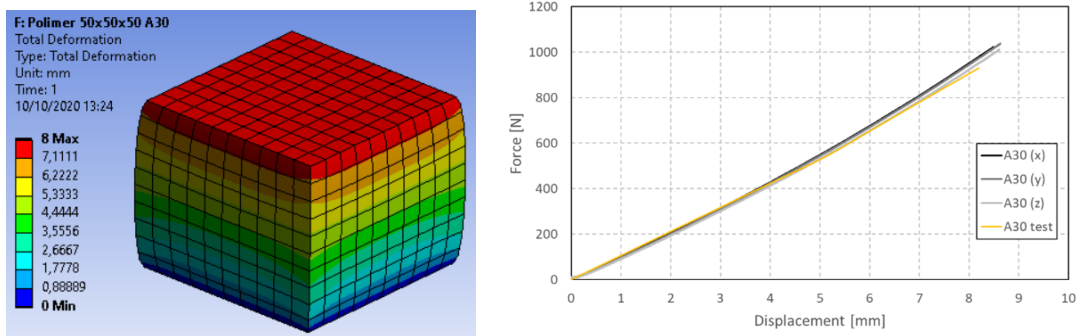


FIGURE 3.3: A30 Simulation condition and F- δ curve $y=-8$ mm

From the previous graphs, Fig.3.3 we can see how the simulated behaviour, A30test, perfectly fits the real trend obtained in the laboratory. From the analysis of the curve we can also conclude that the component has an isotropic behaviour along the three principal directions.

Fig.3.4 shows the simulation results related to stress. We can observe how the most stressed points are located near the outer bases and this confirms the reliability of the test.

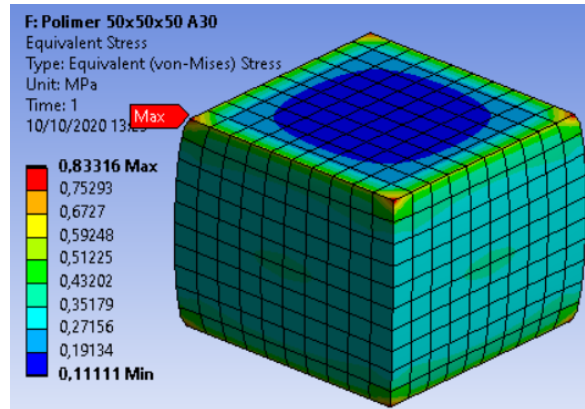


FIGURE 3.4: Stress condition

Subsequent step consists in a compression with a displacement in the (-j) Y direction of 35mm. This was performed in order to analyse the real behaviour of the material taking into account the densification that occurs in the polymer. The simulation results are shown below in Fig.3.5.

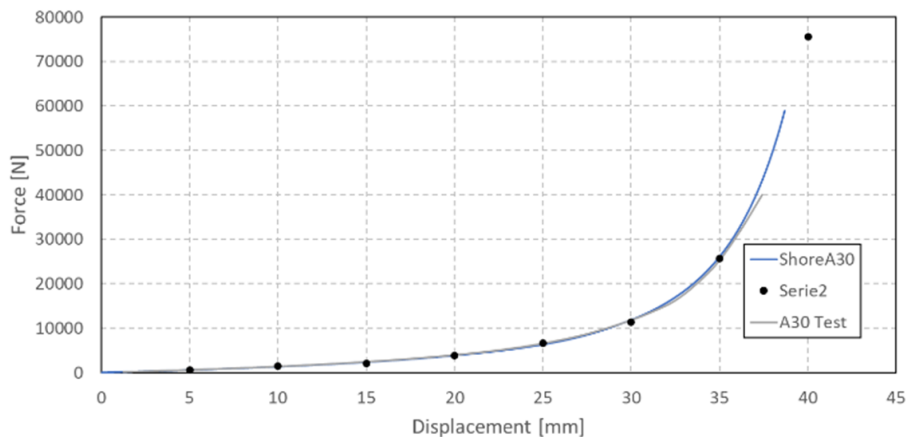


FIGURE 3.5: A30 Simulation condition and F- δ curve $y=-35$ mm

In the plot, Fig.3.5, it can be seen how the simulated behaviour perfectly correspond to the real trend measured in the laboratory.

From the previous graph some conclusions can be drawn regarding the behaviour that occurs in the polymeric material. Three areas of interest can be highlighted. The first occurs for displacements up to 8mm where the polymer shows a perfectly elastic behaviour where the load increases linearly. A second central area where there is a plateau zone, and the load remains at an almost constant value as the displacement

varies. Finally, in the rightmost portion of the graph the polymer densification occurs and as a consequence the force increases exponentially reaching high values for small delta of displacement.

Fig.3.6 shows the simulation results related to stress. The point where the stress reaches the maximum value is highlighted. We can see how, even in this case, the most solicited points are located near the base, and this confirms the reliability of the test.

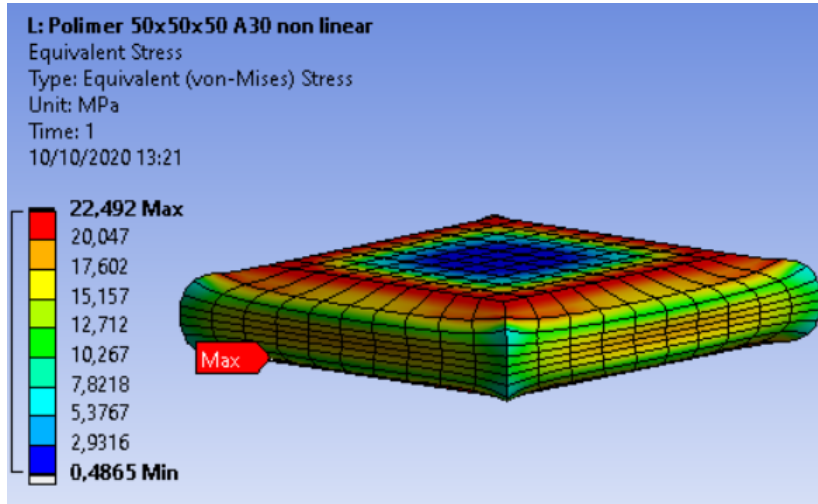


FIGURE 3.6: A30 Stress condition

Below, in Tab., the results obtained from the simulation are reported. To calculate the energy absorbed, Eq.3.2, by the component, the area under the Force-Displacement curve was calculated using the Matlab calculation program.

$$E_s = \frac{\int F dx}{V} \quad (3.2)$$

Where F is the load and V is the volume of the sample.

Displacement [mm]	Force [N]	Max Stress [MPa]	Max Strain [-]	Max Energy [J]
Y= - 8 Sim	951.58	0.7855	0.374	3.73
Y= - 8 Exp	1016.00	0.6752	0.374	4.32
Y= - 35 Sim	22840.00	9.14	0.709	251.70
Y= - 35 Exp	26105.20	10.44	0.709	267.99

TABLE 3.3: A30 results

3.2.2 A60

The simulation of the compression test is performed in a similar way to that performed for rubber of Shore A30 hardness. The results for Shore A60 hardness polymer are summarized below, Fig.3.7.

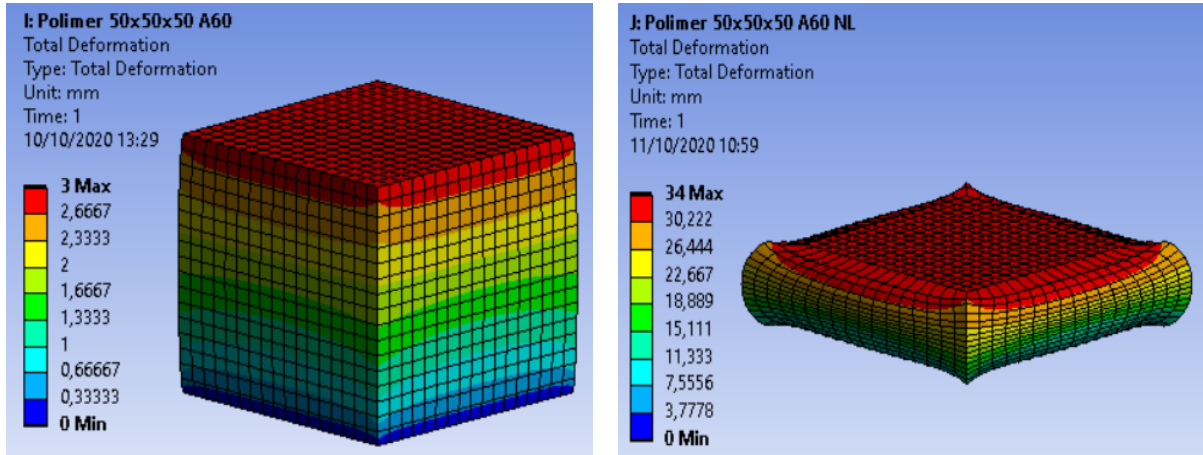


FIGURE 3.7: A60 Simulation condition and $F-\delta$

Fig.3.7 shows the deformation that occurs in the polymer considering two different displacements in the negative direction of the Y axis. On the left panel a displacement of -3mm is considered, in order to be sure of obtaining an elastic response of the material. On the right panel a displacement of -35mm is used, to take into account the densification of the rubber.

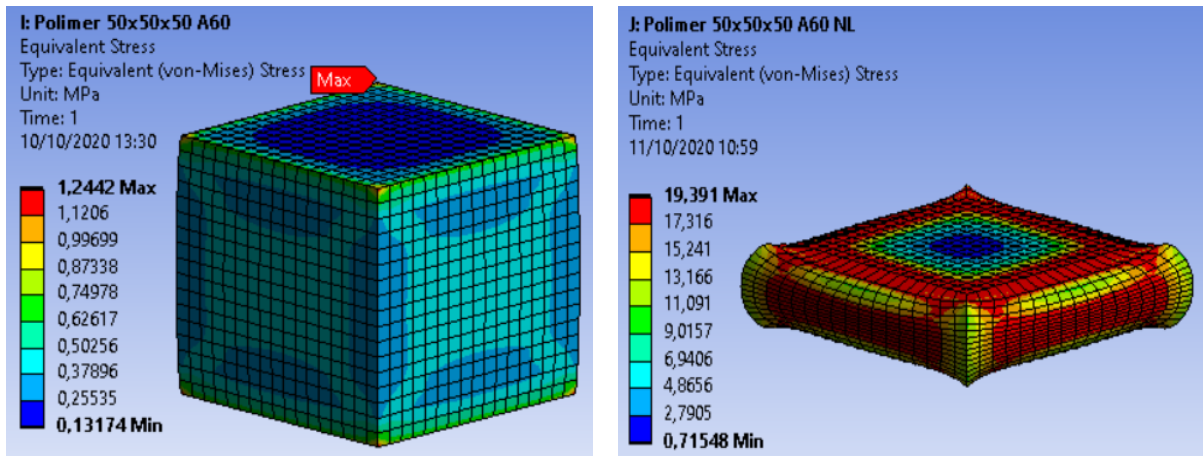


FIGURE 3.8: A60 Simulation condition and $\sigma-\epsilon$

The simulation results related to the stress are reported in Fig.3.8. The point where the stress reaches the maximum value is highlighted. We can see how, even in this case, the most stressed points are located near the outer bases and this confirms again the reliability of the tests.

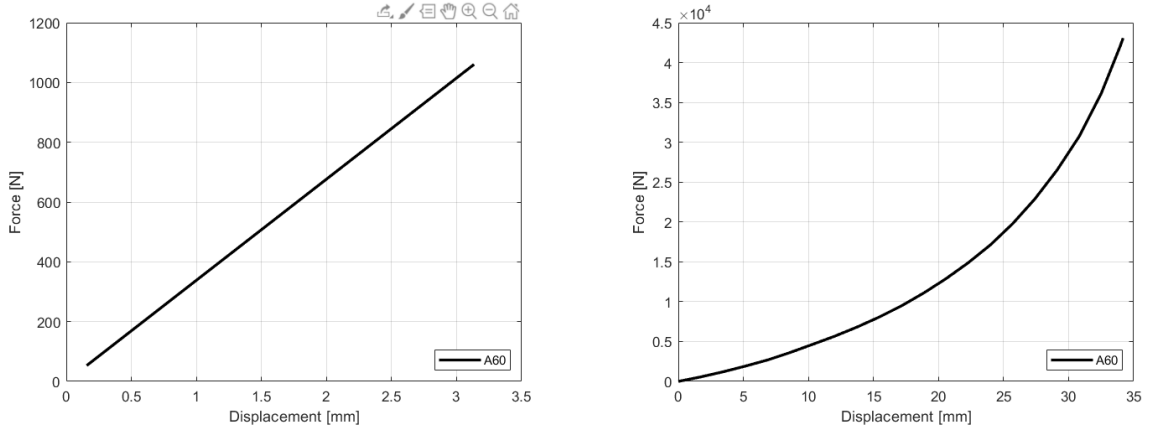


FIGURE 3.9: A60 F- δ curves

Fig.3.9 shows the Force-Displacement curves obtained from the simulations. On the left we can observe a linear trend of the force with respect to the displacement for compressions up to 3mm. Up to this point the rubber behaves like a perfectly elastic material. In the plot on the right instead, we can see how for increasing displacements the polymer response is different and we can denote two characteristic zones. The first one in which, as highlighted above, the behaviour is linear and second zone in which the force has an exponential grow where densification of the rubber occurs.

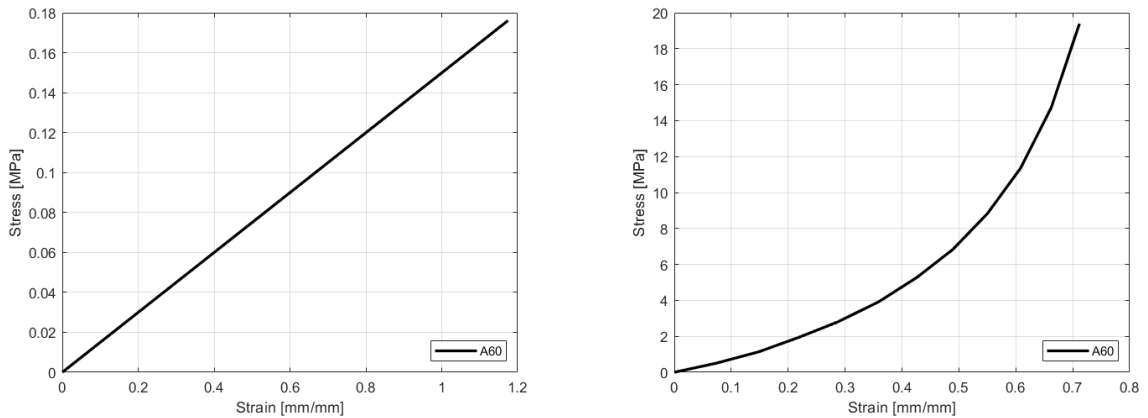


FIGURE 3.10: A60 σ - ϵ curves

In Fig.3.10, the Stress-Strain (σ - ϵ) curve obtained from the simulations are shown. The considerations made previously are also valid considering the σ - ϵ diagram.

In the plot on the left is shown how the polymer responds elastically to a compression of few millimetres, with a linear increase in stress as a function of the deformation. In the curve represented on the right it can be seen that for increasing displacements the response of the polymer is different and we can notice two characteristic zones. The first one in which, as highlighted above, the behaviour is linear and second zone in which the force has an exponential grow where densification of the rubber occurs.

By comparing the simulated results with the experimental ones, we can conclude that the simulation satisfyingly reflects the real trend being the two curves perfectly superimpose, Fig.3.11.

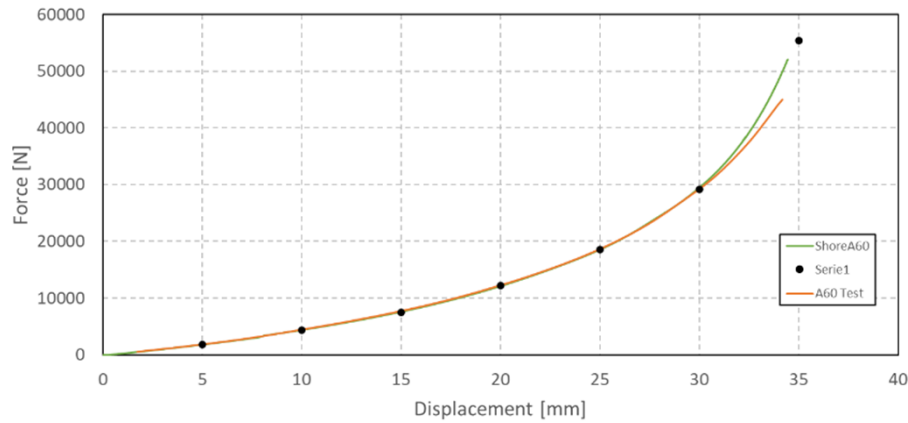


FIGURE 3.11: A60 Comparison experimental vs simulation curves

Below, in Tab.3.4, the results obtained from the simulation are reported. To calculate the energy absorbed by the component, the area under the Force-Displacement curve was calculated using the Matlab calculation program.

Displacement [mm]	Force [N]	Max Stress [MPa]	Max Strain [-]	Max Energy [J]
Y= - 3 Sim	1130.5	0.424	0.063	1.66
Y= - 3 Exp	1047.5	0.419	0.063	1.45
Y= - 34 Sim	45000.0	19.390	0.712	445.80
Y= - 34 Exp	48500.0	19.410	0.680	449.87

TABLE 3.4: A30 results

After having carried out the calibration of the part by verifying that the simulation results match the experimental results, the model is ready.

3.3 Mesh Sensitivity

This subsection analyses how the size of the tetrahedral elements characterizing the mesh can affect the simulation results.

The model of the polymeric component with Shore A30 hardness of $5 \times 5 \times 10 \text{mm}^3$ is taken as a sample. The sensitivity analysis is carried out by repeating the same simulation of compression test changing the size of the mesh from fine to coarse each time. Using an education version of Ansys Workbench software, the minimum size of triangles that constitute the mesh that can be applied is 0.5 mm. Therefore, this results in the lower limit below which we cannot refine the mesh.

Tab.3.5 summarizes the simulations performed and the corresponding Force-Displacement curve, Fig.3.12.

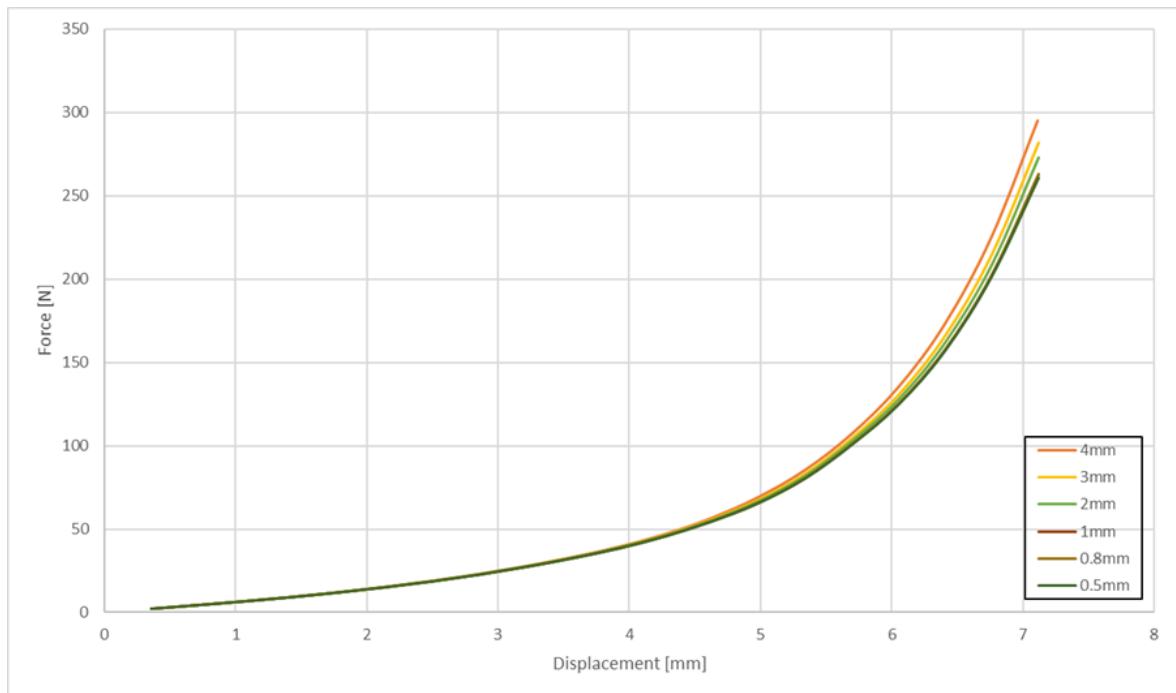


FIGURE 3.12: F- δ curves as a function of mesh size

Mesh size [mm]	Max Force [N]	Node	Element
0.5	260.79	9581	2000
0.8	262.96	3296	637
1	263.18	1416	250
2	272.80	320	45
3	281.72	141	16
4	295.40	111	12

TABLE 3.5: Mesh sensitivity results

From the data reported above some conclusions can be drawn:

- as the mesh size increases, the number of nodes and consequently that of the elements making up the component are reduced;
- the maximum value of the force increases as the discretization becomes coarser;
- the maximum percentage error calculated by comparing the two extreme conditions is 13.3%;
- the trend of the F - δ diagram shows how the mesh size is not an influential parameter in the simulation solution;
- the use of a fine mesh shows a more conservative solution to the problem.

Chapter 4

Static Analysis

The goal of the static analysis is to analyse a mathematical model implementing the mechanical characteristics of the component analysed in the laboratory. This model should allow to obtain correct results regardless of the geometry one wants to analyse, and it should be possible to implement it within a simulation software.

4.1 Polymer

The aim of this study is to isolate a portion of the polymer to make stress and energy considerations. The section of the polymer to be analysed is modelled using the SW 3D software.

Since we want to isolate only a single cross-section of the polymer, which would be of difficult feasibility from a practical point of view, we rely solely on the simulation of the Ansys software. It is possible to compare the results even in macro-scale on realizable components. The polymer section simulated has dimensions of $5 \times 5 \times 10 \text{mm}^3$ and is able to include one reticular cell inside.

The types of rubbers analysed have two different hardness: one Shore A30, the second one Shore A60. They take on different hardness by the different weight ratio of “Extender” present in the mixture of components. Tab.4.1 shows the experimental data relating to the polymers. The data were obtained from a section of dimensions $50 \times 50 \times 50 \text{mm}^3$ on which experimental tests were performed.

Sample name	Polymer hardness	Sample size [mm ³]	Mixture ratio [%]		
			Polyol	Isocyanate	Extender
A30	Shore A30	50x50x50	1	1	4.5
A60	Shore A60				2.0

TABLE 4.1: Polymer specification

Once the 3D section has been performed, the file is exported in the .IGS format. At this point the geometry is imported into the Ansys Workbench environment and the simulation of the compression test is performed. The Ansys Mechanical extension allows the automatic generation of the mesh, Fig.4.1, with predefined values of unit cell sizes. Otherwise, the designer can also assign a precise unit cell size value, managing various discretization parameters of the solid state model, but would require a great deal of experience from the user. The acrlongfe mesh can significantly influence the quality of the solution obtained in the cases of parts of complex spatial configuration.

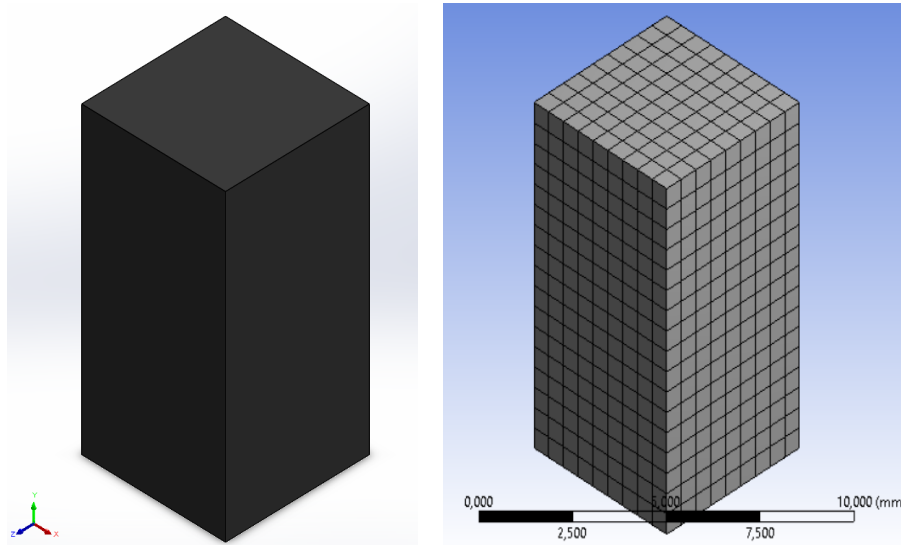


FIGURE 4.1: Polymer mesh generation

For the compression test it is necessary to apply some boundary conditions to the model in order to faithfully reproduce the real test. Boundary conditions are generally represented by external supports and loads. Defining limitations is a necessary condition for performing a correct static analysis. A fixed constraint is applied to the model on the lower face of the polymer. This defines a fully constrained state to simulate the

locking on the machine for the compression test and avoid sliding phenomenon that can be created with the machine platform. Meanwhile on the upper face a displacement in the negative direction of the Y axis is applied. The shift along the Y axis is varied during simulations.

The last step of the static analysis is the definition of the solutions on which the software will perform the calculations through algebraic equations. From the compression test we are interested in investigating the equivalent stresses and deformations according to the Von Mises criterion and the resulting force. They are set by simply clicking with the right mouse button on the item "Solution", see subsection 4.2.1. After that, the software will automatically solve the equations and plot the graphs corresponding to the solutions found.

4.1.1 A30

Two analyses are carried out with relative different displacements. The first is carried out for a negative shift along Y-axis of 0.6mm in order to be sure to fall within the linear part of the deformation. Then a compression test is simulated with a displacement in the (-j) Y-axis of 7mm in order to analyse the real behaviour of the material taking into account the densification that occurs in the polymer. The results of the two simulations are shown below, Fig.4.2.

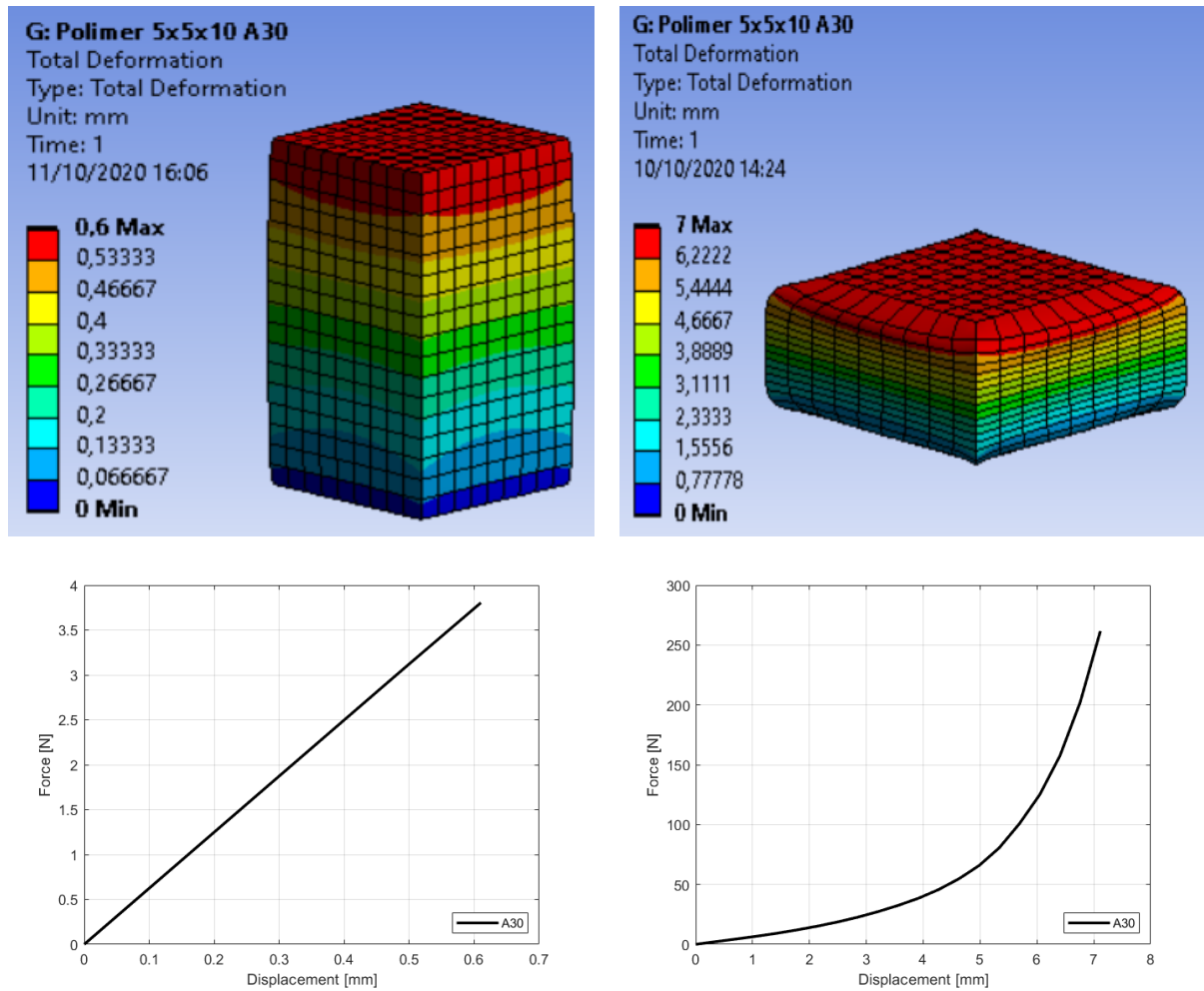


FIGURE 4.2: A30 simulation results

The results obtained from the simulation are shown below in Tab.4.2.

Displacement [mm]	Force [N]	Max Stress [MPa]	Max Strain [-]	Max Energy [J]
Y= - 0.6	3.804	0.238	0.099	0.0012
Y= - 7	261.640	19.862	0.802	0.4098

TABLE 4.2: A30 results

In the plot on the left it is shown how the polymer responds elastically to a compression of a few millimetres with a linear increase in force as a function of the displacement. From the curve represented on the right it is clear that for increasing displacements the response of the polymer is different and we denote three characteristic zones. The first

one in which, as just highlighted, the behaviour is linear, a second one in which the load gradually increases as the displacement varies. The third zone the force undergoes an exponential increase and densification of the rubber occurs.

To calculate the energy absorbed by the component, the area under the F - δ curve was calculated using the Matlab software.

4.1.2 A60

Using the polymer with Shore A60 hardness, the same procedures were adopted and two analyses were carried out with relative different displacements. The first one is carried out for a negative displacement along Y-axis of 0.6mm in order to be sure to fall within the linear part of the deformation. Then a compression test is simulated with a shift in the (-j) Y direction of 4mm in order to analyse the real behaviour of the material taking into account the densification that occurs in the polymer. The results of the two simulations are shown below, Fig.4.3.

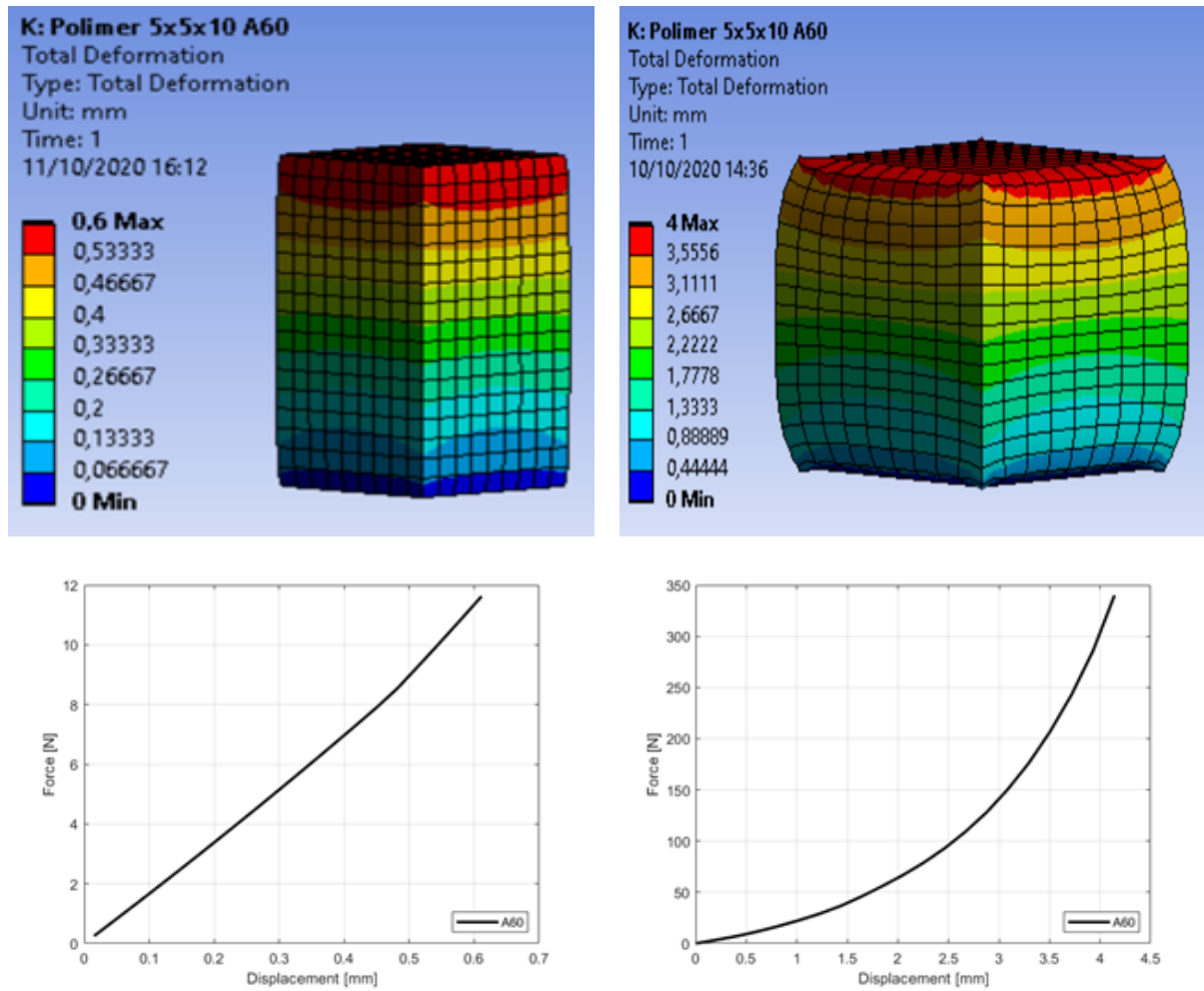


FIGURE 4.3: A60 simulation results

The results obtained from the simulation are shown below in Tab.4.3.

Displacement [mm]	Force [N]	Max Stress [MPa]	Max Strain [-]	Max Energy [J]
Y= - 0.6	11.62	0.78	0.107	0.0033
Y= - 4	340.01	13.39	0.692	0.4061

TABLE 4.3: A60 results

In Fig.4.3, the F- δ diagram obtained from the previous simulations are shown. In the plot on the left it is shown how the polymer responds elastically to a compression of a few millimetres with a linear increase in force as a function of the displacement, while in the curve represented on the right it is clear that for increasing displacements the

response of the polymer is different. We can denote two characteristic zones. The first one in which, as just highlighted, the behaviour is linear, a second one in which the force has an exponential grow where densification of the rubber occurs. To calculate the energy absorbed by the component, the area under the F- δ curve was calculated using the Matlab software.

4.1.3 F- δ curves comparison

Below a comparison of the Force-Displacement curves of the approximated section of the polymer of $5 \times 5 \times 10 \text{mm}^3$ is shown. Both hardness Shore A30 and Shore A60 are reported.

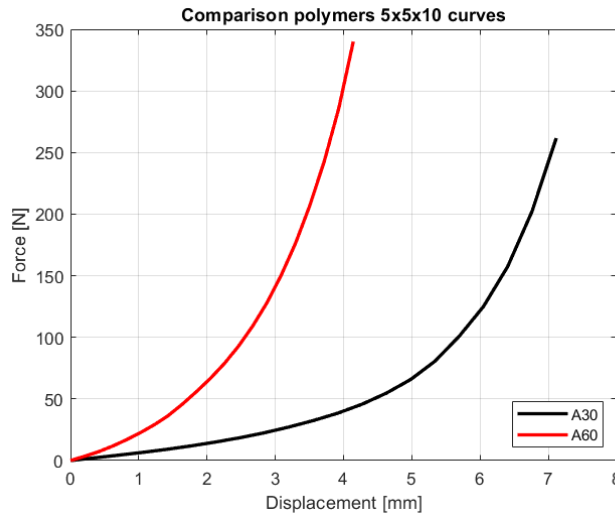


FIGURE 4.4: Polymers F- δ curves comparison

	Displacement [mm]	Max Force [N]	Max Energy [J]
A30	-7	261.64	0.4098
A60	-4	340.01	0.4061

TABLE 4.4: Comparison F- δ results

Some conclusions can be drawn from Fig.4.4 and Tab.4.4. The first one is how a different weight percentage of 'Extender' inside the rubber changes the mechanical properties of the polymer. The A60 polymer results more rigid than the one with

Shore A30 hardness. The elastic modulus is also different, equal to 7.34MPa for the A60 polymer and 2.14MPa for the A30 rubber.

A comparison of the results concerning the energy absorbed can be seen in Tab.4.4. The energy absorbed by the two components is of the same order of magnitude, but the value of the elongation differs in the two cases. It is therefore concluded that polymer A60 absorbs a greater amount of energy than Shore A30 rubber as it assumes the same value of absorbed energy but for a displacement that is half of the previous one.

4.2 Lattice structures

The purpose of the work is to isolate a single reticular unit cell present within a component. A static linear Finite Element analysis is carried out.

The main goal of carrying out a static strength analysis (in this case of compressive strength) is to evaluate a state of stress induced in the structure by forces that remain constant over time. The evaluation of a state of stress allows to characterize the material used and to verify that it can withstand the conditions in use.

The Compression Test was performed on two types of lattice structures (BCC and BCCZ) and the corresponding load and displacement curve were recorded.

Through the FEM analysis it is possible to calculate a stress state of the real three-dimensional model designed in the CAD environment. The reference software used for Finite Element simulation is Ansys Workbench.

Static analysis is performed in several steps. The first step is to create a 3D solid model of the structure that one wants to analyse. It is possible both to create the geometry through WB or through other CAD software and subsequently import it into the Ansys environment. The latter solution was preferred, and the reference software used is Solidworks.

The metal reticular structures to be created are based on the shapes of Body Center Cubic lattice cells (BCC), Fig.4.5a, and Body Center Cubic lattice cells reinforced along the Z-axis (BCCZ), Fig.4.5b.

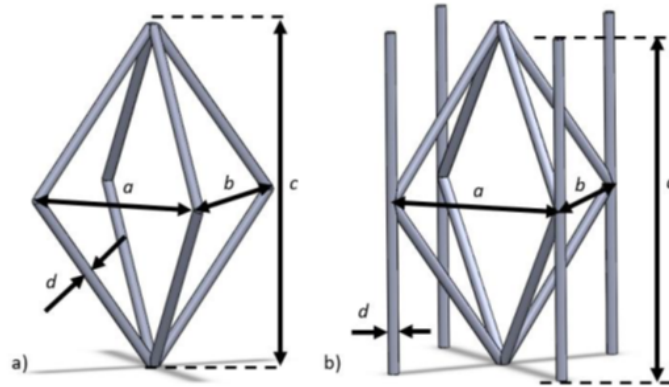


FIGURE 4.5: BCC (a) and BCCZ (b) lattice structures [4]

The properties of the reticular structures are shown in the following Tab.4.5. For each type of lattice, three different thicknesses of the uprights are considered, indicated with the parameter d in the previous figure, which allow to obtain three different values of the relative nominal density of the lattice.

Sample name	Cell dimension [mm]			
	a	b	c	d
BCC-1				0.55
BCC-2	5	5	10	0.65
BCC-3				0.75
BCCZ-1				0.40
BCCZ-2	5	5	10	0.48
BCCZ-3				0.56

TABLE 4.5: Lattice dimensions

For the single cell, the unit sizes are $5 \times 5 \times 10 \text{mm}^3$ and the structural diameter assumes three different values for each type of cell analysed. The material used is 316L steel produced by additive manufacturing with a density of $7.89 \frac{\text{g}}{\text{cm}^3}$.

Beside having two different lattice cell geometries, the study aims to evaluate how the mechanical behaviour and the energy absorbed by the structures during compression changes as the unit diameter of the cell increases.

4.2.1 Design

The first step of this process consists in designing a three-dimensional model using 3D software, in this specific case Solidworks, which must be calibrated. The calibration is carried out in two passages, the first one aims to reproduce the elastic properties of the reticular cell taken into consideration. The next step allows the implementation of non-linear properties that occur for large displacements during compression.

To model this type of lattice structures we started by creating a 3D sketch and generating a sweep function. Subsequently, by the circular repetition command, it was possible to obtain the final geometry, Fig.4.6.

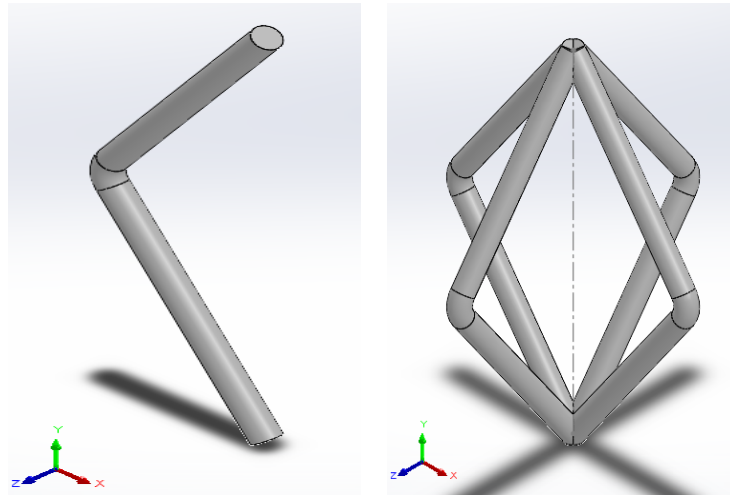


FIGURE 4.6: Sweep and circular repetition

After the modelling part, the 3D file must be converted into an extension readable by Ansys that allows to view the geometry in the simulation environment, in this case .IGS.

The second step is to import the newly created model file into Ansys. Therefore, it is important to define in advance the analysis system on which we want to simulate the behaviour of the structure, in this case a static analysis, to then import the geometry in question.

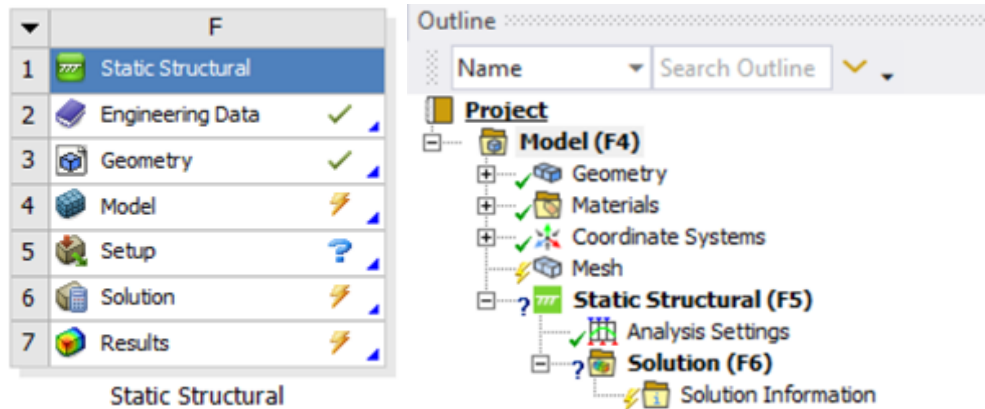


FIGURE 4.7: Definition of parameters for static analysis

Once the geometry has been imported, from the Ansys Mechanical extension it is possible to manage and define a series of parameters that allows to carry out the analysis, Fig.4.7.

The third step is the definition of the lattice material, which allows the software to perform the calculations for the simulation. The metal material chosen for the lattice structure is a stainless steel, 316L. The mechanical characteristics are shown below, Tab.4.6.

Property	Value
Young's modulus	180 ± 15 GPa
Yield stress	530 ± 20 MPa
Ultimate stress	660 ± 20 MPa
Elongation at break	± 5 %
Poisson's coefficient	0.3
Rockwell B hardness	90 ± 6 HRB

TABLE 4.6: Mechanical properties of 316L

One of the fundamental aspects to perform a FEM simulation is the creation of a FE mesh. The surface of the geometry under consideration is discretized with a series of elements of various shapes (triangles, rectangles, etc.), Fig.4.8. The Ansys Mechanical extension allows the automatic generation of the mesh with predefined values of unit cell sizes. Otherwise it is possible to assign a precise unit cell size value, managing

various discretization parameters of the solid state model, but this way is beyond the scope of this work and requires a great deal of experience from the user. The finite element mesh can significantly influence the quality of the solution obtained in the cases of parts of complex spatial configuration.

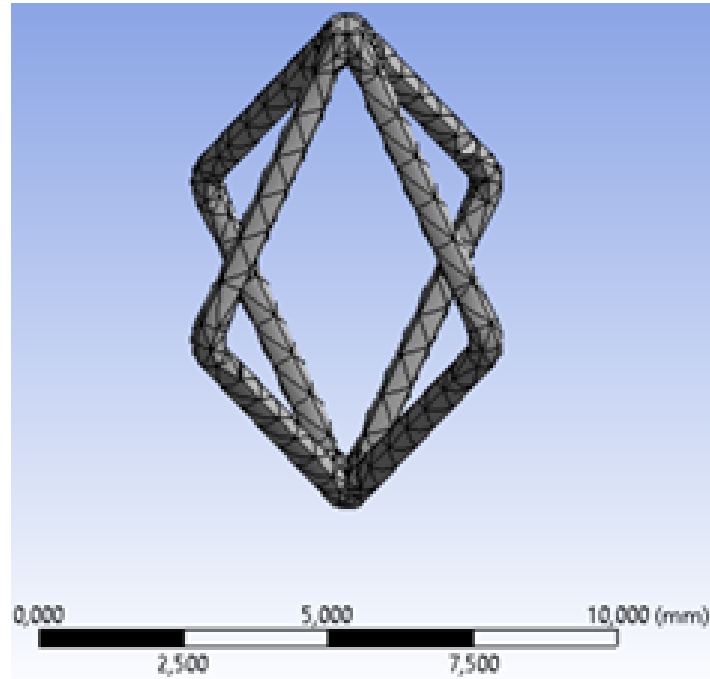


FIGURE 4.8: Lattice mesh generation

The analysis one wants to simulate is a compression test. It is necessary to apply some boundary conditions to the model in order to faithfully reproduce the real test. Boundary conditions are generally represented by external supports and loads. Defining limitations is a necessary condition for performing a correct static analysis. A fixed constraint is applied to the model to the lower face of the reticular structure, which defines a fully constrained state to simulate the locking on the machine for the compression test to avoid the sliding phenomenon that can occur with the machine platform. At the upper face is applied a downward shift in the direction of the Y-axis. The last step of the static analysis is the definition of the solutions on which the software will perform the calculations through algebraic equations.

4.2.2 BCC

4.2.2.1 BCC d=0.55mm

Two analyses are carried out with relative different displacements. The first one is carried out for a negative shift on Y-axis of 0.25mm in order to be sure to fall within the linear part of the deformation, considering a bilinear curve for 316L steel. Then a compression test is simulated with a displacement in the (-j) Y direction of 8mm in order to analyse the real behaviour of the material considering non-linear properties. The results of the two simulations are shown below, Fig.4.9.

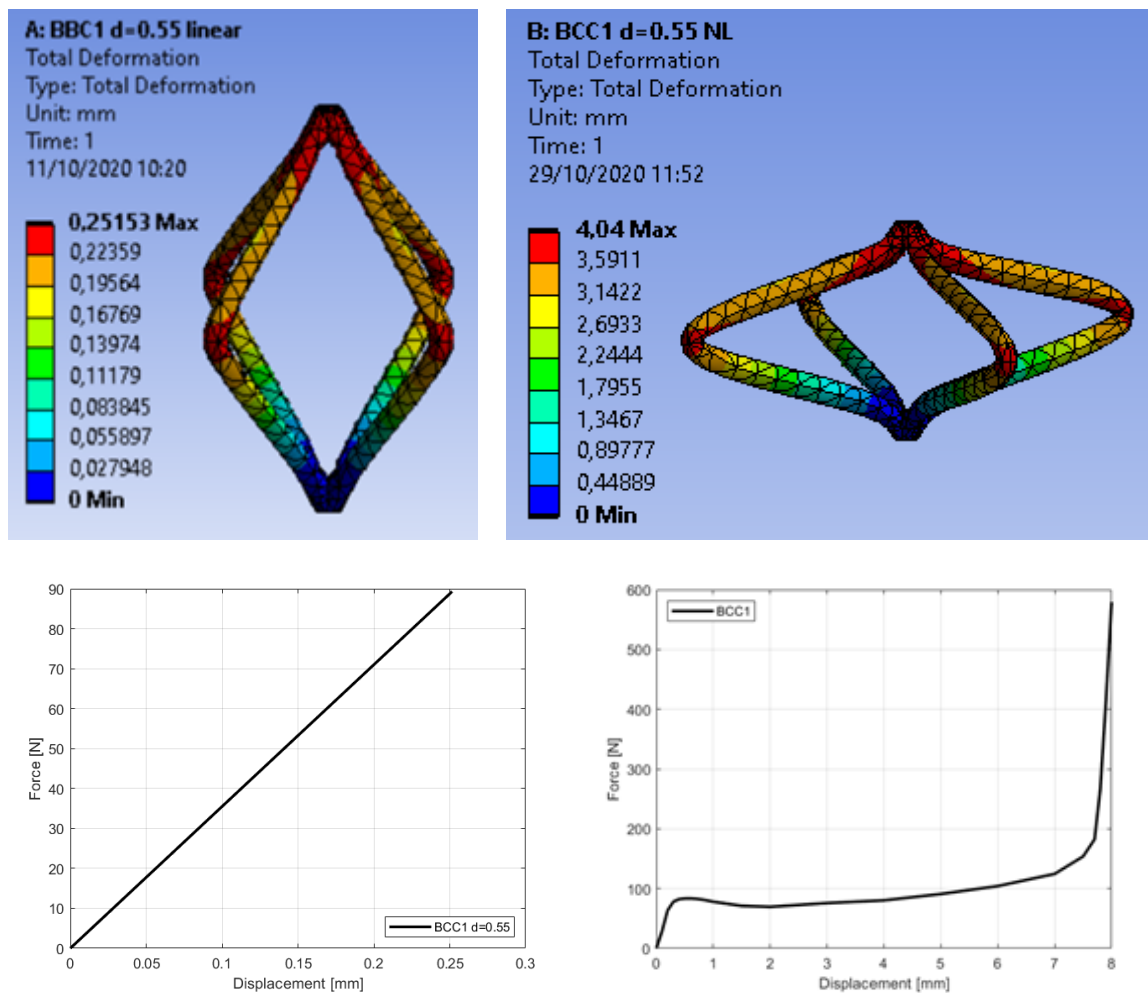


FIGURE 4.9: BCC1 compression simulation results

We can see how the load increases linearly with the displacement in the section in which the reticular cell assumes an elastic behaviour, enlargement on the left, while

once the yield of the material is reached the slope of the curve changes assuming a value of the tangent lower than 1.

The following figure shows the simulation results related to stress. We can see how the most stressed points are located near the internal equatorial vertices and this confirms the reliability of the test, Fig.4.10.

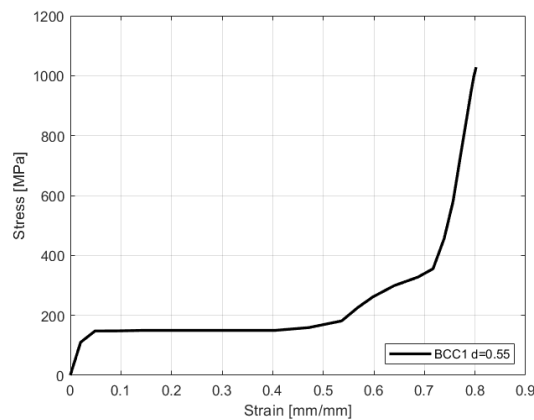
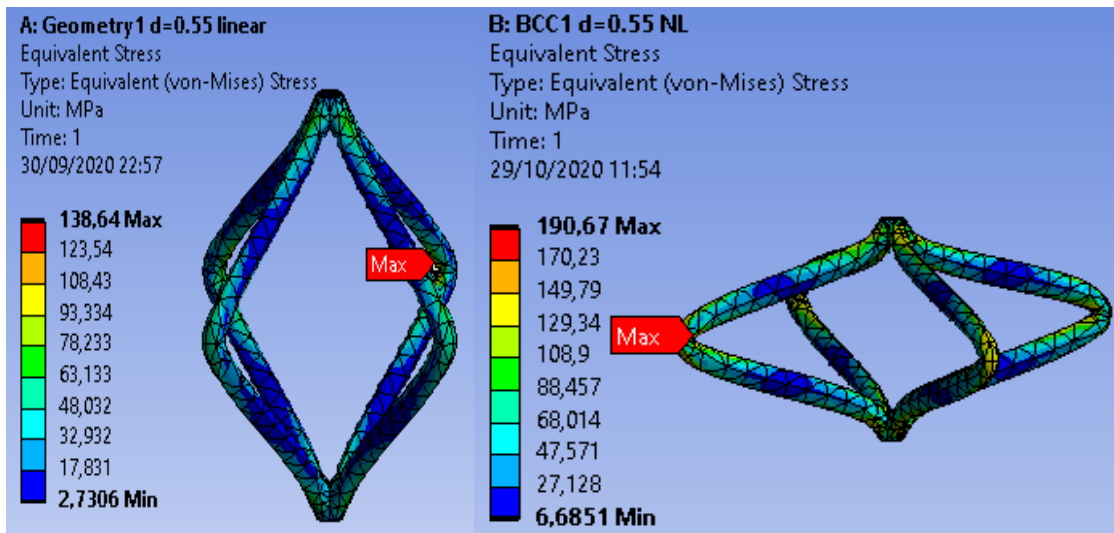


FIGURE 4.10: BCC1 stress simulation results

From the previous diagram we can see how the trend of the single cell is similar to that analysed in the laboratory, albeit for a component of different sizes, this allows us to conclude the reliability of the newly designed model. We can clearly distinguish three different areas on the σ - ϵ diagram. The first zone, on the left, occurs for small deformations displacements in which the material follows a perfectly elastic trend where the stress increases linearly. A second zone where a plateau is highlighted, therefore, the stress remains at an almost constant value as the deformation varies. Finally, in

the rightmost portion of the diagram there is a rapid and exponential increase in stress reaching high values for small delta of deformation, a clear indicator of the nucleation and propagation of cracks within the metal.

The results obtained from the simulation are reported below in Tab.4.7. To calculate the energy absorbed by the component, the area under the Force-Displacement curve was calculated using the Matlab software.

Displacement [mm]	Max Force [N]	Max Stress [MPa]	Max Strain [-]	Max Energy [J]
Y= - 0.25	89.29	138.64	0.054	0.011
Y= - 8	579.39	1028.30	0.802	0.800

TABLE 4.7: BCC1 results

4.2.2.2 BCC d=0.65mm

The simulation of the compression test is performed in a similar way to that performed for the reticular cell with diameter $d = 0.55\text{mm}$. The results for the unit cell diameter $d = 0.65\text{mm}$ are briefly reported below.

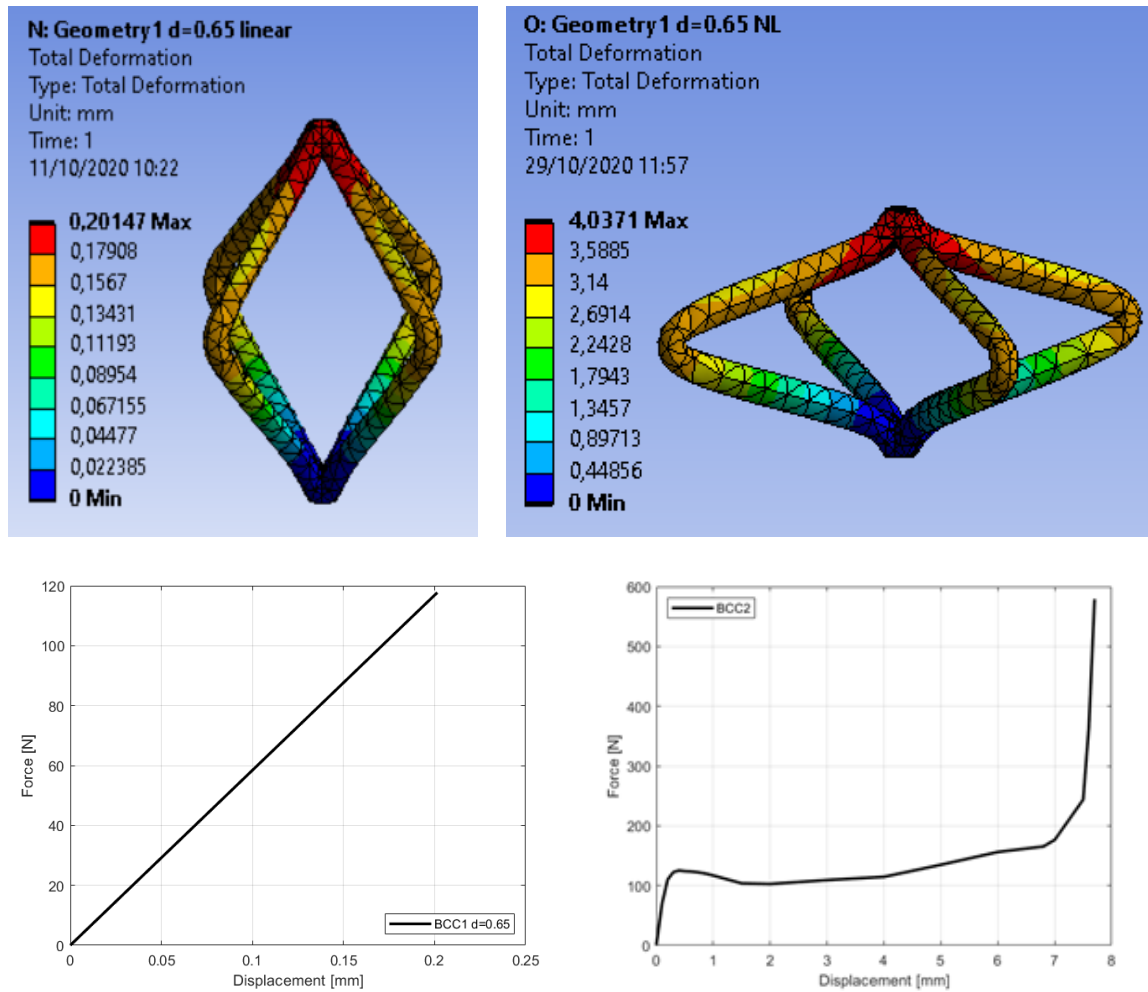


FIGURE 4.11: BBC2 compression simulation results

In Fig.4.11, the deformation that occurs in the lattice is shown. Considering two different displacements in the negative along Y-axis, to the left of -0.2mm in order to be sure to obtain an elastic response of the material, to right of -8mm to take into account the non-linear properties of the material that occurs for larger displacements. As in the previous case, the load increases linearly with the displacement in the section in which the reticular cell assumes an elastic behaviours, enlargement to the left, while once the yield of the material is reached, the slope of the curve changes assuming a value of the tangent less than 1.

The following figure shows the simulation results related to stress. We can see how the most stressed points are located near the internal equatorial vertices and this confirms the reliability of the test, Fig. 4.12.

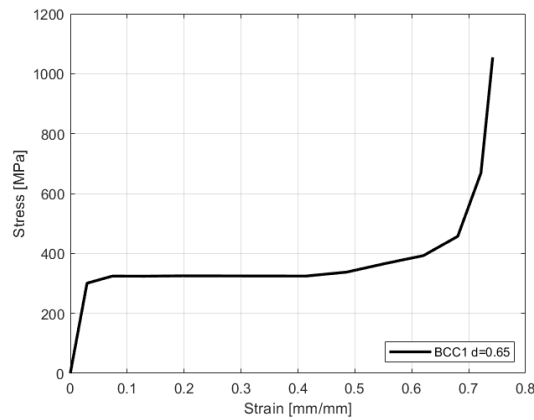
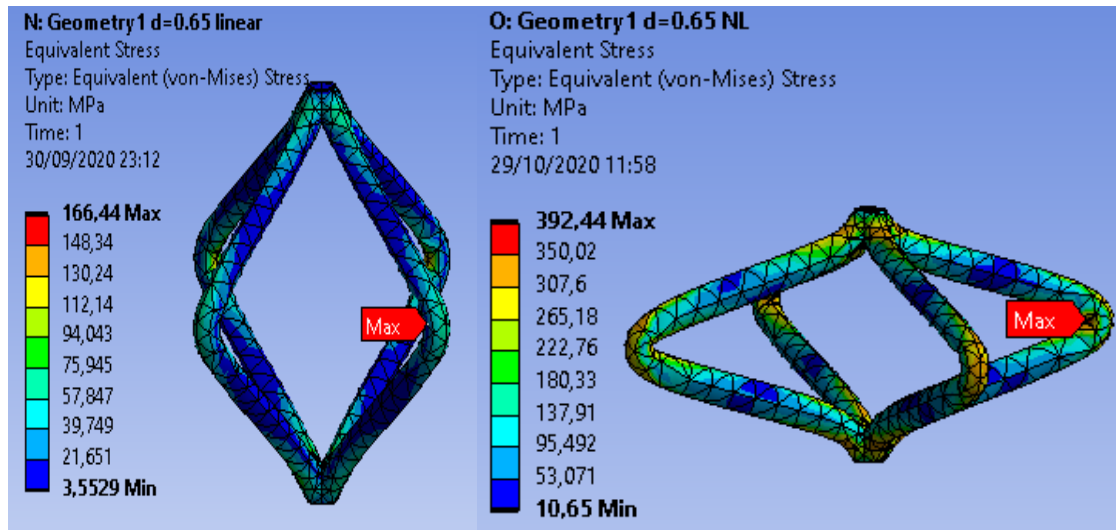


FIGURE 4.12: BBC2 stress simulation results

From the previous diagram we can see how the trend of the single cell is similar to that analysed in the laboratory, albeit for a component of different sizes, this allows us to conclude the reliability of the newly designed model. We can clearly distinguish three different areas on the σ - ϵ diagram. The first zone, on the left, occurs for small deformations displacements in which the material follows a perfectly elastic trend where the stress increases linearly. A second zone where a plateau zone is highlighted, therefore, the stress remains at an almost constant value as the deformation varies. Finally, in the rightmost portion of the diagram there is a rapid and exponential increase in stress reaching high values for small delta of deformation, a clear indicator of the nucleation and propagation of cracks within the metal.

The results obtained from the simulation are reported below in Tab.4.8. To calculate

the energy absorbed by the component, the area under the Force-Displacement curve was calculated using the Matlab software.

Displacement [mm]	Max Force [N]	Max Stress [MPa]	Max Strain [-]	Max Energy [J]
Y= - 0.2	117.71	166.44	0.066	0.012
Y= - 8	585.21	1177.78	0.7421	1.050

TABLE 4.8: BCC2 results

4.2.2.3 BCC d=0.75mm

Also in this case the simulation of the compression test is performed in the same way as the previous ones. The results for the unit cell diameter $d = 0.75\text{mm}$ are briefly reported below.

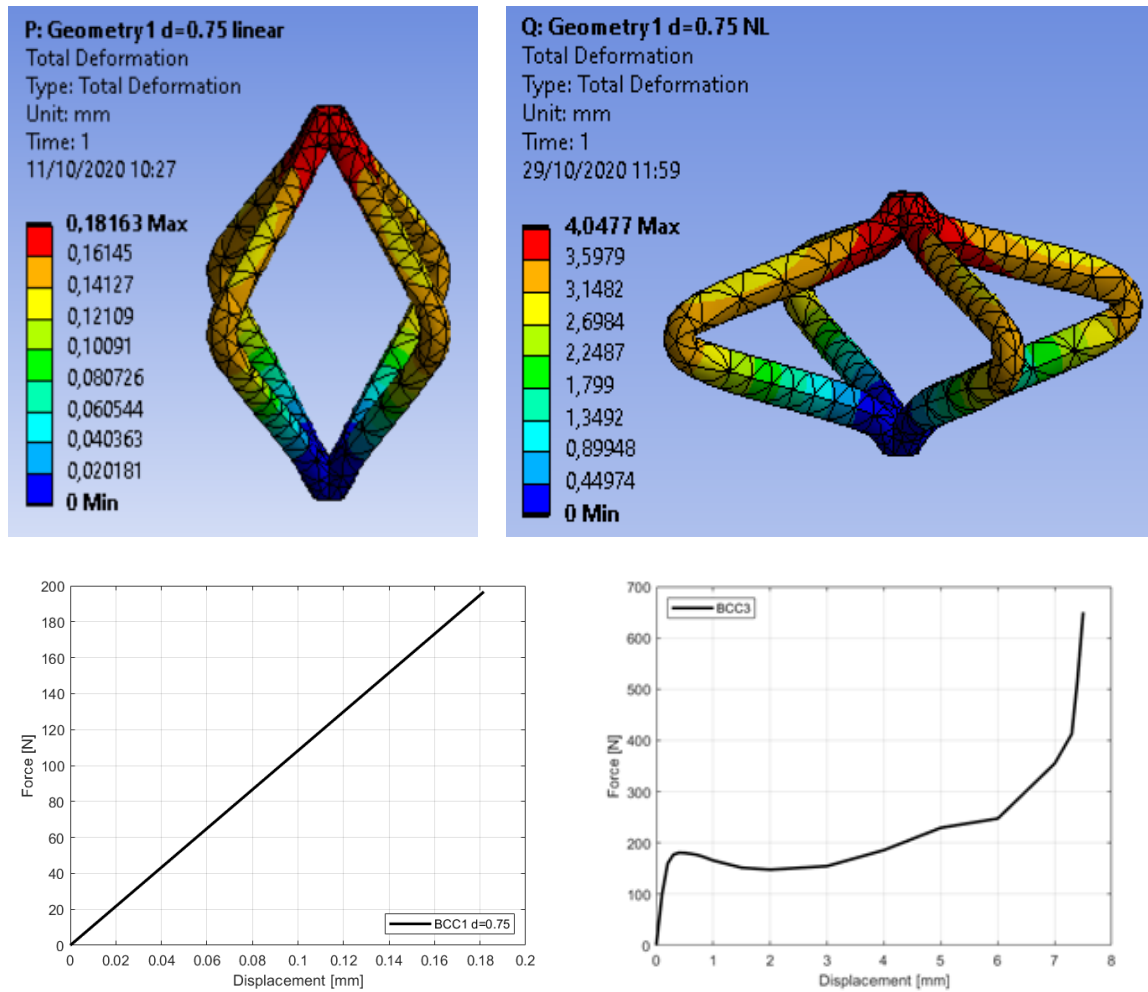


FIGURE 4.13: BBC3 compression simulation results

In the previous figure, Fig.4.13, above the deformation that occurs in the lattice is shown considering two different displacements in the negative direction of the Y axis, to the left of -0.18mm in order to be sure to obtain an elastic response of the material, to right of -8mm to take into account the non-linear properties of the material that occurs for larger displacements.

As in the previous cases, the load increases linearly with the displacement in the section in which the reticular cell assumes an elastic behaviour, enlargement to the left, while once the yield of the material is reached the slope of the curve changes taking on a value of the tangent lower than 1.

The following figure shows the simulation results related to stress. We can see how the most stressed points are located near the internal equatorial vertices and this confirms the reliability of the test, Fig.4.14.

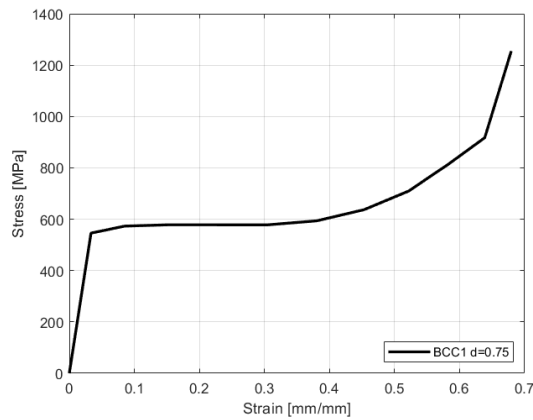
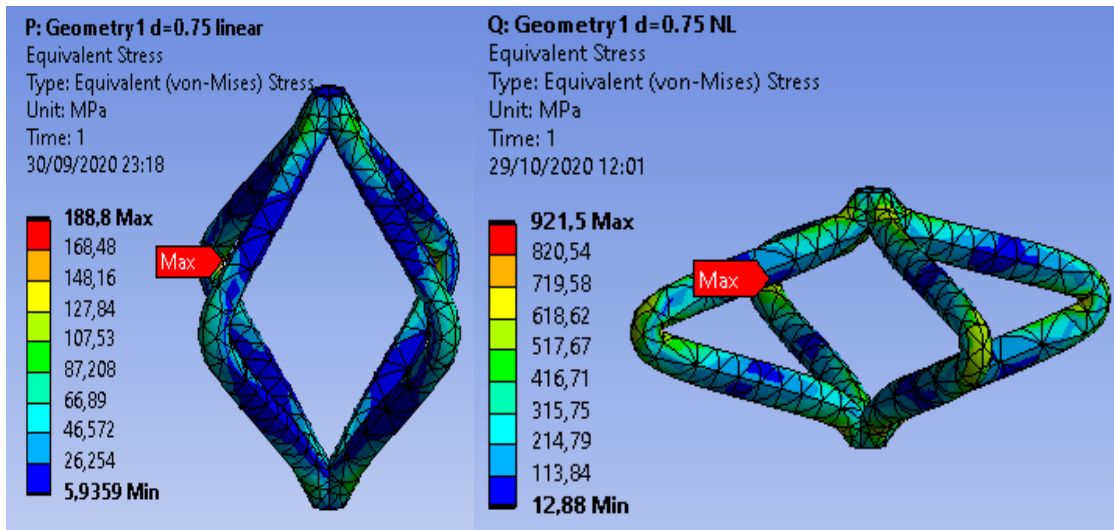


FIGURE 4.14: BBC3 stress simulation results

The considerations made for the reticular cells analysed previously are valid and similar also for this one, as shown by the trend of the Stress-Strain curve in Fig.4.14. Below, in Tab.4.9, the results obtained from the simulation are reported. To calculate the energy absorbed by the component, the area under the Force-Displacement curve was calculated using Matlab.

Displacement [mm]	Max Force [N]	Max Stress [MPa]	Max Strain [-]	Max Energy [J]
Y= - 0.18	196.65	188.80	0.075	0.018
Y= - 8	650.14	1113.10	0.679	1.601

TABLE 4.9: BCC3 results

4.2.3 BCC comparison

A comparison chart of BCC lattice materials is given below, Fig.4.15.

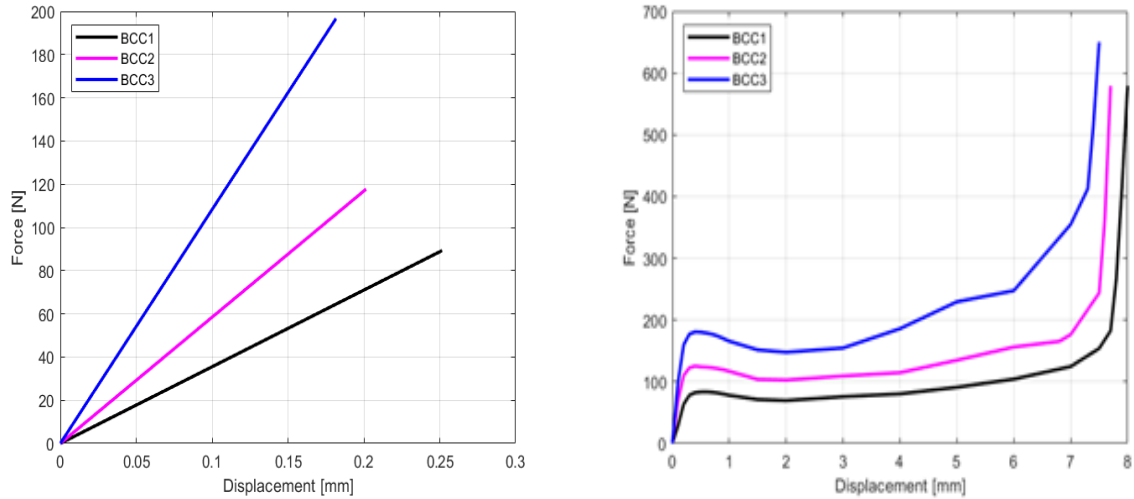


FIGURE 4.15: BCC F- δ curves comparison

	Max Force [N]	Max Energy [J]
d = 0.55mm	579.39	0.800
d = 0.65mm	585.21	1.050
d = 0.75mm	650.14	1.601

TABLE 4.10: BCC comparison results

In Fig.4.15 it can be seen how the behaviours changes according to the diameter of the lattice structures. The load supported by the component increases with the increase in the cell diameter. Tab.4.10 shows the energies absorbed by the lattice cells. An increase in the diameter of the structure of 0.1mm strongly affects the energy absorbed by the component. With the 0.2mm increase in the structure, the absorbed energy doubles the initial value.

4.2.4 BCCZ

After analysing the behaviour of the component in the form of a BCC reticular cell, it is now studied how a different type of truss lattice structure behaves after being subjected to a compression test. The procedure is similar to the one done previously, therefore only the results obtained from the simulation are reported. The unit cell diameter can assume three different value. They are taken into consideration between different diameters, $d = 0.40\text{mm}$, $d = 0.48\text{mm}$ and $d = 0.56\text{mm}$ respectively identified with the subscripts 1,2,3 in Fig.4.15 and Fig.4.16.

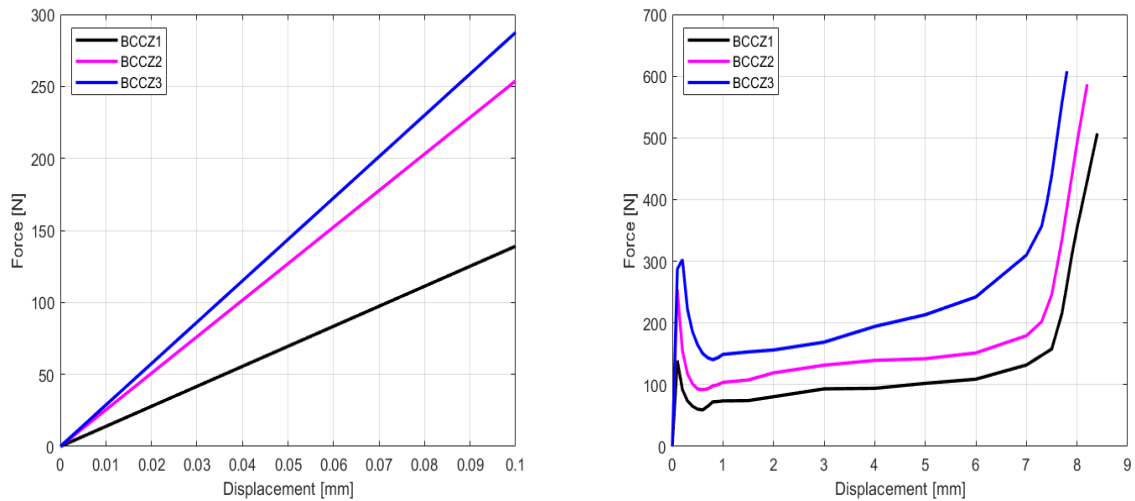


FIGURE 4.16: BCCZ F- δ curves comparison

	Max Force [N]	Max Energy [J]
d = 0.40mm	507.23	1.02
d = 0.48mm	586.80	1.33
d = 0.56mm	607.99	1.72

TABLE 4.11: BCCZ comparison results

In Fig.4.16 it can be seen how the behaviour changes according to the diameter of the lattice structure. The load supported by the component increases with the increase in the unit cell diameter. Tab.4.11 shows the energies absorbed by the lattice cells. It can

be seen how an increase in the diameter of the structure of 0.1mm affects the energy absorbed by the component.

4.3 Hybrid Material

After having calibrated the mathematical model related to the lattice structures and the polymer component, it is possible to start the design of the final component.

The aim of this subsection is to model a component of a metal lattice cell surrounded by a polymer cross-section, and to study its compression behaviour by discretizing the model by means of FEM analysis.

Starting from the Ansys simulation software, a static structural analysis is carried out in which the geometry of the assembly including the single reticular cell and a portion of polymer that surrounds it is considered. As far as the polymeric part is concerned, a rectangular section is approximated to completely include the reticular structure within it.

The approach followed is to design and upload an assembly geometry. This part was carried out on a different 3D modelling software (Solidworks) in which a cube of solid polymer material is modelled and then the excess material is removed, corresponding to the negative of the reticular structure that will be surrounded by the polymer, Fig4.17. After the modelling part, the 3D file must be converted into an extension readable by Ansys that allows you to import the assembly into the simulation environment (.IGS).

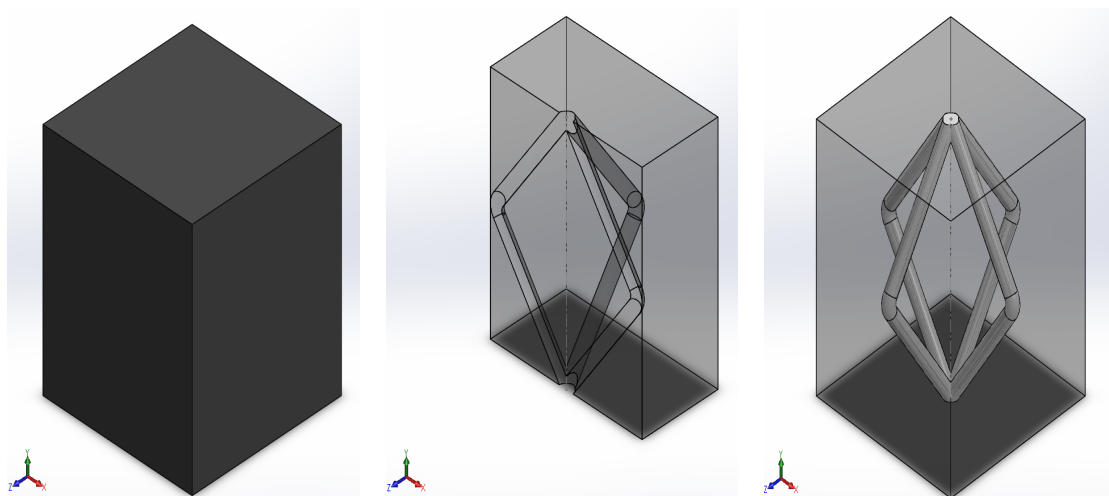


FIGURE 4.17: Hybrid material design

After importing the geometry, the software recognizes the two geometries as separate solid bodies, namely the lattice structure and the polymeric part, to which physical and mechanical properties must be assigned. In this regard, it is necessary to assign the material corresponding to each individual solid present in the assembly. The lattice structure is produced in 316L stainless steel by the additive manufacturing process; the polymer, on the other hand, is based on three different percentages of polyol, isocyanate and extender with variable compositions, which allow to obtain different hardness of the polymer itself, as already detailed in the Chapter 4.1. To simulate the compression test in Ansys, it is necessary, as a first step, to generate the mesh in model space. The mesh can be assigned a precise size value of the unit cell or manage this aspect independently from the software. A mesh discretization element size of 0.5mm is assigned. The next step is to define the boundary conditions of the assembly for the compression test. A fixed (locked) constrain is assigned to the lower face, while a variable downwards shift of the Y axis is imposed on the upper face. The last passage of the static analysis is the definition of the solutions on which the software will perform the calculations through algebraic equations.

4.3.1 BCC1/A30 & BCC1/A60

The first simulation test is carried out considering the reticular cell with diameter $d = 0.55\text{mm}$. The simulation of the compression test is carried out for a negative shift in the direction of the Y axis of 8mm in order to analyse the real behaviour of the material taking into account the densification that occurs in the polymer. The results of the two simulations are shown below, Fig.4.18. The figures show a progressive downward movement of the structure.

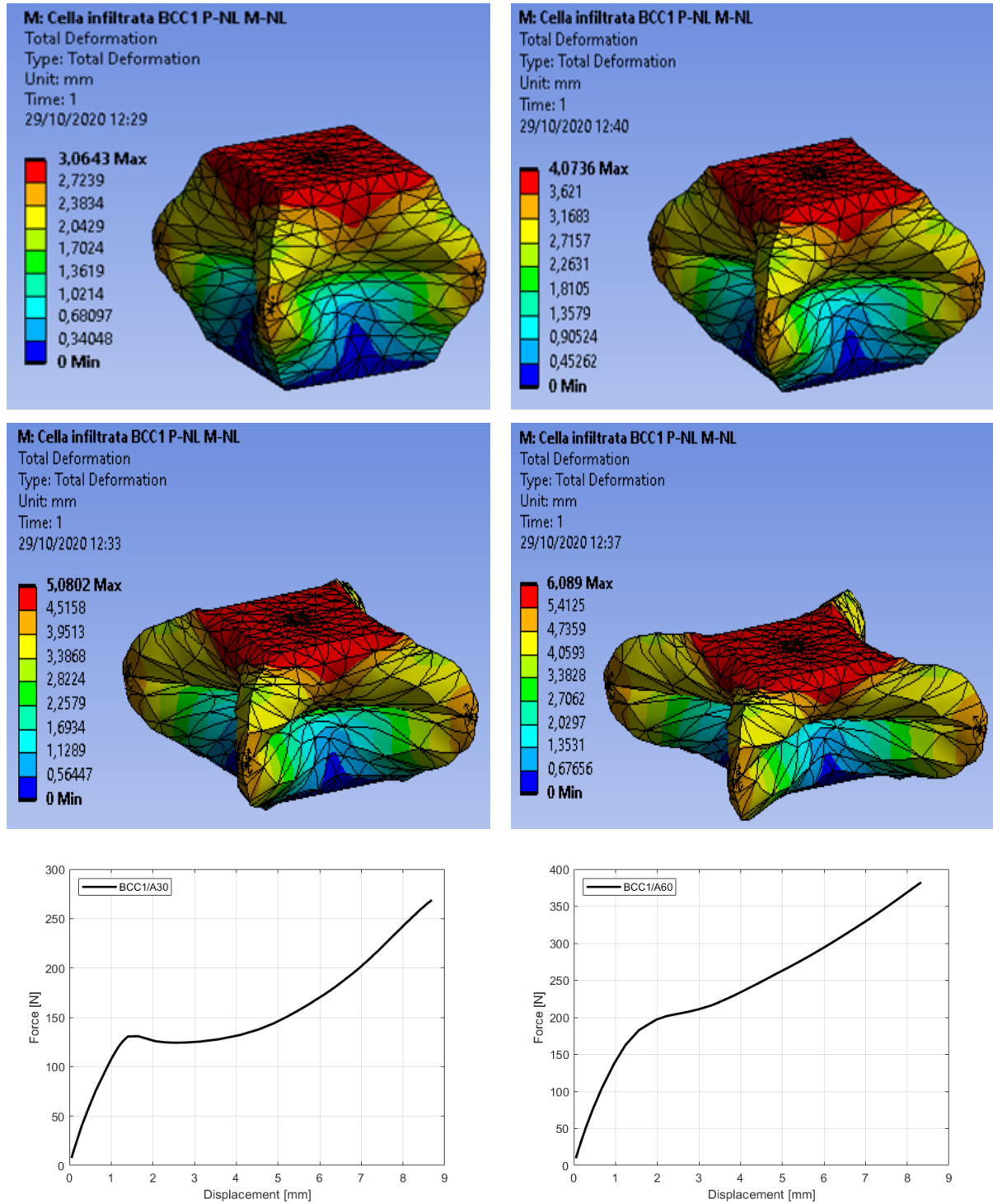


FIGURE 4.18: BCC1/A30 & BCC1/A60 simulation results

We can clearly distinguish three different zones on the Force-Displacement diagram. The first zone, on the left, occurs for small displacements, up to 1mm point where there is a peak of the applied force and this indicates the yield of the component, in

which the material follows a perfectly elastic trend where the load increases linearly, a second one where a plateau zone is highlighted. Finally, in the right part of the plot there is a rapid and exponential increase in force reaching high values for small delta displacement, a clear indicator of the formation and propagation of cracks within the metal material. Below, in Tab.4.12, the results obtained from the simulation are reported. To calculate the energy absorbed by the component, the area under the Force-Displacement curve was calculated using the Matlab calculation program.

	Displacement [mm]	Max Force [N]	Max Energy [J]
BCC1/A30	-8.100	268.80	1.32
BCC1/A60	-8.067	336.44	1.54

TABLE 4.12: BCC1/A30 & BCC1/A60 results

4.3.2 BCC2/A30 & BCC2/A60

The second simulation test is performed considering the reticular cell with diameter $d = 0.65\text{mm}$. The simulations of the compression test are performed in a similar way to that performed for the infiltrated reticular cell with diameter $d = 0.55\text{mm}$. The results for the unit cell size $d = 0.65\text{mm}$ are briefly reported below, Fig.4.19. The figures on the left refer to the component infiltrated with the Shore A30 hardness polymer while those shown on the right show the behaviour of the cell infiltrated with the Shore A60 hardness rubber.

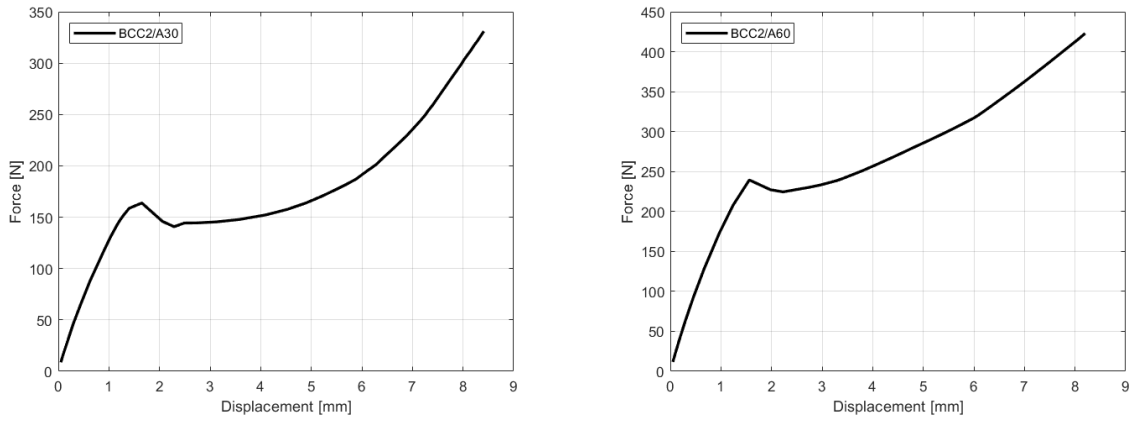


FIGURE 4.19: BCC2/A30 & BCC2/A60 simulation results

We can clearly distinguish three different zones on the $F-\delta$ diagram. The first zone on the left, occurs for small displacements, up to 1.5mm point where there is a peak of the applied force. This indicates the yield of the component, in which the material follows a perfectly elastic trend where the load increases linearly. Then it's present a second zone where a plateau is highlighted. Finally, in the right part of the plot there is a rapid and exponential increase in force reaching high values for small delta displacement, a clear indicator of the formation and propagation of cracks within the metal material. Below, in Tab.4.13, the results obtained from the simulation are reported. To calculate the energy absorbed by the component, the area under the Force-Displacement curve was calculated using the Matlab calculation program.

	Max Force [N]	Max Energy [J]
BCC2/A30	330.99	1.46
BCC2/A60	372.16	1.91

TABLE 4.13: BCC2/A30 & BCC2/A60 results

4.3.3 BCC2/A30 & BCC2/A60

The last simulation test is carried out considering the reticular cell with diameter $d = 0.75\text{mm}$.

Compression test simulations are performed similar to and above. The results for

the lattice structure diameter $d = 0.65\text{mm}$ are briefly reported below, Fig.4.20. The figures on the left refer to the component infiltrated with the Shore A30 hardness polymer while those shown on the right show the behaviour of the cell infiltrated with the Shore A60 hardness rubber.

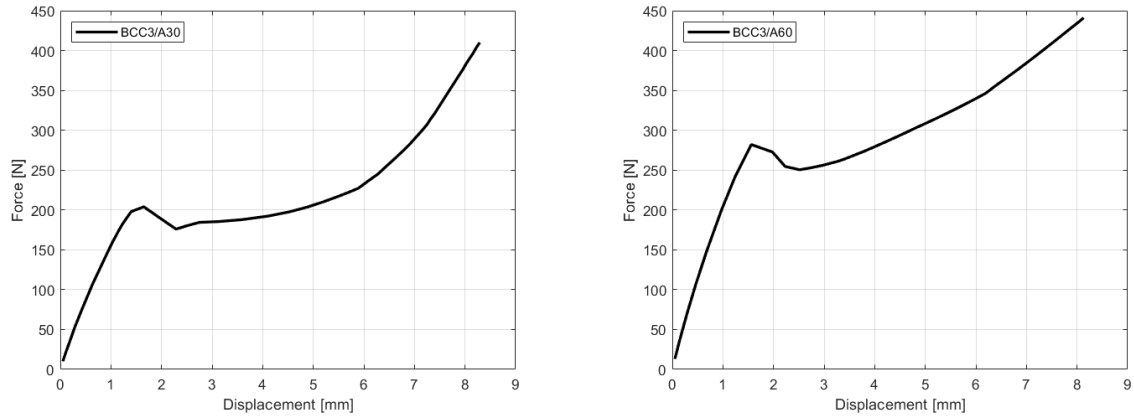


FIGURE 4.20: BCC3/A30 & BCC3/A60 simulation results

As for the previous cases we can clearly distinguish three different zones on the $F-\delta$ diagram. The first zone, on the left, occurs for small displacements, up to 1.5mm point where there is a peak of the applied force and this indicates the yield of the component, in which the material follows a perfectly elastic trend where the load increases linearly, a second one where a plateau zone is highlighted. Finally, in the right part of the plot there is a rapid and exponential increase in force reaching high values for small delta displacement, a clear indicator of the formation and propagation of cracks within the metal material.

The results obtained from the simulation are reported below in Tab.4.14. To calculate the energy absorbed by the component, the area under the Force-Displacement curve was calculated using the Matlab calculation program.

	Max Force [N]	Max Energy [J]
BCC3/A30	410.00	1.76
BCC3/A60	388.11	2.20

TABLE 4.14: BCC3/A30 & BCC3/A60 results

4.3.4 BCC/A30 comparison

Below is a comparison graph of the BCC lattice infiltrated with the A30 polymer, Fig.4.21.

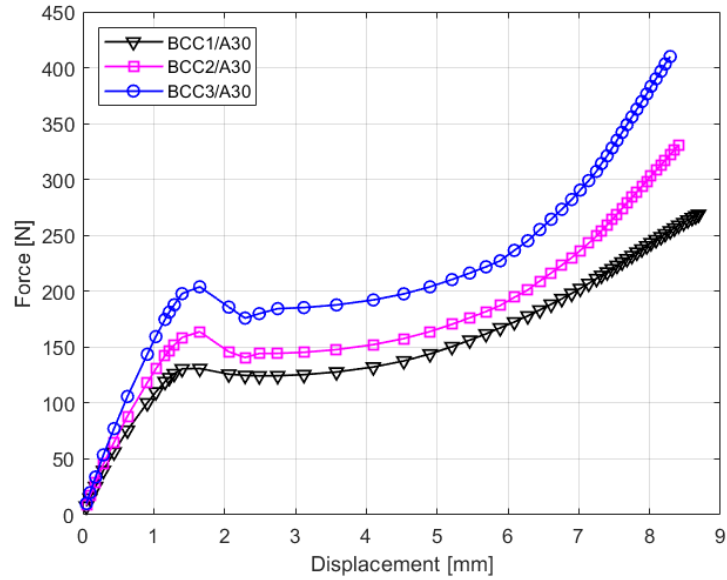


FIGURE 4.21: BCC/A30 F- δ curves comparison

	Max Force [N]	Max Energy [J]
BCC1/A30	268.80	1.32
BCC2/A30	330.99	1.46
BCC3/A30	410.00	1.76

TABLE 4.15: BCC/A30 results

In Fig.4.21 it can be seen how the behaviour changes according to the diameter of the lattice. The load beared by the component increases with the increase in the cell diameter. Tab.4.15 shows the energies absorbed by the lattice cells. It can be seen that an increase in the diameter of the structure of 0.1mm strongly affects the energy absorbed by the component.

4.3.5 BCC/A60 comparison

Below is a comparison graph of the BCC truss lattice structures infiltrated with the A60 polymer, Fig.4.22.

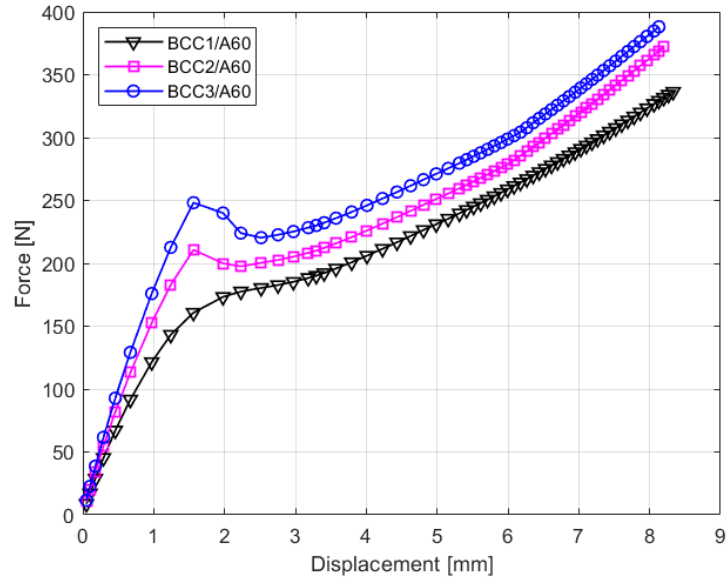


FIGURE 4.22: BCC/A60 F- δ curves comparison

	Max Force [N]	Max Energy [J]
BCC1/A60	336.44	1.54
BCC2/A60	372.16	1.91
BCC3/A60	388.11	2.20

TABLE 4.16: BCC/A60 results

In Fig.4.22 it can be seen how the behaviour changes according to the diameter of the lattice. The load supported by the component increases with the increase in the cell diameter. Tab.4.16 shows the energies absorbed by the lattice cells. It can be seen that an increase in the diameter of the structure of 0.1mm strongly affects the energy absorbed by the component.

4.3.6 BCCZ/A30 & BCCZ/A60 comparison

Once having analysed the behaviour of the components in the form of a reticular BCC cell, it is now studied how a different type of architecture behaves after being subjected to a compression test. The procedure is similar to the one done previously, therefore only the results obtained from the simulation are reported.

The unit cell diameter can assume three different value. They are taken into consideration between different thicknesses, $d = 0.4\text{mm}$, $d = 0.48\text{mm}$ and $d = 0.56\text{mm}$ respectively identified with the subscripts 1,2,3 in Fig.4.23 and Fig.4.24.

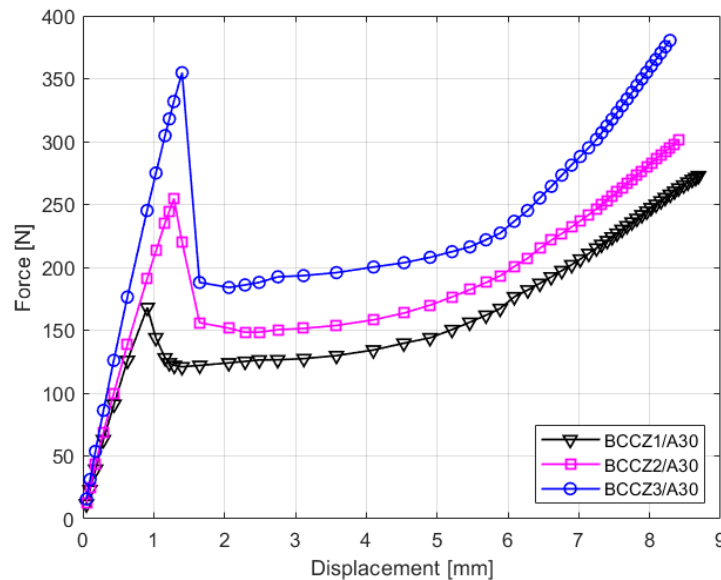


FIGURE 4.23: BCCZ/A30 F- δ curves comparison

Fig.4.23 shows the Force-Displacement diagram for the BCCZ cell infiltrated with the polymer of Shore A30 hardness. It can be seen how the behaviour changes according to the diameter of the lattice. The load supported by the component increases with the increase in the cell diameter. Tab.4.17 shows the energies absorbed by the lattice cells. It can be seen how an increase in the diameter of the structure of 0.1mm affects the energy absorbed by the component.

	Max Force [N]	Max Energy [J]
BCCZ1/A30	272.80	1.37
BCCZ2/A30	300.99	1.55
BCCZ3/A30	380.40	1.89

TABLE 4.17: BCCZ/A30 results

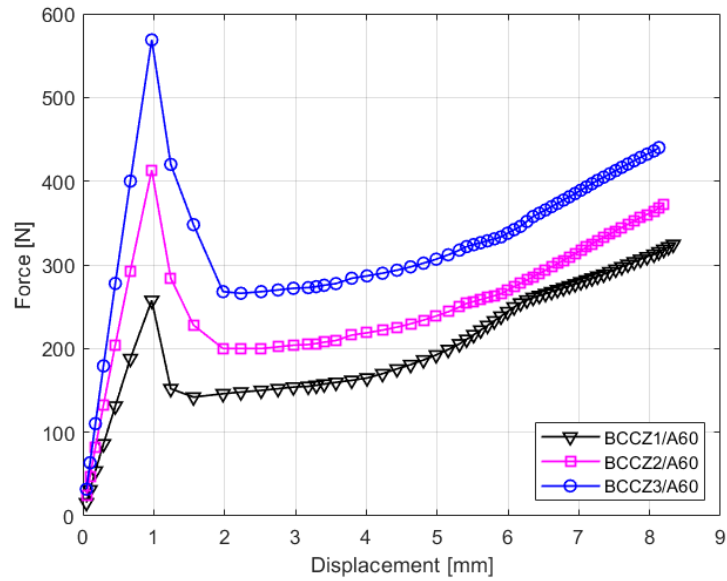


FIGURE 4.24: BCCZ/A60 F- δ curves comparison

Fig.4.24 shows the F- δ diagram for the BCCZ cell infiltrated with the polymer of Shore A60 hardness. It can be seen how the behaviour changes according to the diameter of the lattice structure. The load supported by the component increases with the increase in the cell diameter. Tab.4.18 shows the energies absorbed by the lattice cells. An increase in the diameter of the structure of 0.1mm strongly affects the energy absorbed by the component.

	Max Force [N]	Max Energy [J]
BCCZ1/A60	324.44	1.66
BCCZ2/A60	413.19	2.07
BCCZ3/A60	568.75	2.57

TABLE 4.18: BCCZ/A60 results

Chapter 5

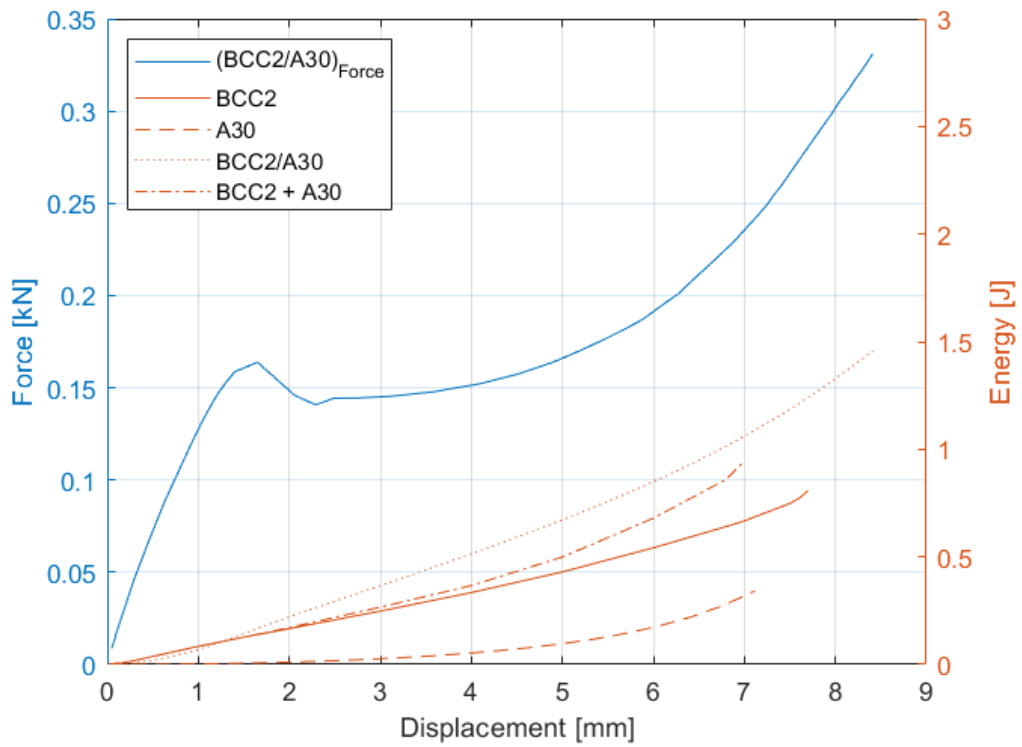
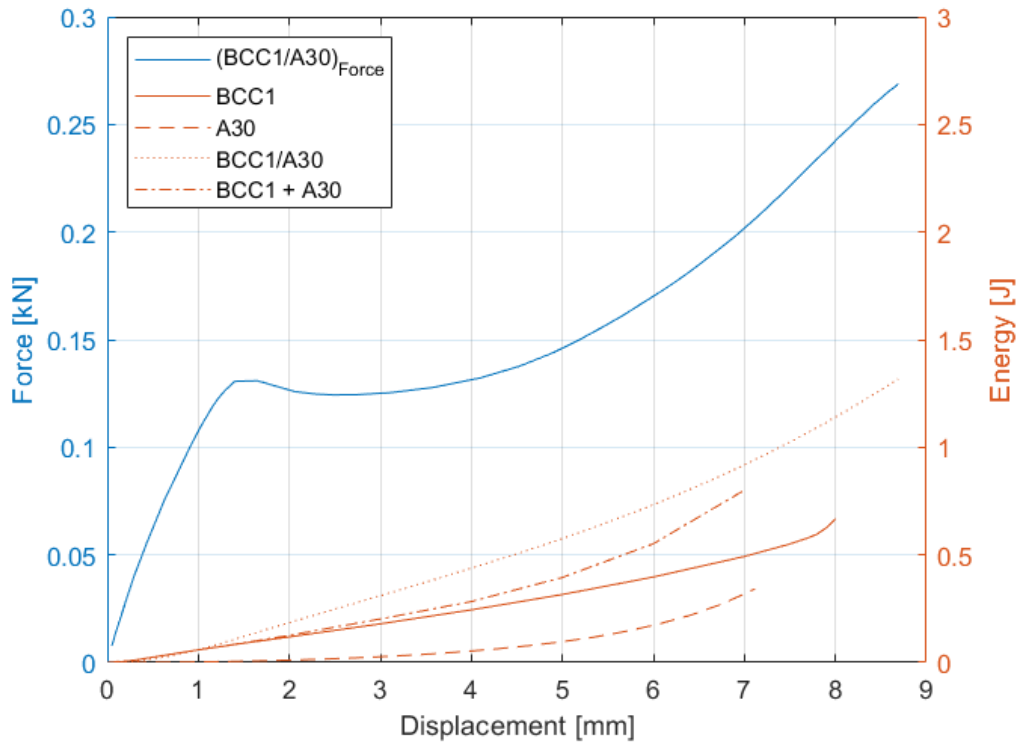
Energy absorption analysis

In this chapter, the different types of infiltrated lattice structures are compared in terms of absorbed energy.

What we want to analyse is the increase in energy of the infiltrated structure compared to the components taken individually.

In the following figures, the Force-Displacement curve of the infiltrated structure is shown in blue, while the curve of the energy absorbed as a function of the displacement is plotted in orange. The orange continuous line defined the energy absorbed by a part composed by metal lattice structure alone. The dashed orange line represent the energy that a component made up only polimer is able to absorb. Now, the point-by-point summation of these two energies is displayed by an orange dash-dot line in the plots. This sum is compared with the energy absorbed by a component made up hybrid materials. The energy of hybrid materials is showed with an orange dot line.

5.1 BCC/A30



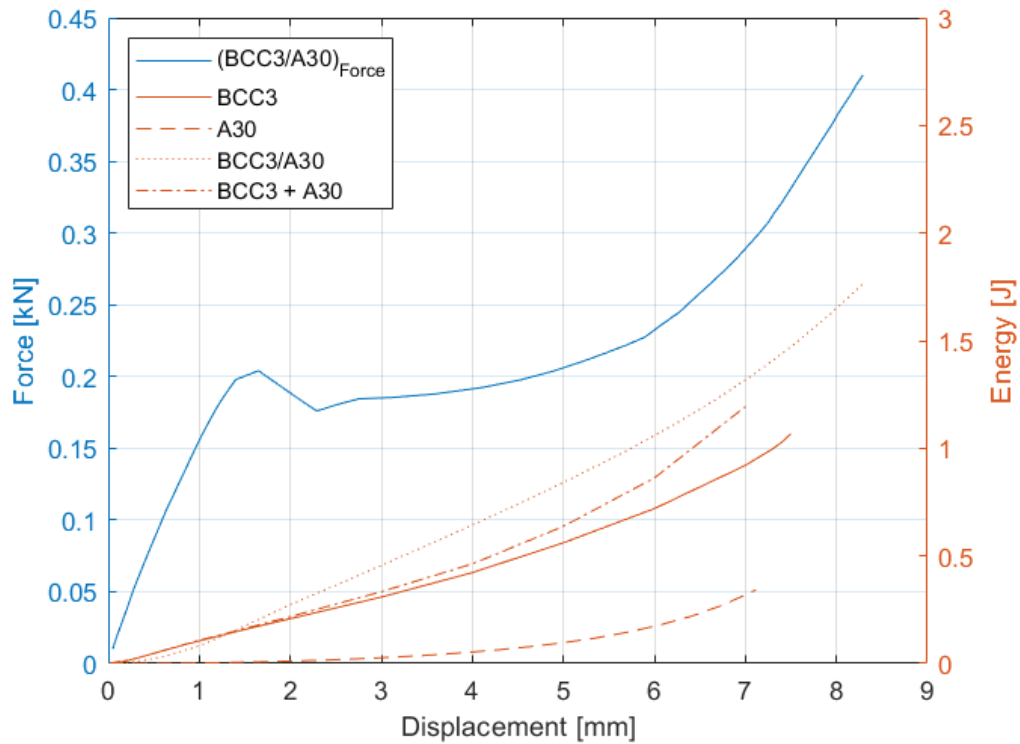


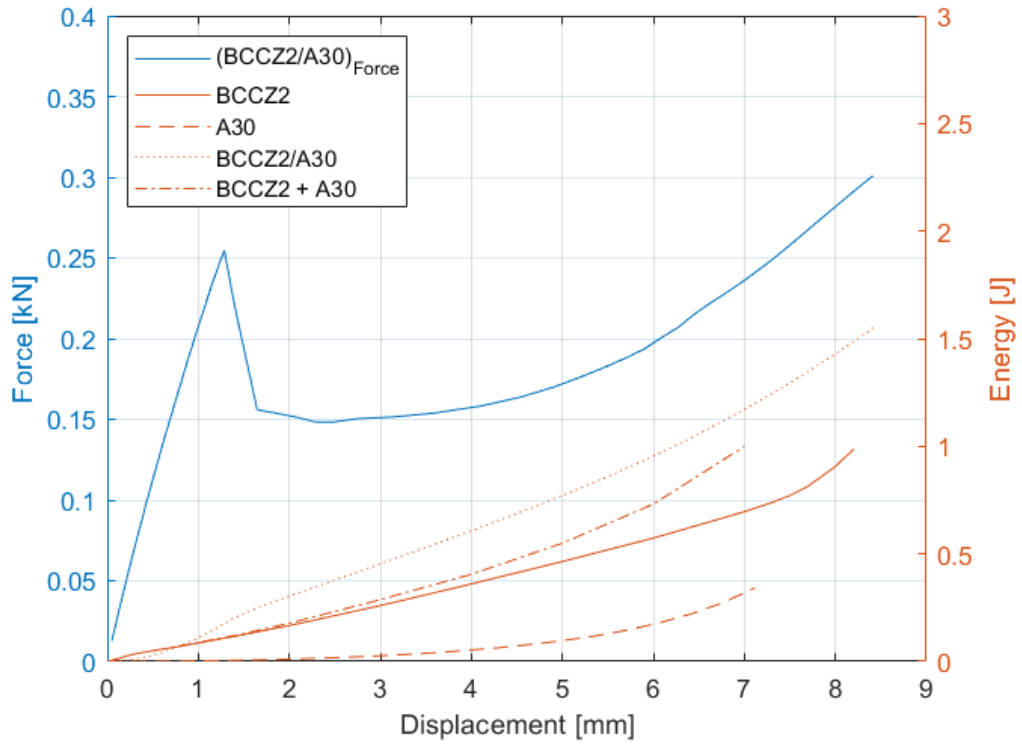
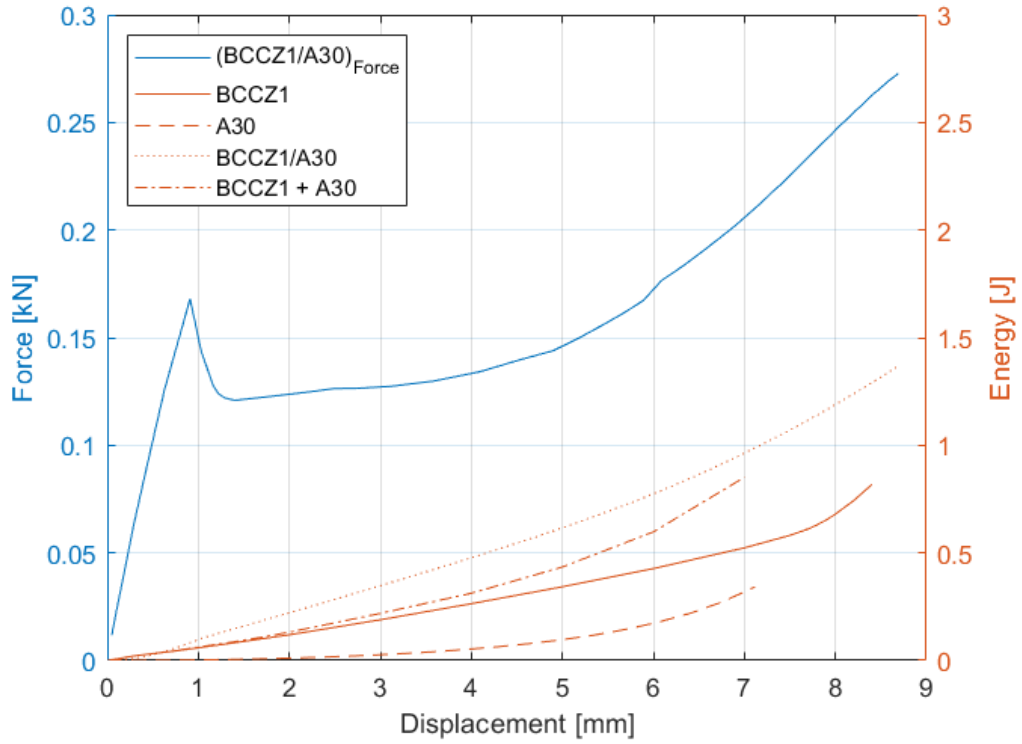
FIGURE 5.1: BCC/A30 energy comparison

Fig.5.1 shows the response trend to the compressive force for the hybrid structures BCC/A30, in blue colour, while the absorbed energy is shown in orange.

With this type of analysis, we want to analyse how the energy absorbed by the hybrid component is related to that absorbed by the components that compose it individually. The dashed orange line shows the energy that the polymeric material is able to absorb, while the continuous one coloured in orange represents the energy absorbed by the metal lattice structure. Finally, the dotted orange curve indicates the energy that the hybrid component is able to absorb during stress.

It can be seen that the energy absorbed by the hybrid component is greater than the sum of the energies of the individual components that make it up. We can conclude that the energetic properties of a hybrid component are not the sum of the capacities that the individual components that constitute it have to absorb energy during a compressive stress.

5.2 BCCZ/A30



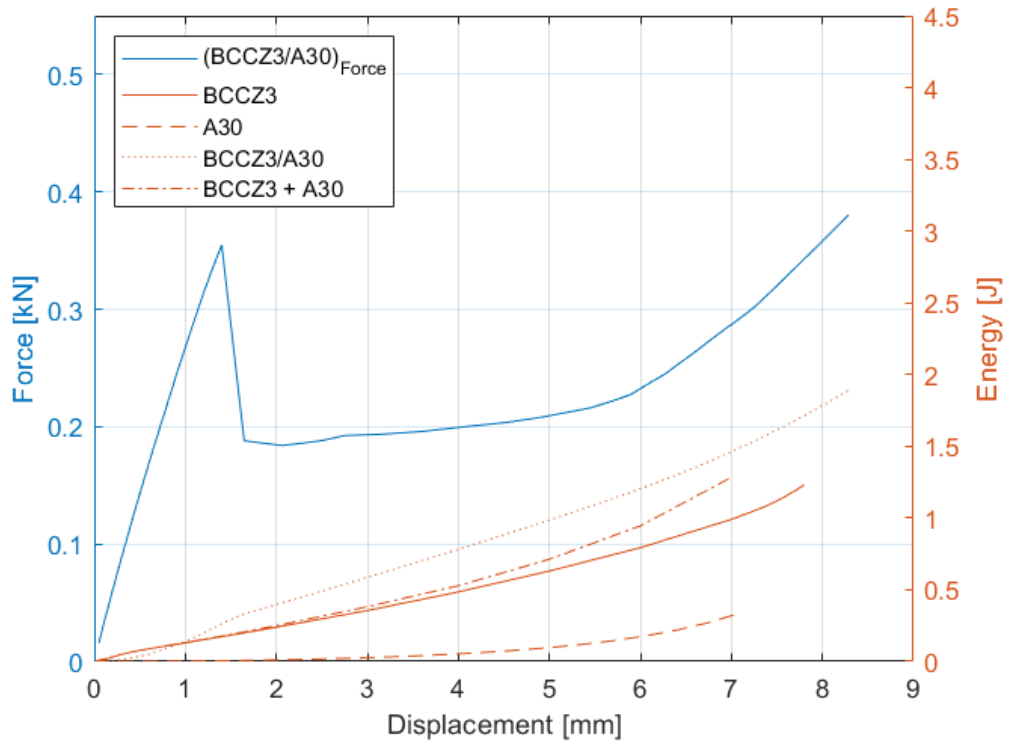
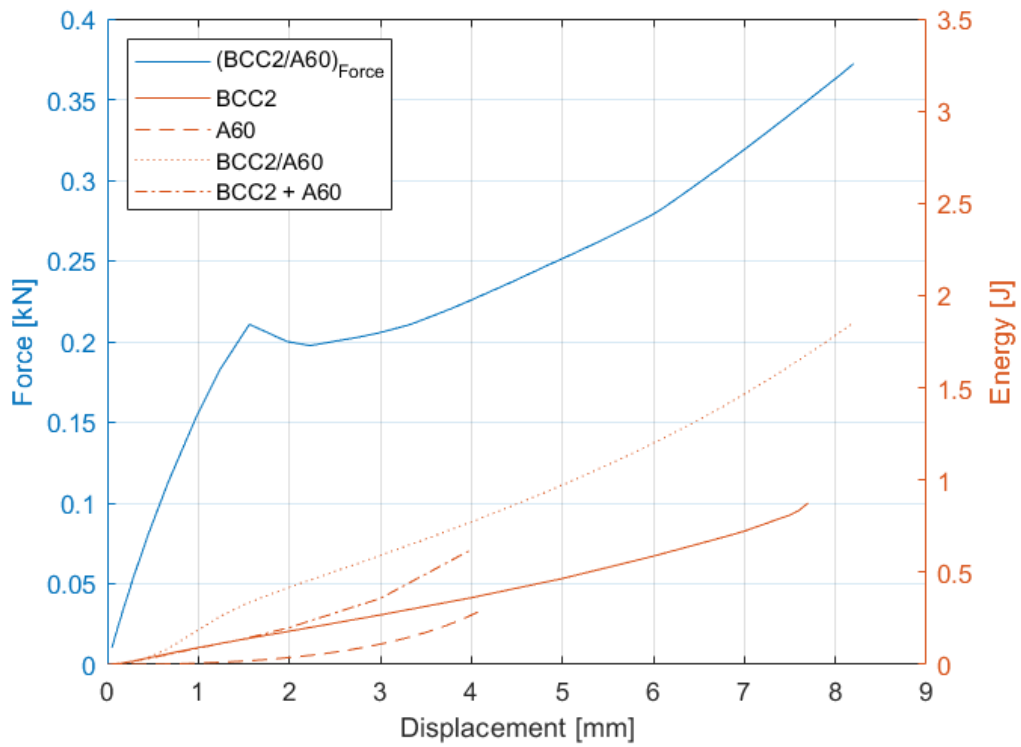
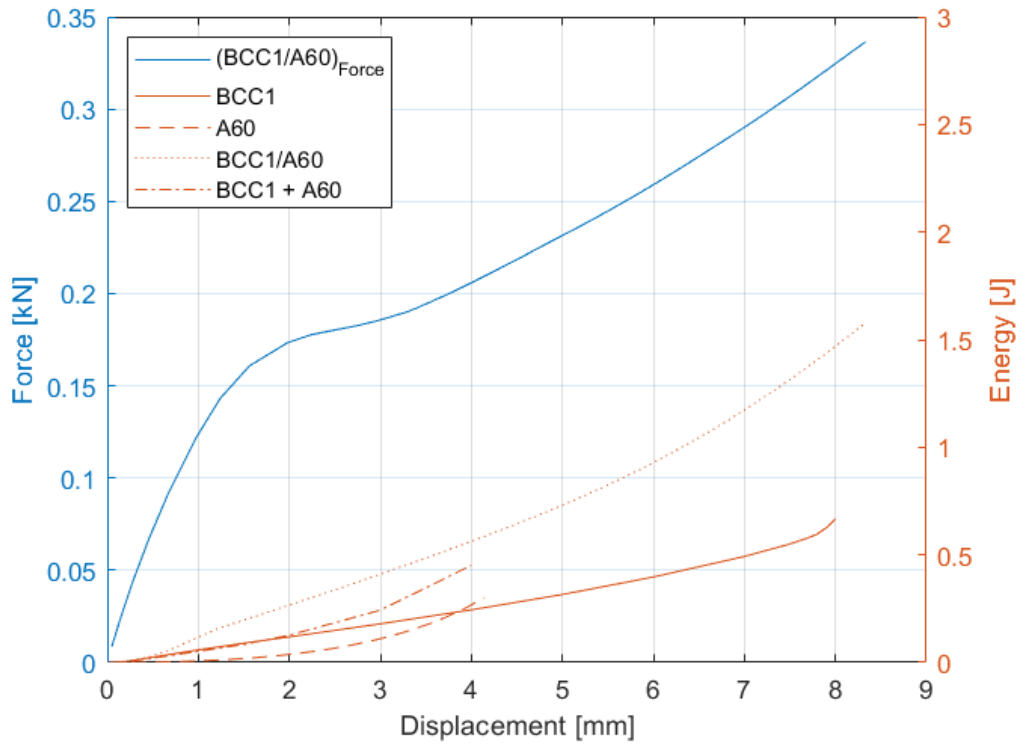


FIGURE 5.2: BCCZ/A30 energy comparison

Fig.5.2 shows the response trend to the compressive force for the hybrid structures BCCZ/A30, in blue colour, while the absorbed energy is shown in orange. The considerations made in the previous section are also valid for the geometry examined here.

5.3 BCC/A60



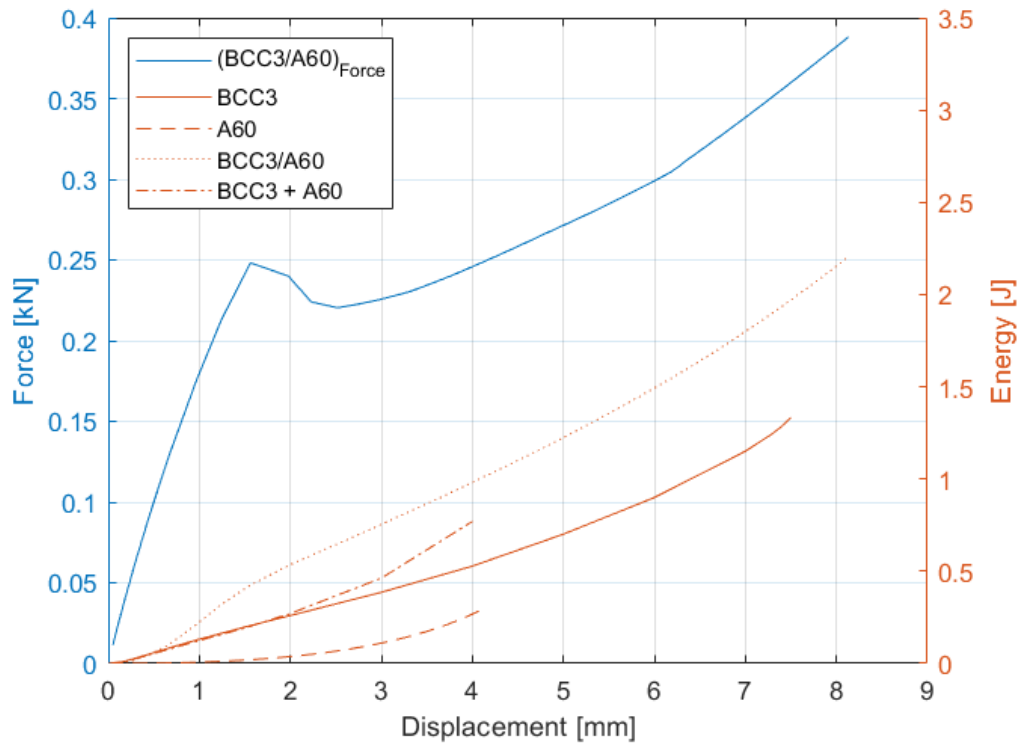
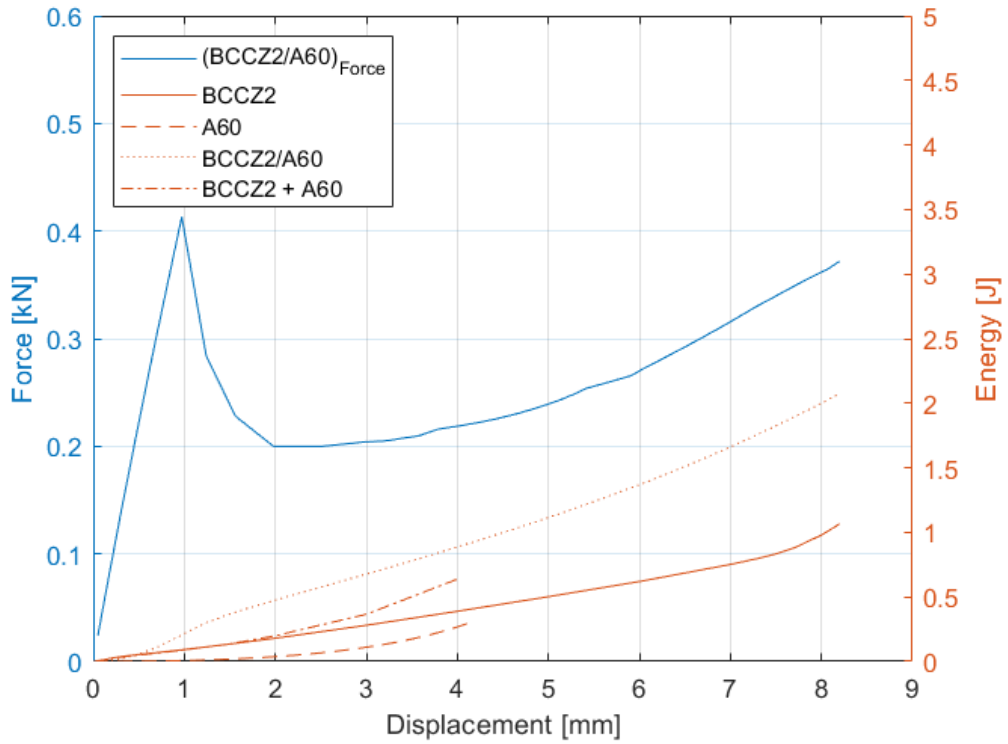
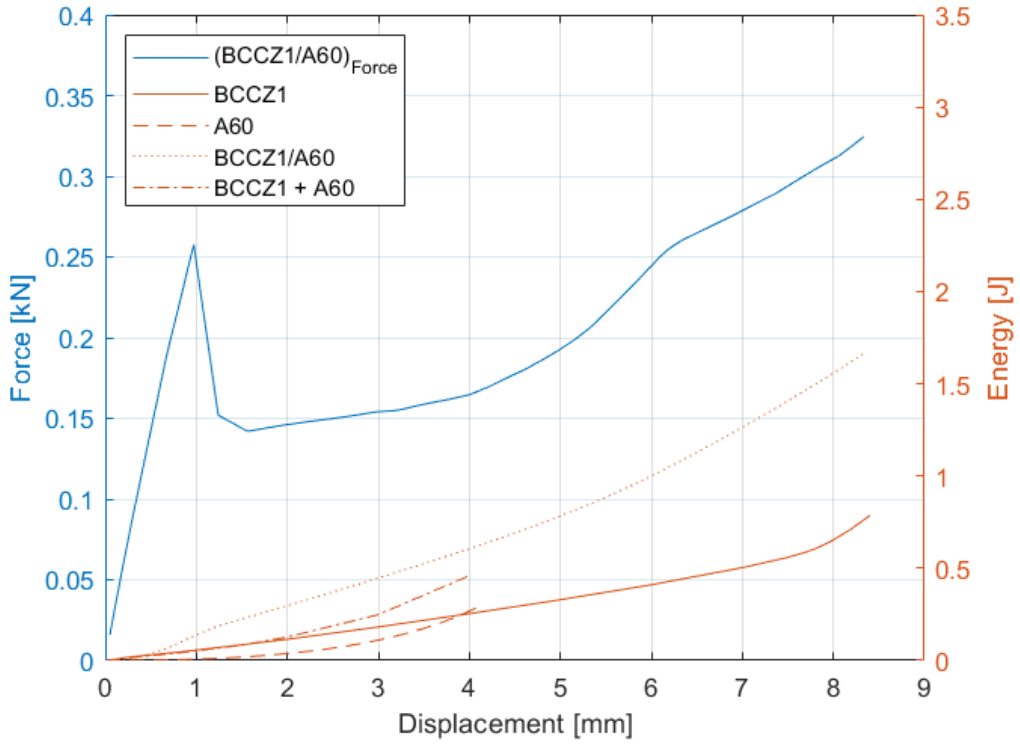


FIGURE 5.3: BCC/A60 energy comparison

Fig.5.3 shows the response trend to compressive force for the hybrid structures BCC/A60, in blue, while the absorbed energy is shown in orange. The considerations made in section 5.1 are also valid by varying the polymer considered here.

5.4 BCCZ/A60



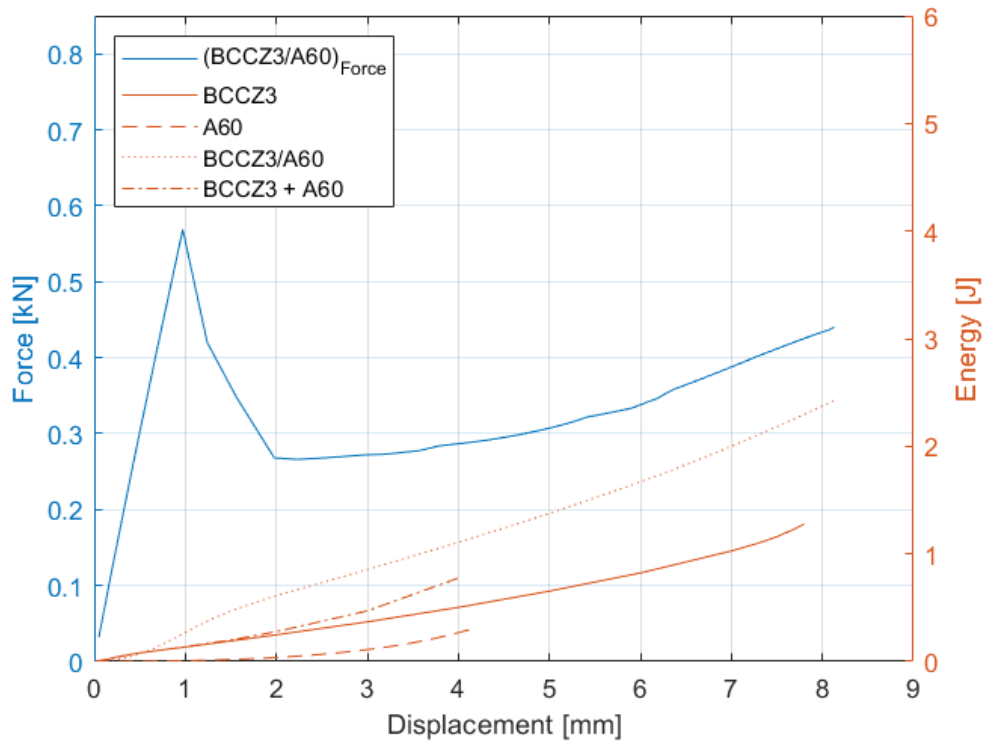


FIGURE 5.4: BCCZ/A60 energy comparison

Fig.5.4 shows the response trend to the compressive force for the hybrid structures BCCZ/A60, in blue colour, while the absorbed energy is shown in orange. The considerations made in section 5.2 are also valid by varying the polymer considered here.

5.5 Influence of the number of cells

In this subsection we want to investigate how to extend the results obtained from the simulations of a single cell to a component formed by a number n of cells.

In this way, the results achieved with a previous thesis work [4] in which a $50 \times 50 \times 50 \text{mm}^3$ structure made up of 500 lattice structures was tested. In Fig.5.5 you can see how despite considering a structure with more cells, the energy absorbed of the hybrid material is greater than the sum of the energies of the components that compose it.

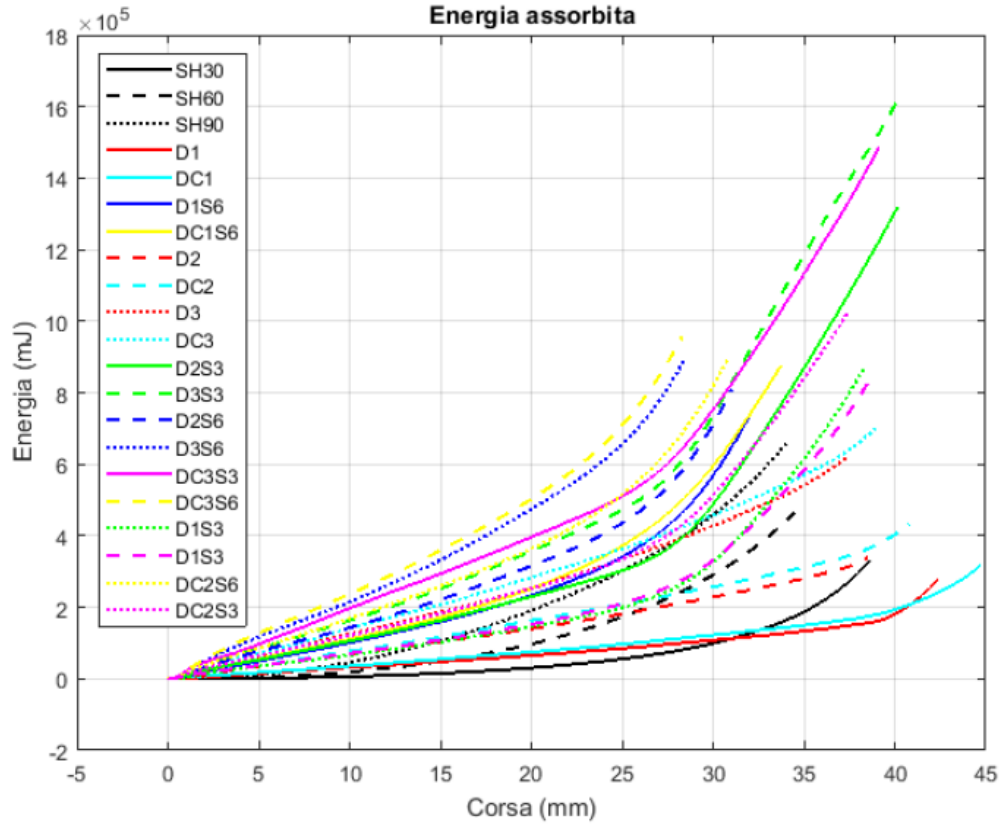


FIGURE 5.5: Energy absorption as a function of displacement [4]

A more analytical approach to the problem can be investigated by considering the stiffness of a complete structure. A final component with regular shape consists of an n number of cells. Some cells are arranged in XY to form a plane while others are arranged on the Z-axis by superimposing different planes. The hybrid structure formed by a reticular cell and the polymer can be considered as a spring of stiffness K . From the simulations carried out on the different components, the stiffness value K of the single cell is obtained. The complete structure will show a stiffness which will be the sum of the stiffnesses of the individual cells. In terms of equivalent stiffnesses, the lattice present on the same plane, i.e. XY plane, are connected in parallel with each other. They are then connected in series with the cells present on different planes in the direction of the Z-axis. The Equivalent stiffness (K_{eq}) for springs in parallel and in series are reported in Eq.5.1 and Eq.5.2.

$$K_{eq//} = \sum_{i=1}^n k_i \quad (5.1)$$

$$K_{eq_{series}} = \sum_{i=1}^n \frac{1}{k_i} \quad (5.2)$$

The K_{eq} for springs in parallel is calculated as the sum of the stiffnesses of the cells, the K_{eq} for springs in series as the sum of the reciprocals of the stiffnesses.

Finally, the stiffness of a final component is defined by the sum of the reciprocals of the equivalent stiffnesses taking into account the cells present on the different planes that make up the structure, Eq.5.3.

$$K_{eq_{tot}} = \sum_{i=1}^n \frac{1}{(k_{xy})_i} \quad (5.3)$$

Chapter 6

Dynamic analysis

6.1 Modal analysis

The goal of the modal analysis is to analyse the dynamic behaviour of infiltrated structures when subjected to vibrations. With modal analysis it is possible to evaluate in detail the response and dynamic properties of the system in the frequency domain. The vibrational behaviour of a system can be analysed by evaluating the natural frequency value and the associated proper modes of vibration.

The modal analysis was performed on two types of hybrid materials and the values of the corresponding natural frequencies were recorded. Through the designed mathematical model, Chapter 5, it is possible to carry out a dynamic analysis using Ansys Workbench. We proceed step by steps. The first step is to import the model that we want to analyse as .IGS extension file into simulation environment.

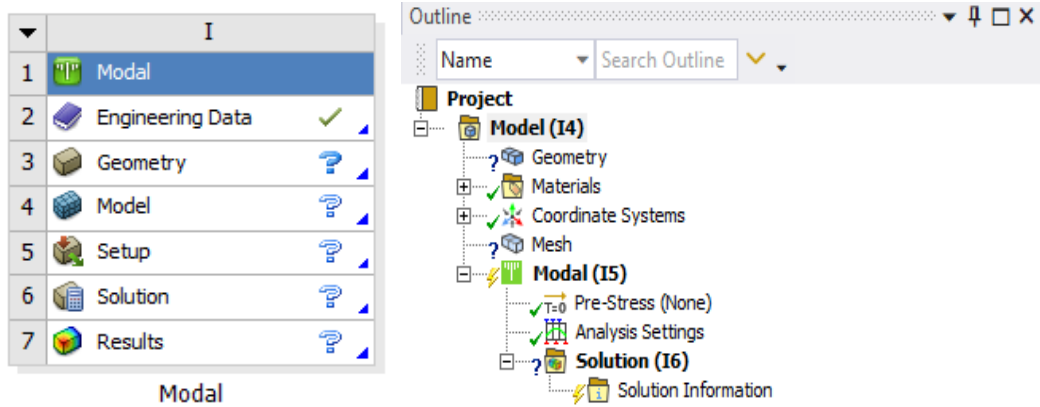


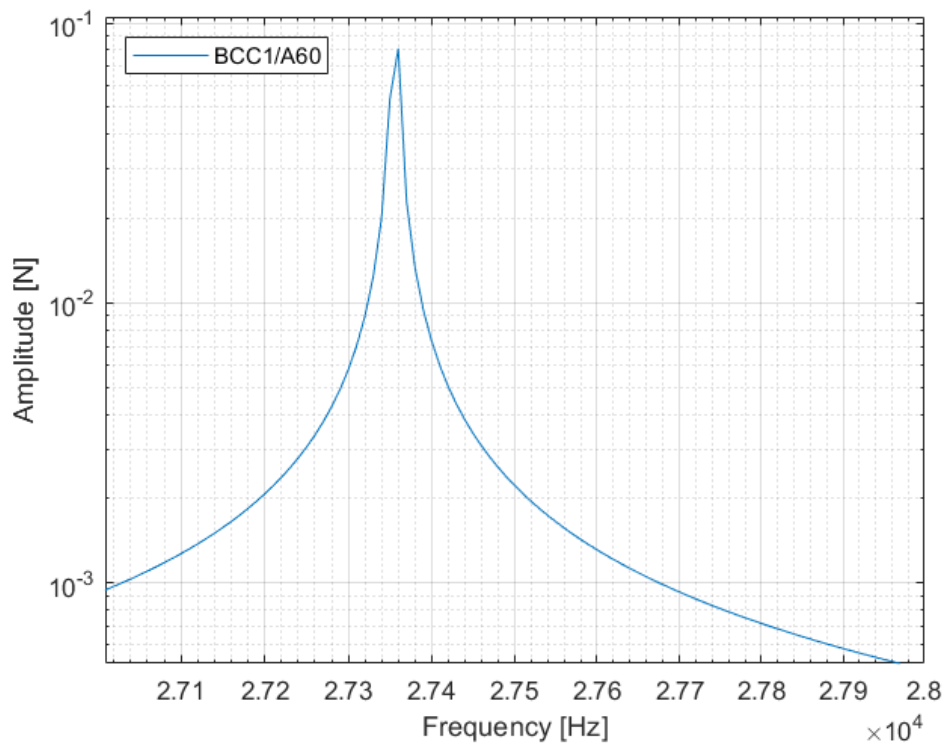
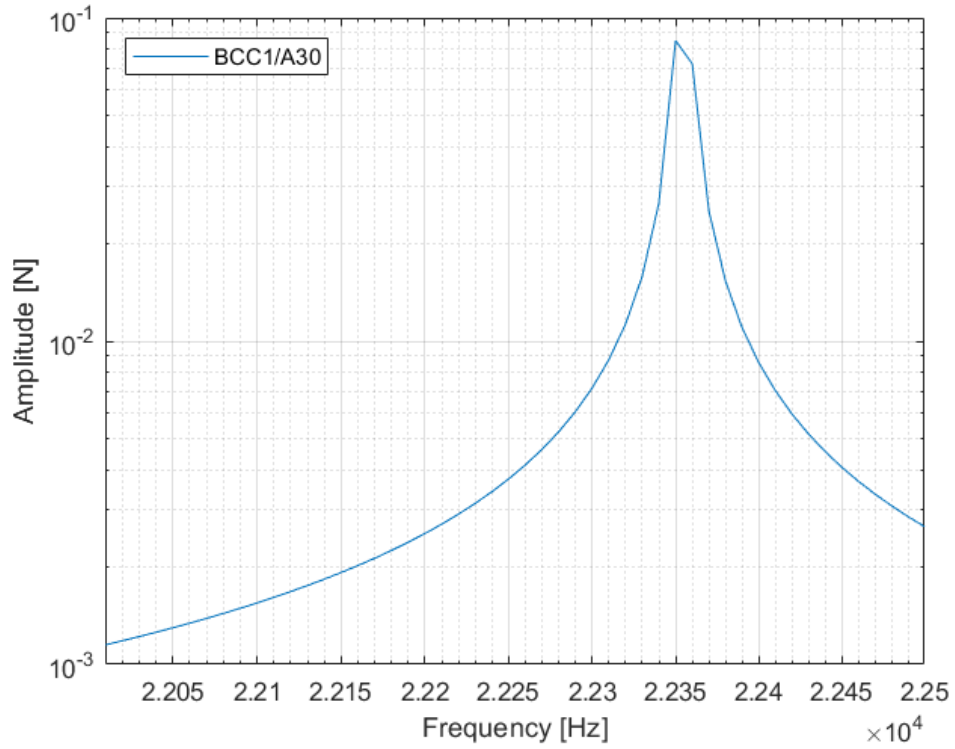
FIGURE 6.1: Definition of parameters for modal analysis

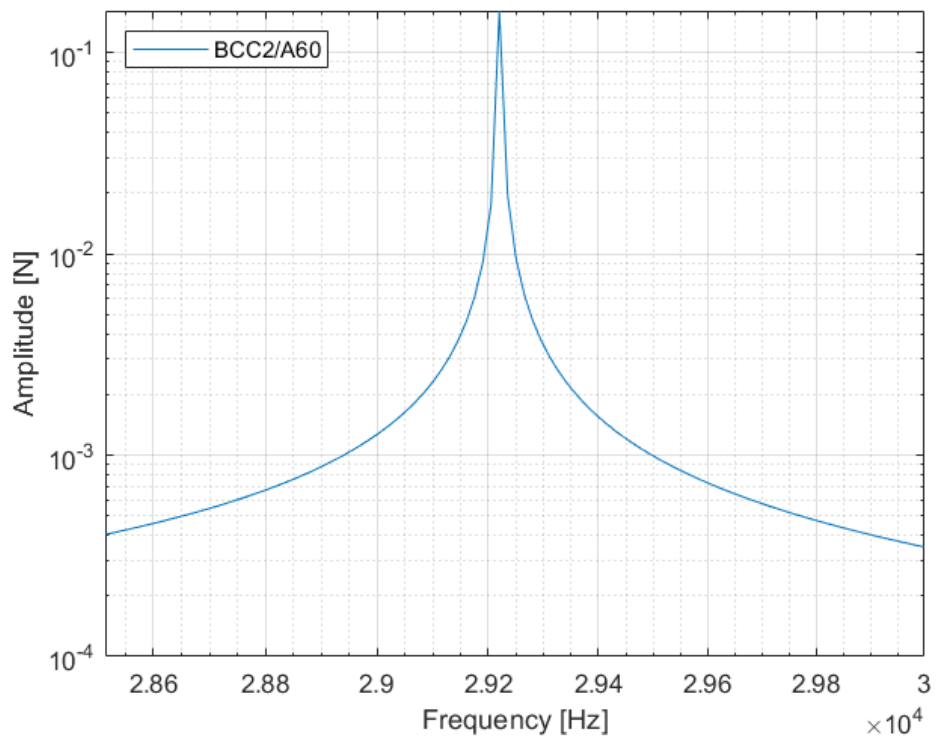
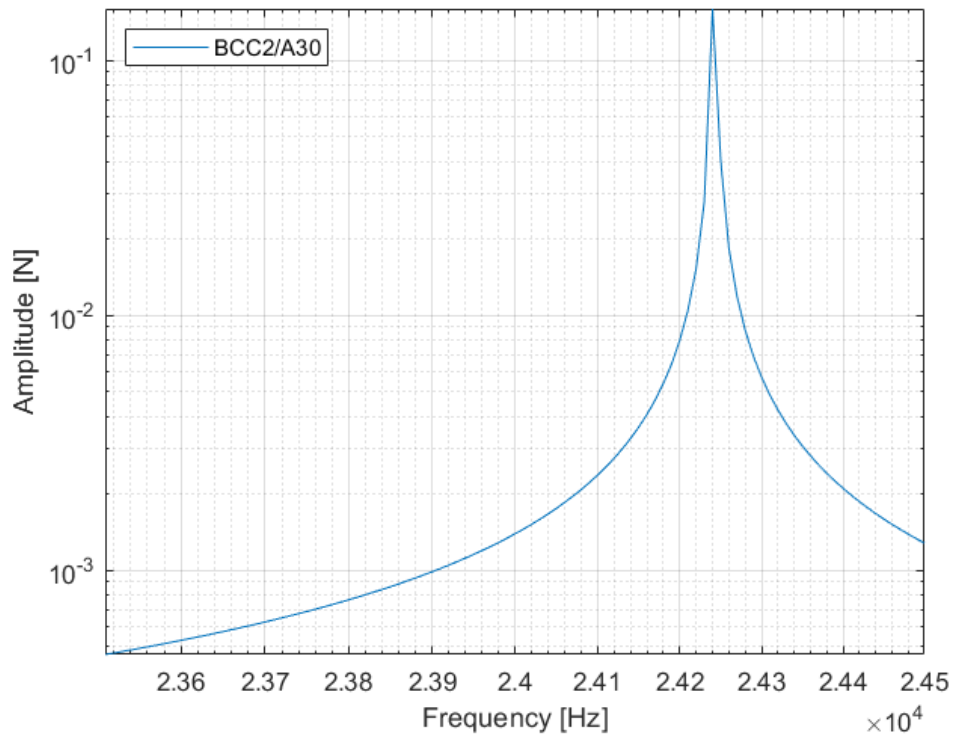
It is important to define in advance the analysis system on which we want to simulate the dynamic behaviour of the structure, in this case a modal analysis, to then import the geometry in question. Once the geometry has been imported, from the Ansys Mechanical extension it is possible to manage and define a series of parameters that allows to carry out the analysis, Fig.6.1.

The hybrid structure is composed by a lattice structure made with 316L filled with polymer. One of the fundamental aspects to perform a FEM simulation is the creation of a Finite Element mesh. The surface of the geometry under consideration is discretized with a series of elements of various shapes (triangles, rectangles, etc.). The Ansys Mechanical extension allows the automatic generation of the mesh with predefined values of unit cell sizes. Otherwise it is possible to assign a precise unit cell size value, managing various discretization parameters of the solid state model, but this way is beyond the scope of this work and requires a great deal of experience from the user. The mesh size is set to 0.5mm. It is necessary to apply some boundary conditions to the model in order to faithfully reproduce the real test. A fixed constraint is applied to the model to the lower face of the filled structure, which defines a fully constrained state.

After that, the maximum modes to find are defined. For our investigation are set 10 modes. Of these ten modes for the type of analysis we want to carry out, only one value has a relevant meaning, namely the frequency at which the compressive stress occurs. From the modal analysis, the frequency at which the resonance peak occurs is obtained. Fig.6.2 shows the Frequency Response Function (FRF) of the hybrid

structures analysed. In Tab.6.1 the natural frequencies for the various structures are reported.





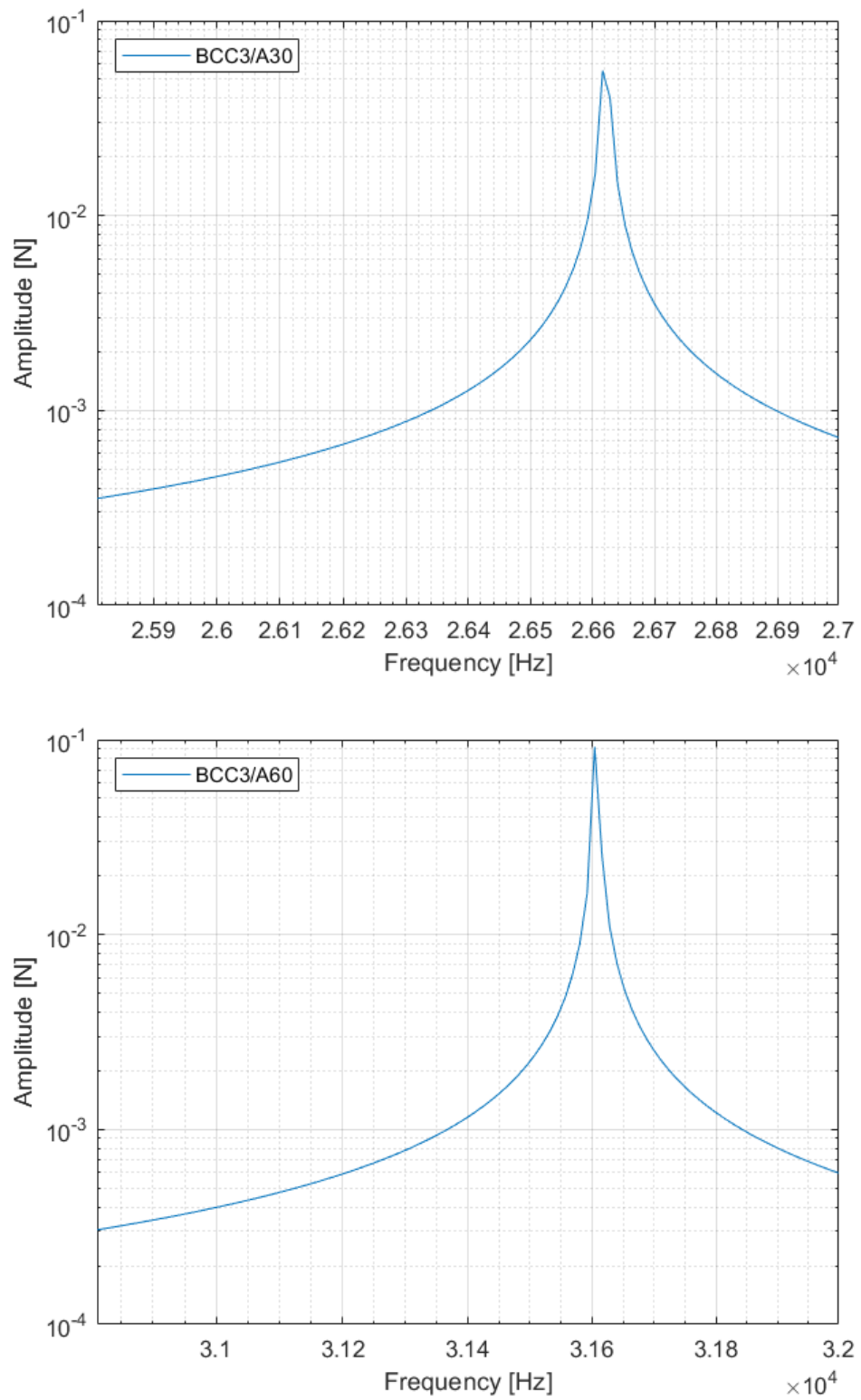
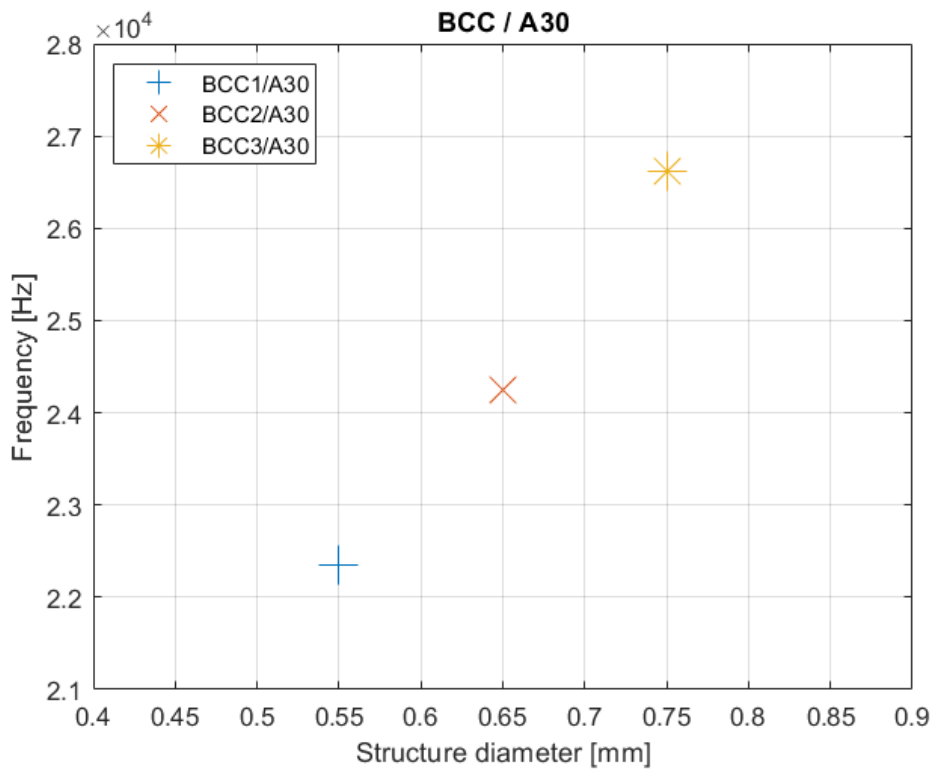


FIGURE 6.2: Frequency Response Function of the hybrid materials

Filled Structure	Natural frequency [Hz]
BCC1/A30	22350
BCC1/A60	27360
BCC2/A30	24240
BCC2/A60	29220
BCC3/A30	26616
BCC3/A60	31604

TABLE 6.1: Results of modal analysis

In Fig.6.3 we can visualize how the natural frequency change in relation to the structural diameters of the lattice structures. Increasing the uprights dimension the natural frequency reached by the hybrid structures increase as well. The first plot is referred to the lattice structures filled with polymer of Shore A30 hardness. The second one to the polymer of Shore A60 hardness. The last graph compares the hybrid materials as a function of the filler.



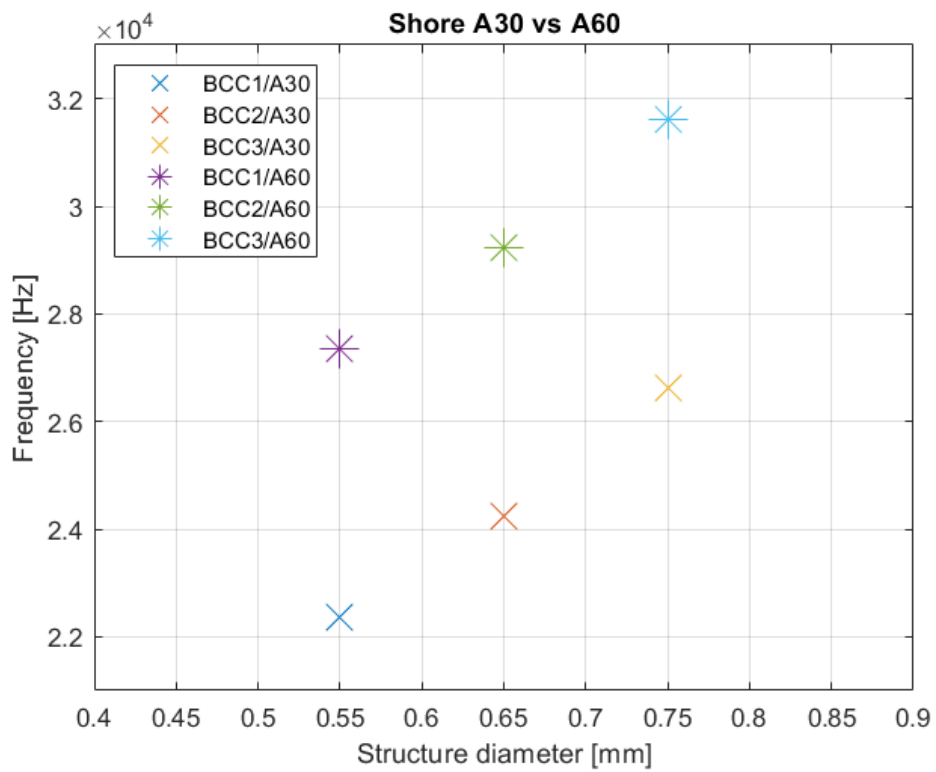
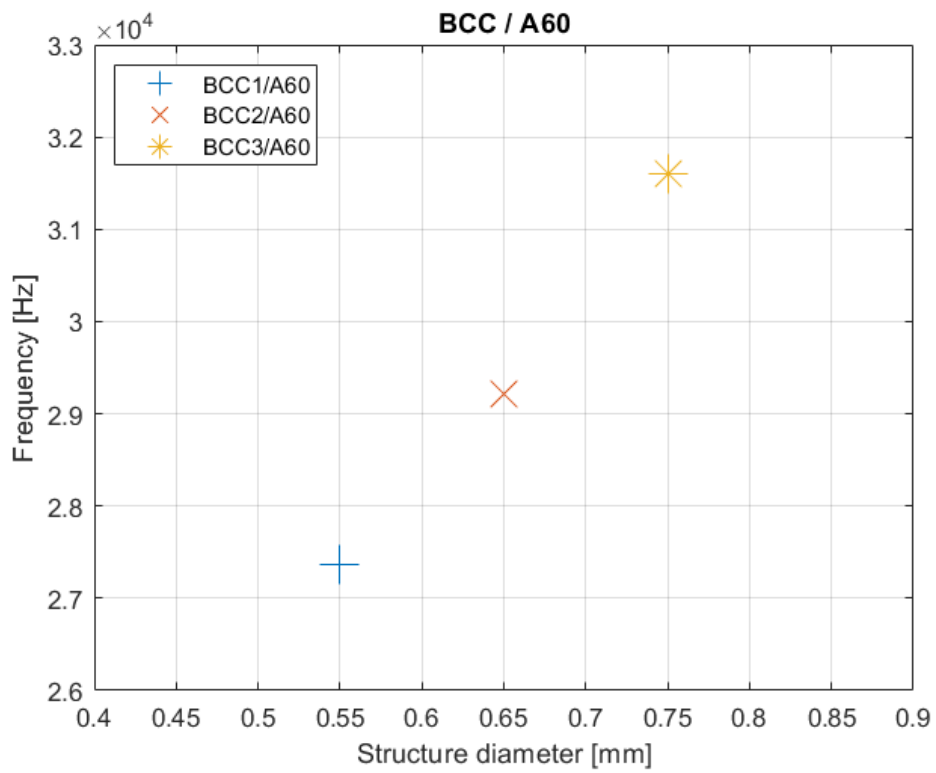


FIGURE 6.3: Influence of the lattice on the natural frequency of the hybrid material

6.2 Harmonic analysis

Frequency response is used to characterize dynamic systems. It is the measure of the output spectrum in response to a stimulus.

The modal analysis was performed on two types of hybrid materials and the graphs of the Frequency Response Function were recorded. Harmonic analysis is connected to the modal analysis. In fact, the simulation software allows you to connect a previously performed dynamic analysis to a harmonic. To do this, simply connect the fields "engineering data", "geometry" and "model", Fig.6.4. In this way the material properties, geometry and parameters related to the mesh size remain unchanged.

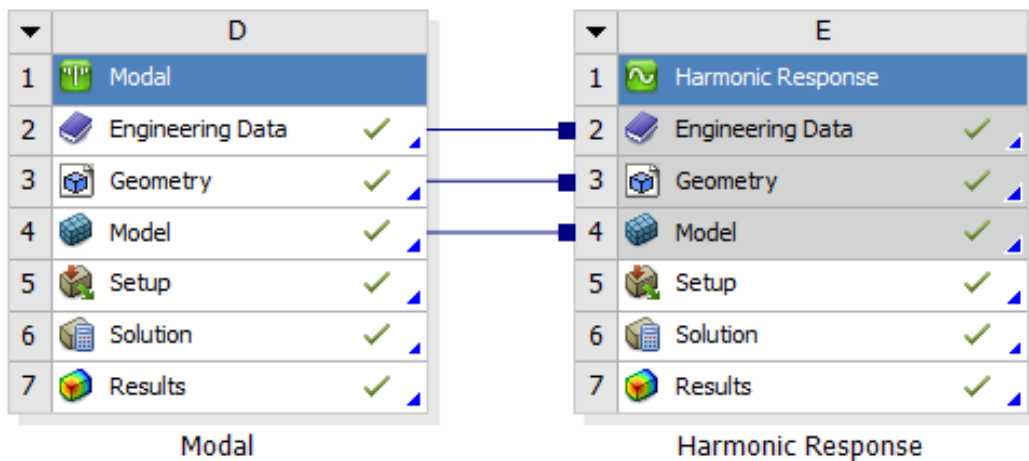


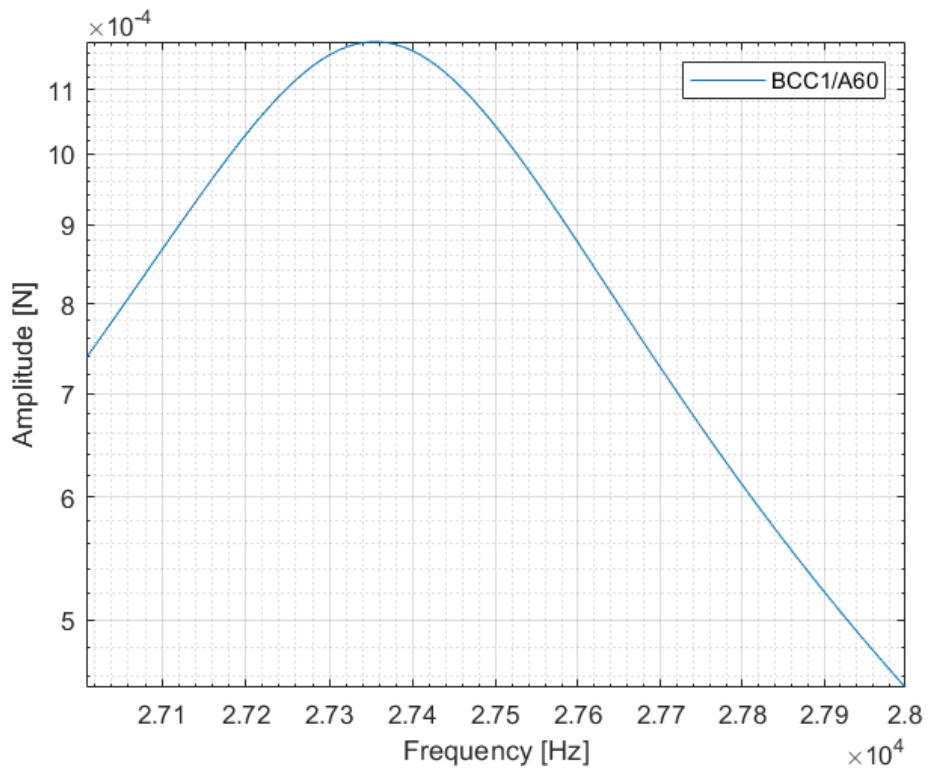
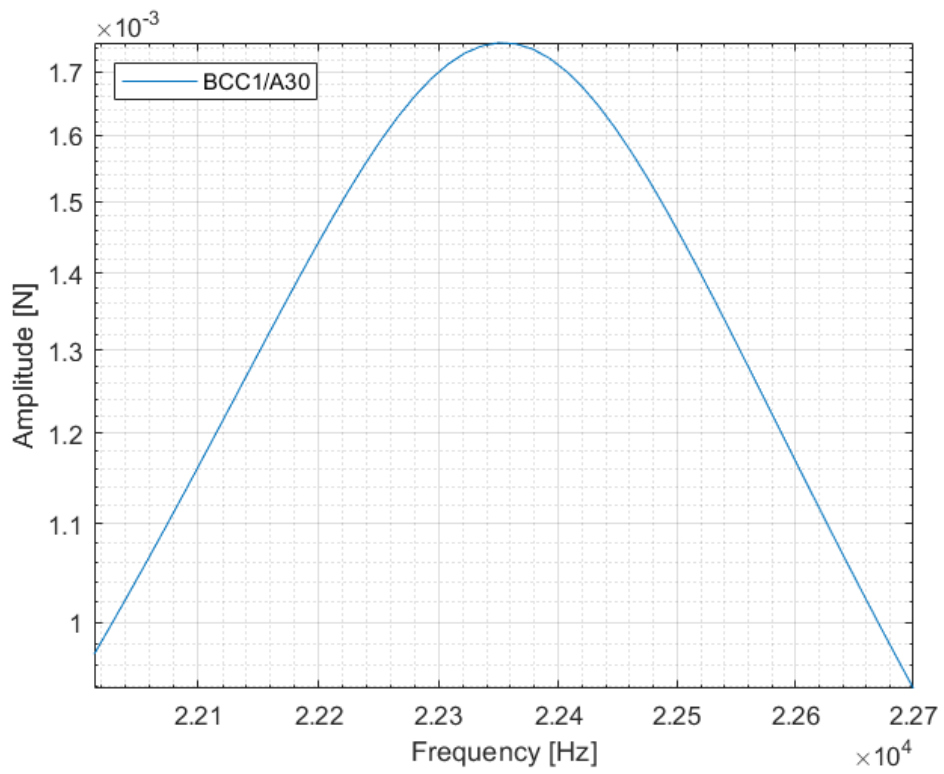
FIGURE 6.4: Definition of parameters for harmonic analysis

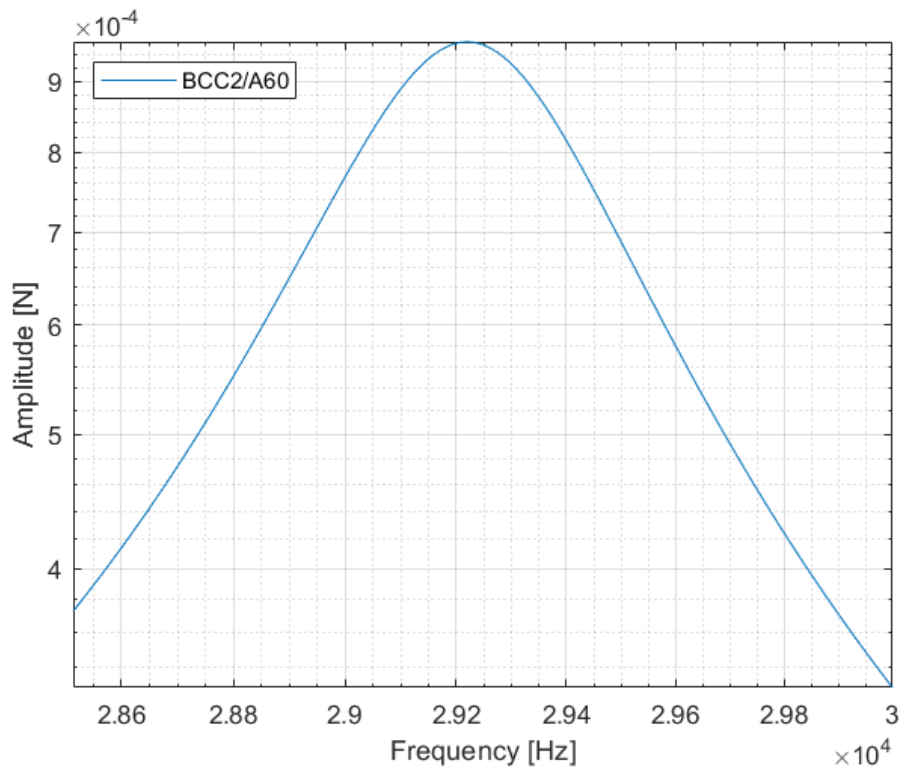
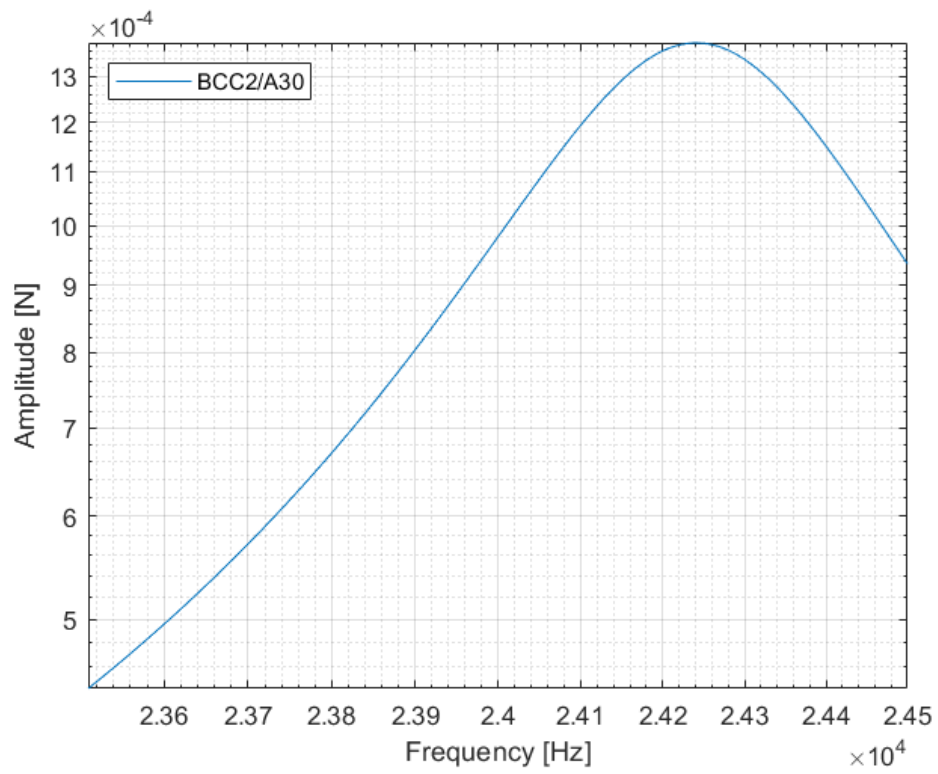
In simulated harmonic analysis, to reflect a real test, the damping coefficients of the elements that make up the infiltrated structure must be taken into account. The damping coefficient is an important parameter in all dynamic type analyses. Since it is difficult to calculate by analytical approaches, it is obtained experimentally. From the literature [18] [19] [20], a damping coefficient is assumed for the metal structure $c_{316L} = 0.02 \frac{Ns}{m}$, while for the polymeric structure $c_{pol} = 0.05 \frac{Ns}{m}$. The assumed damping coefficients are an average value from those found in the literature, Tab.6.2.

Fig.6.5 shows the Frequency Response Function of the hybrid structures analysed. Tab.6.3 shows the amplitudes for the various structures.

Ref	\mathbf{c}_{316L} $\left[\frac{Ns}{m}\right]$	\mathbf{c}_{pol} $\left[\frac{Ns}{m}\right]$
[18]	0.02	0.05
[19]	[0.02 ÷ 0.04]	≈ 0.05
[20]	0.016	≈ 0.05
Average	0.02	0.05

TABLE 6.2: Damping coefficient





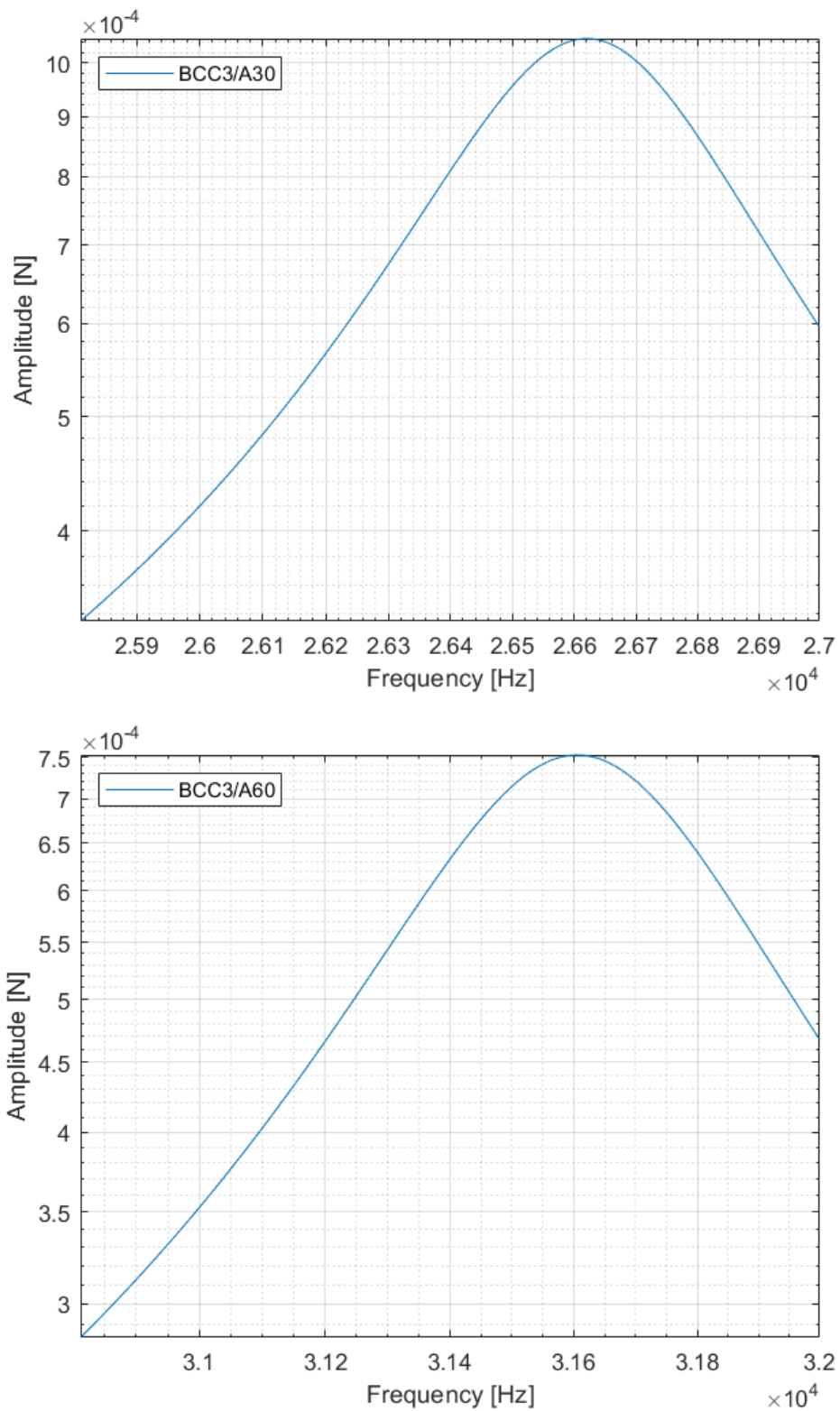


FIGURE 6.5: Frequency Response Function of damped hybrid materials

Filled Structure	Max Amplitude	Max Amplitude
	[N]	[dB]
BCC1/A30	0.0017	-55.1459
BCC1/A60	0.0012	-58.5571
BCC2/A30	0.0014	-57.2053
BCC2/A60	0.00096	-60.3440
BCC3/A30	0.0010	-59.5926
BCC3/A60	0.00075	-62.4613

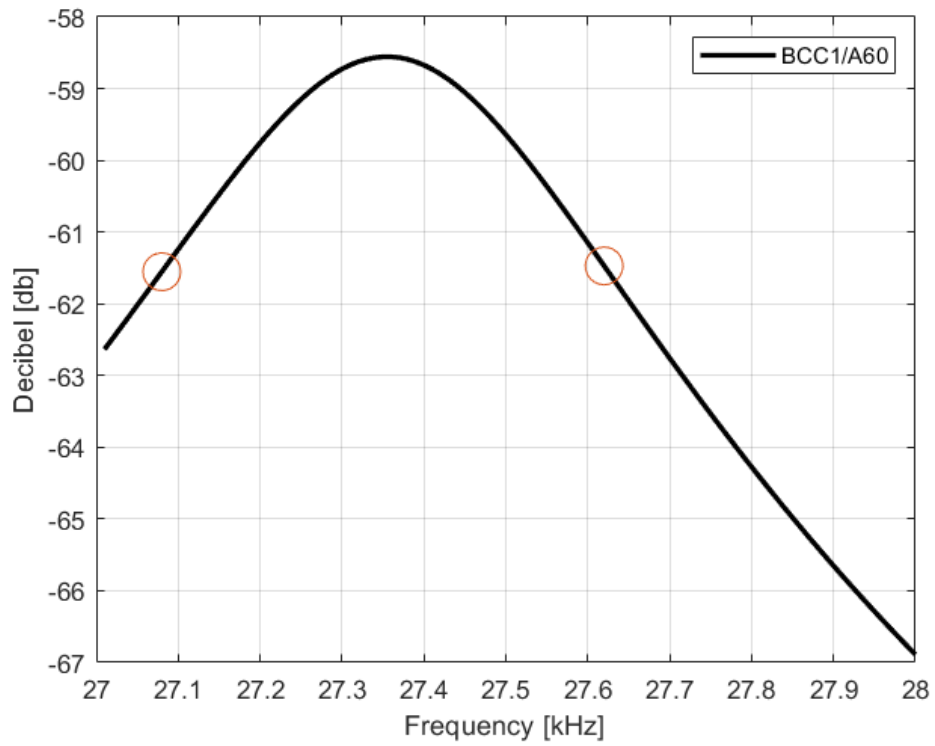
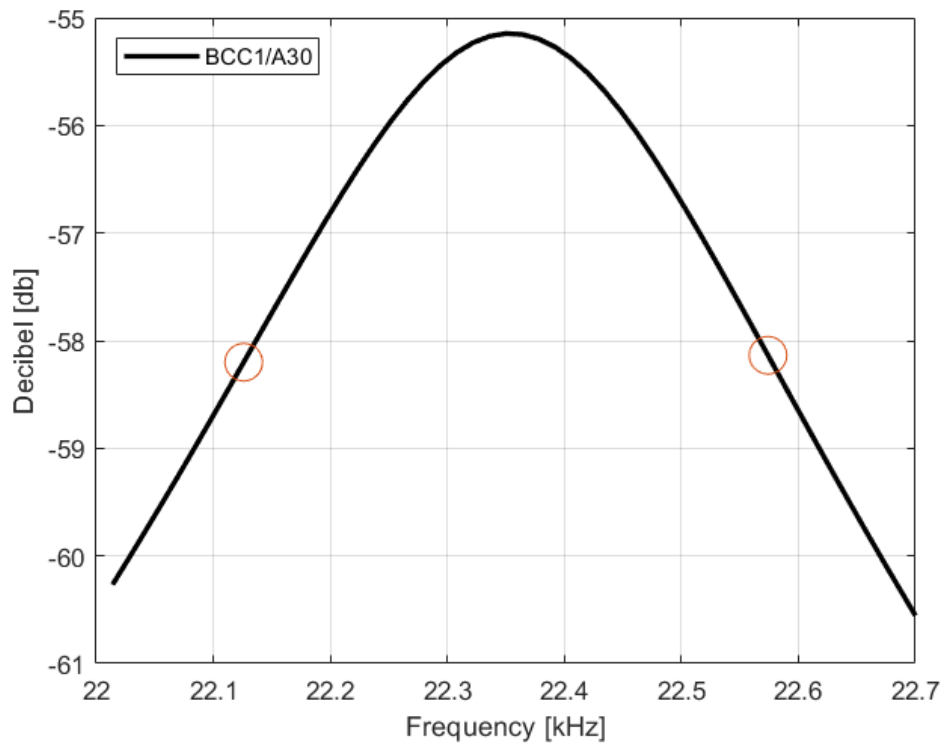
TABLE 6.3: Results of harmonic analysis

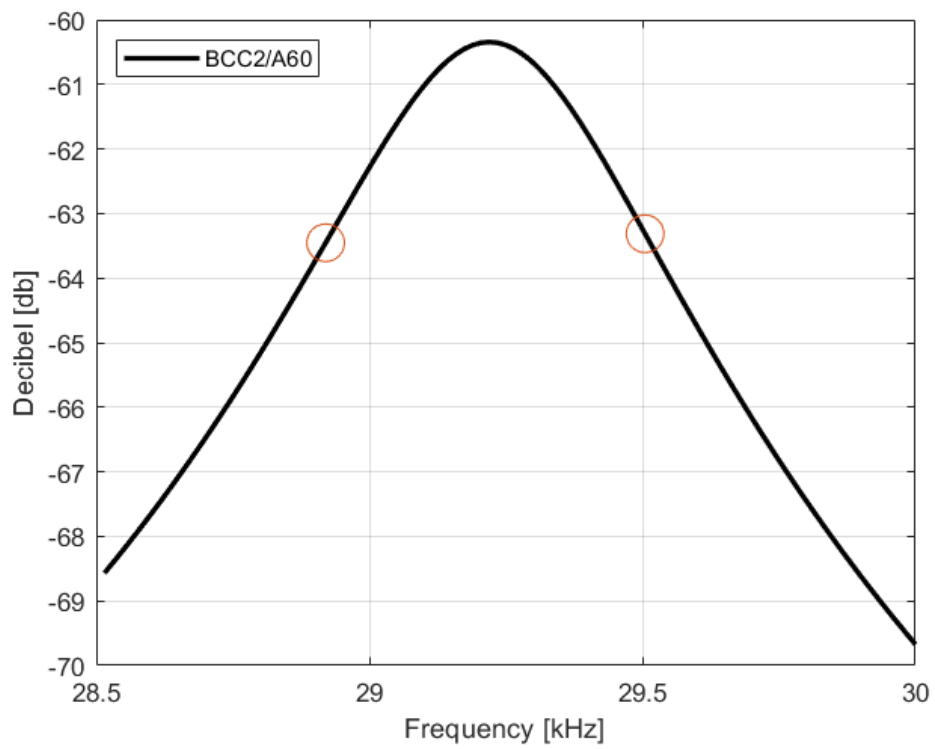
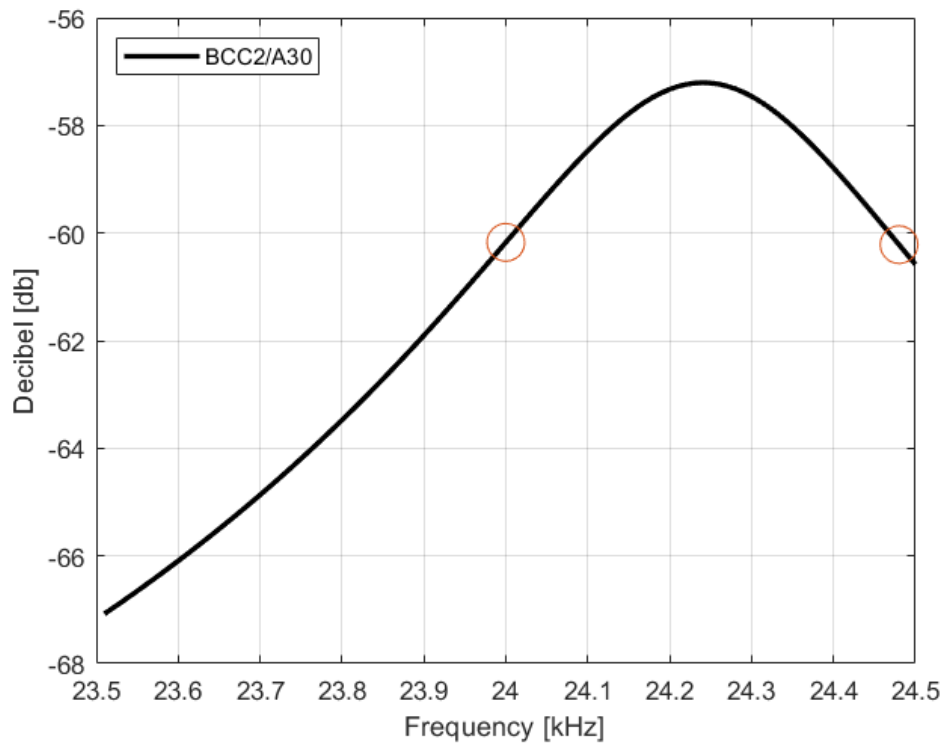
The ultimate goal of harmonic analysis is to be able to analytically calculate the energy absorbed by the hybrid structure. From the frequency response it is necessary to convert the amplitude from Newton (N) to decibels (dB). The conversion formula is shown in Eq.6.1.

$$dB = 20 \cdot \log_{10}(N) \quad (6.1)$$

Once the amplitude has been converted, the FRF $H(\Omega)$ is defined to which the half power point method (-3dB) can be applied. This method is widely used for Single-Degree-Of-Freedom (SDOF) and Multi-Degree-Of-Freedom (MDOF) structures with linear viscous damping. Considering an SDOF system excited by a harmonic forcing, it is possible to analytically calculate the energy absorbed by the system. The maximum value that the function assumes corresponding to the resonance peak is identified on the FRF. Then a quantity equal to 3dB is subtracted from the maximum value. Two points of frequency ω_1 and ω_2 , Eq.6.2, are identified on the FRF (assuming $\omega_1 > \omega_2$) on both sides of the function $H(\Omega)$, Fig.6.6.

$$\omega = 2\pi f \quad (6.2)$$





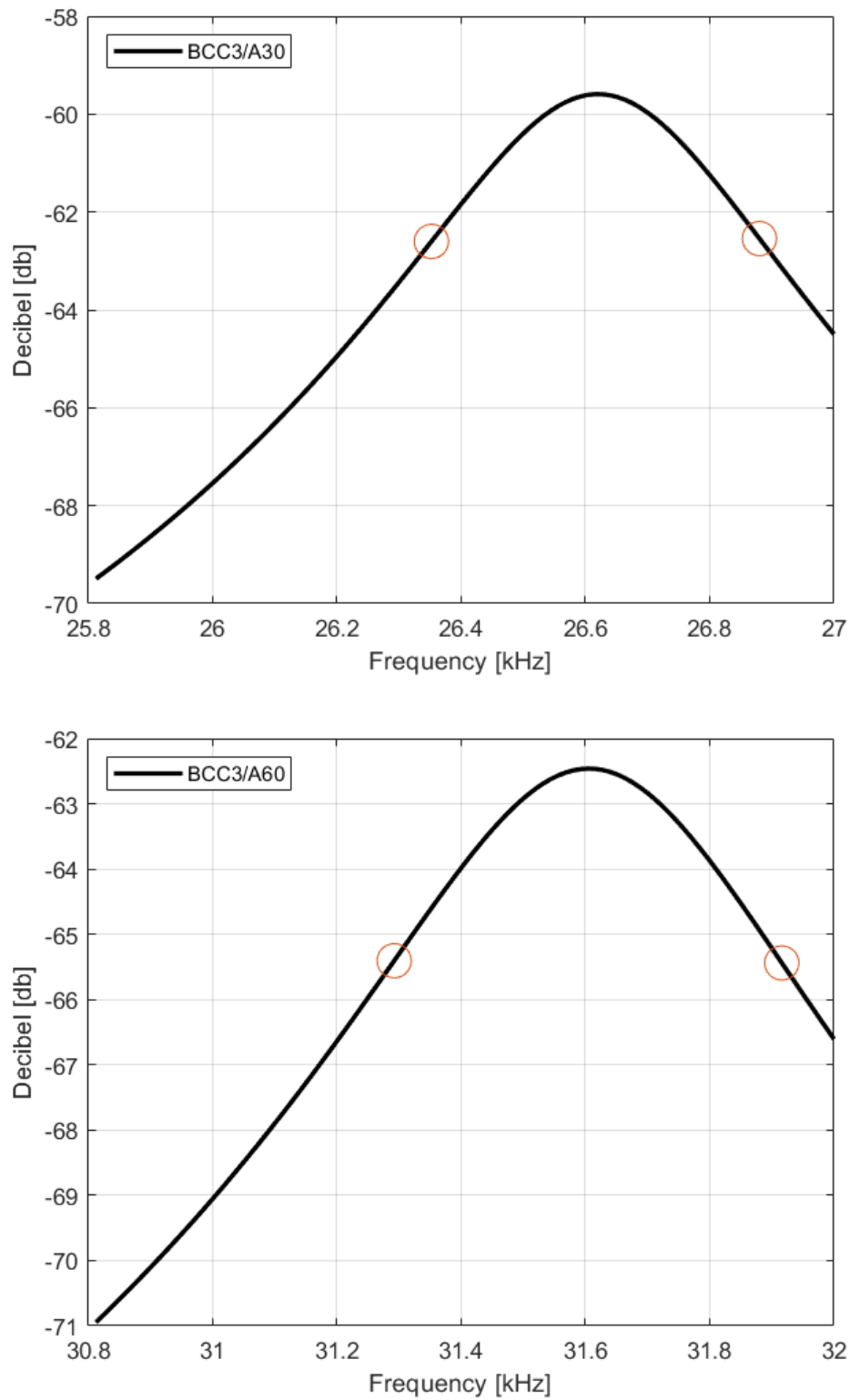


FIGURE 6.6: Half power method of damped hybrid materials

Typically, a vibration energy harvesting system can be modelled as a simple spring-mass model of a linear inertial-based generator, Fig.6.7. The system which consists of a seismic mass m , a spring of stiffness k and a damper with damping coefficient c .

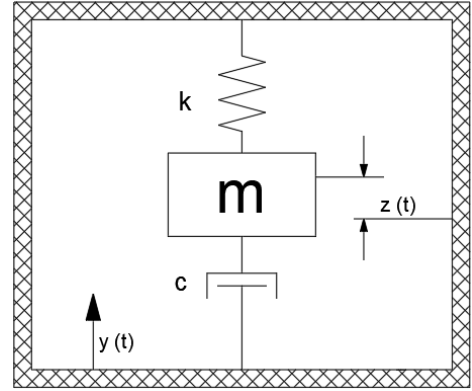


FIGURE 6.7:
Spring-mass-
damper system

These components are located within the inertial frame which is excited by the external mechanical vibration. The vibration is represented by

$$y(t) = Y_0 \cdot \sin(\omega t) \quad (6.3)$$

where Y_0 is the amplitude of the external excitation, Eq.6.3 The system can be described with the differential equation, Eq.6.4.

$$m\ddot{z}(t) + c\dot{z}(t) + kz(t) = -m\ddot{y}(t) \quad (6.4)$$

where the $z(t)$ represent spring deflection and $y(t)$ is the input displacement. The steady state solution is given by

$$z(t) = \frac{\omega^2}{\sqrt{\left(\frac{k}{m} - \omega^2\right)^2 + \left(\frac{c\omega}{m}\right)^2}} Y_0 \sin(\omega t - \phi) \quad (6.5)$$

where ϕ is the phase angle, Eq.6.5. The maximum energy can be obtained when the excitation frequency ω is equal to the natural frequency ω_n of the system. The energy dissipated in resonance can be expressed by [21]

$$E_D = \int f_D(t) dy = \int_{\omega_1}^{\omega_2} c\dot{y}(t)\dot{y}(t) dt = c \int_{\omega_1}^{\omega_2} [Y_0\omega \cos(\omega t - \phi)]^2 dt = 2\pi\zeta\omega_n k Y_0^2 \quad (6.6)$$

where ζ is the damping ratio, Eq.6.6. The damping ratio can be estimated by the half power method, Eq.6.7 and it is given by [22]

$$\zeta = \frac{\Delta f}{2f_n} \quad (6.7)$$

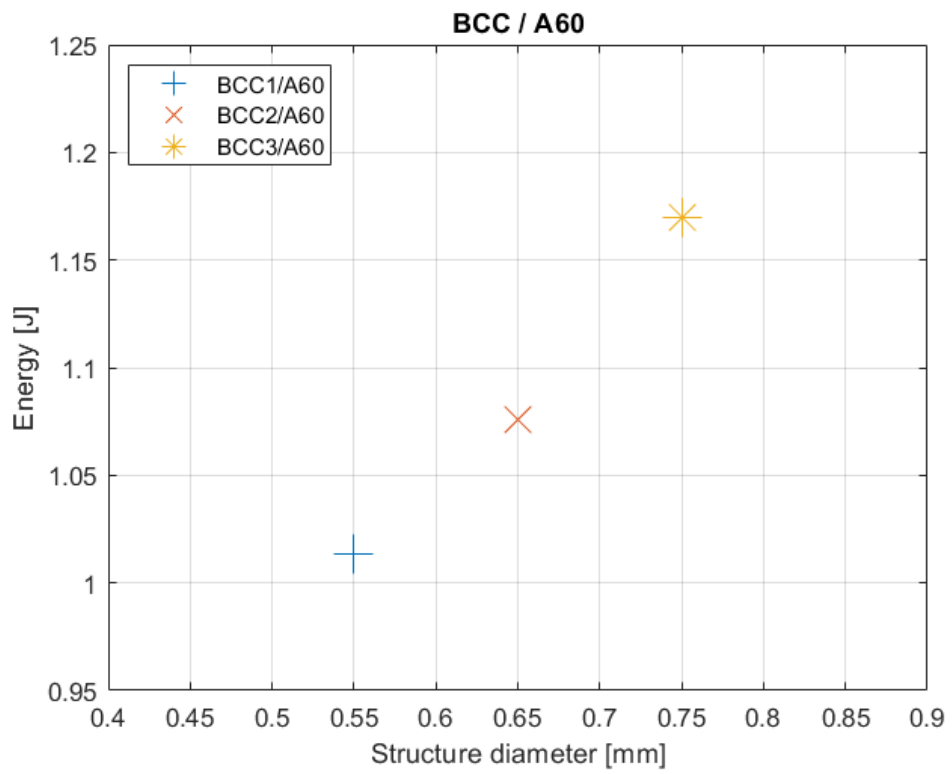
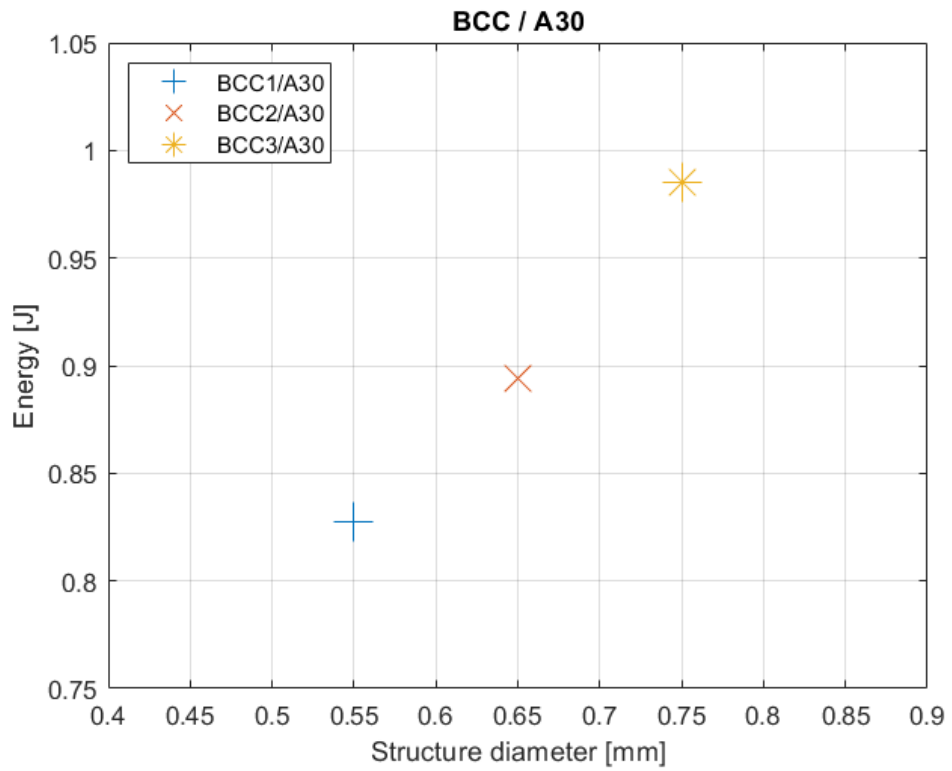
At this point it is possible to calculate the energy absorbed by the hybrid structure. Tab.6.4 shows the results of the harmonic analysis for hybrid structures.

Filled Structure	Max Amplitude	Frequency1	Frequency2	Max Energy
	-3dB			
	[dB]	[Hz]	[Hz]	[J]
BCC1/A30	-58.1459	22126	22574	0.8276
BCC1/A60	-61.5571	27080	27620	1.0134
BCC2/A30	-60.2053	24000	24480	0.8938
BCC2/A60	-63.3440	28920	29505	1.0759
BCC3/A30	-62.5926	26352	26880	0.9854
BCC3/A60	-65.4613	31292	31916	1.1696

TABLE 6.4: Results

Analysing the results we can see how, as the diameter of the elementary cell of the metal structure increases, the absorbed energy increases considerably. For materials infiltrated with A30 polymer, an increase of 0.2mm in the size of the unit cell leads to a 30% increase in the energy absorbed by the structure. For materials infiltrated with A60 polymer, the increase in absorbed energy is 30% for an increase in size of 0.16mm.

In Fig.6.8 we can visualize how the energy absorbed change in relation to the structural diameters of the lattice structures. Increasing the uprights dimension the energy absorbed by the hybrid structures increase as well. The first plot is referred to the lattice structures filled with polymer of Shore A30 hardness. The second one to the polymer of Shore A60 hardness. The last graph compares the hybrid materials as a function of the filler.



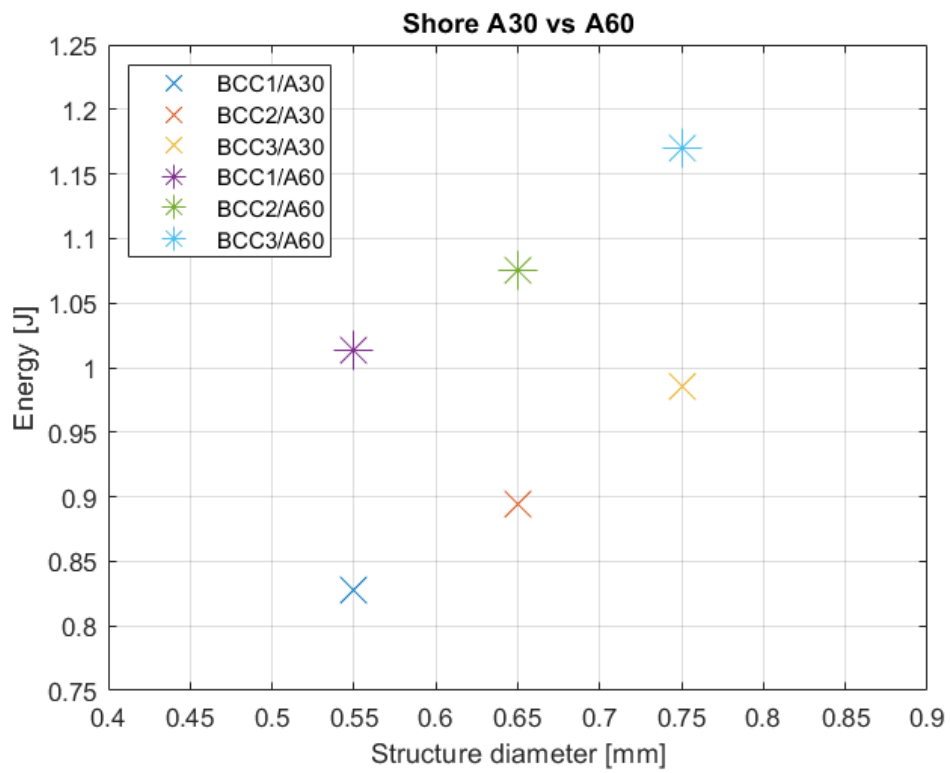


FIGURE 6.8: Influence of the lattice on the energy absorption of the hybrid material

Chapter 7

Conclusion and future development

The goal of this thesis was the creation of a mathematical model that was able to evaluate the absorption of energy by hybrid materials. The different types of hybrid materials present in the literature and how they interacted with the constituent components were analysed.

The thesis study, through a static analysis and a subsequent dynamics of the structures, led to several conclusions. Both showed how both the geometry of the lattice structures and the composition of the polymer influence the energy behaviour of the hybrid structure. With an increase of a few tenths of millimetres in the lattice material and/or using a polymer with different hardness, it was verified that the load borne by the structure increases considerably.

From the energetic behaviour, it can be seen that the energy absorbed by the hybrid component is greater than the sum of the energies of the individual components that make it up. We can conclude that the energetic properties of a hybrid component are not the sum of the capacities that the individual components that constitute it have to absorb energy during a compressive stress.

In the future, it is possible to design a component that allows to demonstrate the reliability of the mathematical model. The applications in which this model fits are in the automotive and aerospace sectors.

Furthermore, a more in-depth study of the materials making up the hybrid material can be the starting point for a subsequent work. In particular, reference is made to composite materials, given the exponential growth they have had in recent years.

References

- [1] Guoying Dong et al. “Design and optimization of solid lattice hybrid structures fabricated by additive manufacturing”. In: (2020).
- [2] Chunze Yan et al. “Evaluations of cellular lattice structures manufactured using selective laser melting”. In: (2012).
- [3] Xiaoliang Geng et al. “A FEM study on mechanical behavior of cellular lattice materials based on combined elements”. In: (2018).
- [4] Giorgio De Pasquale and Stefano Sibona. “Hybrid materials based on polymers-filled AM steel lattices with enhanced energy absorption capabilities”. In: ().
- [5] H. Niknam and A. H. Akbarzadeh. “Graded lattice structures: Simultaneous enhancement in stiffness and energy absorption”. In: (2020).
- [6] Yingying Xue, Wen Wang, and Fusheng Han. “Enhanced compressive mechanical properties of aluminum based auxetic lattice structures filled with polymers”. In: (2019).
- [7] Uzair Ahmed Dar et al. “Experimental and numerical investigation of 3D printed micro-lattice structures for high energy absorption capabilities”. In: (2020).
- [8] Dirk Herzog et al. “Additive manufacturing of metals”. In: (2016).
- [9] Ramona Hölker et al. *Hot Extrusion Dies with Conformal Cooling Channels Produced by Additive Manufacturing*. 2015.
- [10] Thaisa T. Oliveira and Andréa C. Reis. “Fabrication of dental implants by the additive manufacturing method: A systematic review”. In: (2019).
- [11] Xipeng Tan et al. “Application of electron beam melting (ebm) in additive manufacturing of an impeller”. In: (2014).

- [12] Anon. “Laser sintering ushers in new route to PM parts”. In: (1997).
- [13] Daniel R.A. Cluff and Shahrzad Esmaeili. “Compressive properties of a new metal-polymer hybrid material”. In: 44 (2009).
- [14] J. E. Campbell et al. “Periodic cellular metal/polyurethane foam hybrid materials”. In: (2009).
- [15] Tianlin Zhong et al. “Mechanical properties of lightweight 316L stainless steel lattice structures fabricated by selective laser melting”. In: (2019).
- [16] Recep Gümrük, U?ur Mazlum, and R. A.W. Mines. “Compressive mechanical behaviors of hybrid composite materials based on micro lattice structure and rubberlike materials”. In: (2015).
- [17] Mahmoud M. Osman et al. “Compressive behavior of stretched and composite microlattice metamaterial for energy absorption applications”. In: (2020).
- [18] Andrea Avi. “Il metodo dell’analisi statica dell’energia per il dimensionamento preliminare delle strutture”. PhD thesis. Università degli Studi di Padova, 2014, p. 225.
- [19] F. Orban. “Damping of materials and members in structures”. In: (2011).
- [20] Lazan and Benjamin Joseph. “Damping of materials and members in structural mechanics”. In: (1968).
- [21] Adolfo Santini. *Dinamica delle strutture*. 2015.
- [22] Svend Gade and Henrik Herlufsen. “Digital Filter vs FFT techniques for damping measurements”. In: (1990).